UILU-ENG 88-3603

Report No. 142

A LONG-LIFE REGIME PROBABILITY-BASED FATIGUE DESIGN METHOD FOR WELDMENTS

by

Sahng Kyoo Park and F. V. Lawrence, Jr.
Department of Materials Science and Engineering

A Report of the

MATERIALS ENGINEERING - MECHANICAL BEHAVIOR

College of Engineering, University of Illinois at Urbana-Champaign

June 1988

A LONG-LIFE REGIME PROBABILITY-BASED FATIGUE DESIGN METHOD FOR WELDMENTS

ABSTRACT

A probability-based fatigue design methodology for crack initiation and early growth is presented which estimates the average fatigue strength of weldments and its uncertainty using a Monte Carlo simulation. The underlying analytical model considers several different kinds of fatigue variables: applied or induced bending stresses; notch severity; notch-root residual stresses; and notch-root mechanical properties. Each of the fatigue variables is treated as a random variable, and the uncertainty of each is modeled by an appropriate probability distribution function developed from laboratory data.

The suggested design method can determine the fatigue strength for a given design life with a certain reliability, and it can be applied to both constant amplitude and variable load history applications. The method also permits the designer to factorize the contribution of each of the fatigue variables to the overall uncertainty in fatigue strength and thus determine the economic merits of reducing the uncertainty in any one of the fatigue variables.

For this study, fatigue test data of three types of weldments, load-carrying fillet-welded cruciform weldments, non-load carrying fillet-welded cruciform weldments and butt weldments, were used for the simulation of fatigue strength and its related uncertainty.

TO MY PARENTS AND MY WIFE

ACKNOWLEDGEMENTS

I would like to express my deep appreciation to Professor F. V. Lawrence, Jr. not only for his academic supervision, but also for his fatherly guidance. Both have been valuable inspirations all through.

I also would like to express my gratitude to Professor W. H. Munse for his valuable comments on my study, and to Dr. S. Bhat in Inland Steel Company for providing valuable data. I must extend my gratitude to my colleagues in NCEL B124 for their encouragement and valuable discussions during my study.

This study was initiated with a fund from U. S. Coast Guard and continued with a fund from the University of Illinois Fracture Control Program supported by a consortium of midwest industries. A special acknowledgement is also due to the Caterpillar Tractor Company for their financial support.

I hereby wish to express my deep appreciation to my parents and family for their limitless devotion during my study. In addition, I wish to express my sincere gratitude to my wife Soo-Eun and my daughter Connie JaKyung for their excessive love and patience.

TABLE OF CONTENTS

1. INTRODUCTION

1.1 Fatigue Design of Weldments

The fatigue design strength of weldments is governed by the desired service period and level of reliability as well as by weldment geometry, stress history and fatigue properties. While the effects of geometry, stress history and material properties have been extensively studied in the past [1,2,3,4], much recent attention has been given to the desired service period and the level of reliability.

The reliability of weldment fatigue strength estimates depends upon the variability of weldment fatigue behavior. The variability of the weldment fatigue strength can be decomposed into systematic errors and random variability. The systematic errors result from factors or variables which are not considered in the prediction model and which cause a consistent bias of the estimated behavior. For example, the systematic errors in the estimated fatigue strength can be corrected using appropriate average "bias factors" [5] such as the Morrow mean stress correction to the Basquin Equation (See Eq.10 and Fig. 1).

Random variability results from uncertainty in the "bias factors" and the inherent randomness of the fatigue process. The uncertainty in the "bias factors" results in a scatter about the average fatigue strength although the extent of this scatter differs for each fatigue model since each model differs in the success with which it deals with the many fatigue variables, and since each uses different means to represent the systematic variations of fatigue behavior. The random variability must be quantified in order to ensure the required structural reliability.

1.2 Probabilistic Fatigue Design of Weldments

Due to the inherent complexity of the weldments as a mechanical structural component, the physical attributes and their related fatigue variables which determine the performance of welded structural components are generally random. In the design of a group of weldments, one can not avoid variations in geometry, material properties and distortion among the weldments even though they are fabricated by the same welding process. However, the physical attributes of a weldment which control the fatigue process exhibit statistical regularity so that weldment fatigue design can be based on probability concepts. Two recent methods are described below:

1.2.1 S-N Diagram Approach: The Munse Fatigue Design Procedure

The fatigue behavior of a group of structural components with the same overall geometry and loading condition can be characterized by a mean S-N curve. The S-N curve (the result of a linear regression analysis of the collected fatigue data often written in the form of Eq. 1 below) represents the mean fatigue life, and the scatter about the mean represents the uncertainty of the empirically (statistically) determined "C" and "m" values (See Fig. 2):

$$N = C / \Delta S^{m} \qquad (1)$$

where N = Mean fatigue life

ΔS = Applied Nominal Stress Range

C, m = Empirical Constants

Much effort [6,7,8] has been recently given to developing fatigue design criteria using statistical concepts to quantify the scatter of component

fatigue data. Munse and Ang [8,9] proposed a fatigue design procedure which takes into accounts the desired reliability by modeling the total uncertainties of S-N relationship. The Munse Fatigue Design Procedure (MFDP) [9] is an effective structural fatigue design method based on S-N diagrams and deals with the complex geometries, the variable load histories, and the desired reliability encountered in the fatigue design of weldments (See Fig.3).

The maximum design fatigue strength (ΔS_D^{max}), which is the maximum stress range occurring once in the design life time, is determined by three factors: the mean S-N constant amplitude fatigue resistance of weld details (ΔS), the Random Load Factor (ξ), and the Reliability Factor (R_F) as follows.

$$\Delta S_D^{max} = \Delta S \quad R_F \quad \xi \tag{2}$$

The MFDP obtained the mean fatigue resistance values from the University of Illinois Fatigue Data Bank [10] which contains S-N data for a large variety of welded components subjected to different types of loading.

To obtain the reliability factor, the MFDP takes all uncertainties into account and provides a rational frame work for designing structural details to a desired level of reliability. The total uncertainty includes the natural scatter in fatigue data together with the uncertainties in fabrication and the stress analysis. The uncertainties (Ω) are quantitatively represented in the form of coefficient of variations (COV):

$$\Omega_N^2 = \Omega_f^2 + \Omega_C^2 + m^2 \, \Omega_S^2 \tag{3}$$

where Ω_N = the total uncertainty in fatigue life.

Ω_f = the uncertainty in the fatigue data life.

$= \sqrt{\Delta_f^2 + \delta_f^2}$; in which δ_f is the coefficient of variation in the fatigue life data about the S-N regression lines; and Δ_f is the error in the fatigue model (the S-N equation, including such effects as mean stress), and the imperfections in the use of the linear damage rule (Miner) and the Weibull distribution approximations.

Ω_C = the uncertainty in the mean intercept of the regression lines, and includes in particular the effects of workmanship and fabrication.

Ω_S = measure of total uncertainty in mean stress range, including the effects of impact and error of stress analysis and stress determination.

Having estimated the total uncertainty in fatigue life Ω_N, the reliability factor R_F is estimated after assuming an appropriate distribution (Weibull in MFDP) of the fatigue life data to specify a desired level of reliability of fatigue strength as shown in following equation [9].

$$R_F = \left[\frac{[P_F(N)]^{\Omega_N^{1.08}}}{\Gamma(1 + \Omega_N^{1.08})}\right]^{1/m} \qquad (4)$$

The product of the mean fatigue resistance and the reliability factor gives the constant amplitude fatigue design strength for a given reliability level. To apply this value to the variable amplitude load, an equivalent stress range (ΔS_e) which causes the same damage as a certain variable load history for a given design period is estimated through Miner's linear cumulative damage rule. The Random Load Factor [9] was obtained as;

$$\text{Random Load Factor} = \xi = \Delta S_D^{max} \; / \; \Delta S_e \qquad (5)$$

The MFDP uses probability distribution functions to represent the variable amplitude loading. One must determine which distribution provides the best fit to a given loading history.

1.2.2 Probabilistic Analysis of Propagation Life:

The Study of Engesvik and Moan

The fatigue life from the initial crack to the critical crack size can be predicted analytically through a correlation between crack growth rate and cyclic stress intensity factor (ΔK_I). The correlation was first proposed by Paris [11] as:

$$da \; / \; dN = C \; (\Delta K_I)^n \qquad (6)$$

where da/dN = Fatigue Crack Growth Rate

C, n = Empirical Material Constant

Then the fatigue propagation life (N_P) can be estimated as:

$$N_P = \frac{1}{C} \int_{a_i}^{a_f} (\Delta K_I)^{-n} \, da \qquad (7)$$

where a_i = Initial Crack size

a_f = Final Crack Size

Engesvik and Moan [12] used a Monte Carlo simulation technique to simulate the fatigue crack propagation life based on the linear elastic

fracture mechanics (Eq.7) [13] using appropriate statistics for the related fatigue variables influencing the fatigue crack propagation life. They simulated the fatigue life for given nominal stress range considering: initial crack size, weldments geometry (toe flank angle(θ) and local radius of toe (r)), and material properties (fatigue propagation exponent (n) and coefficient (C) of the Paris' law) as random variables with certain statistical regularities. They studied the contribution of individual fatigue variables to the randomness of the weldment fatigue crack propagation life.

Forty-two specimens of 32 mm thick non-load-carrying fillet welded cruciform joint were tested under constant amplitude load (ΔS = 150 MPa) with nominal mean stress ratio R = 0. The test results were compared with the Monte Carlo simulation results.

The distributions of fatigue life data both from fatigue test and simulation showed a positively skewed log-normal distribution. Their sensitivity study predicted that the lower tail (shorter fatigue life, $< 10^5$ cycles) should have a lesser sensitivity to the uncertainty of fatigue variables than the upper tail region (longer fatigue life, 2×10^6 cycles). Their simulation results indicated that the scatter in constant amplitude fatigue life is primarily caused by the uncertainty in the following variables listed in order of importance : weld toe radius (r), initial crack size (a_i), material properties (C and n) and toe flank angle (θ).

1.3 Limitations of the S-N Diagram and LEFM Approach

1.3.1 S-N Diagram Approach

The classical S-N diagram approach, design based on the results of constant amplitude tests on weldments, is still the basis of the most weldment fatigue design codes even though this approach requires costly and time-consuming laboratory tests, especially for the fatigue data in the long-life regime.

Although one of the main advantages of the S-N approach is that a massive quantity of fatigue data has been generated for various types of structural details, not much fatigue data are available for the long-life regime. Also, due to the nearly infinite number of loading, material or weld geometry, data for the application at hand are generally unavailable.

The scatter in the S-N diagrams is used as the basis of the determination of reliability. The scatter in the fatigue data for welded components is generally larger than for plain plate due to the complex nature of stress distribution in weldments and by the variation in weld geometry. This large scatter results from not only the randomness of the fatigue behavior but also from the systematic errors resulting from the neglect of many fatigue variables as: mean stress, residual stress, local geometric variation and joint distortion; thus the characteristically large amount of scatter in S-N diagrams from systematic errors result in more conservative fatigue design strength.

The S-N diagram approach is inherently costly and time-consuming, and also causes an unnecessary conservatism in fatigue design due to its

inability to deal with the many fatigue variables and the consequent systematic errors inherent in S-N diagrams of fatigue data banks.

1.3.2 The LEFM Approach: Propagation Life Only

The use of fracture mechanics models [13,14,15] to estimate weldment fatigue life using Eq. 7 is based on three main assumptions: (1) that fatigue crack initiates from pre-existing crack-like defects or geometrical discontinuities; (2) that the stress intensity factor at the tip of pre-existing crack-like discontinuities can be calculated using linear elastic fracture mechanics (LEFM); and (3) that the fatigue crack propagation rate for the pre-existing discontinuities is equal to the propagation rate obtained by testing standard specimens.

These assumptions lead this design method to be characterized as a prediction method of the "residual life" of the structural components after a dominant crack has initiated. This design method has been successfully utilized in design and service maintenance of aircraft. However, in the design of weldments, the above assumptions are violated in many ways.

First, it is questionable whether weld discontinuities should be classed as pre-existing cracks. Smith and Smith [16] investigated 278 weld discontinuities at the toe of BS4360-43A SMAW fillet weldments. They reported the depth of the weld toe notch in the range of 0 to 120μm with average being 45μm. Similar results were reported by other investigators [17,18]. It is questionable whether 45μm average depth discontinuities can be characterized by a linear elastic stress intensity factor. Seeger [19] recently wrote with reference to the results of Smith and Smith:

"Despite the high amount of data evaluated, the question whether the initial flaws of the weld should be considered cracks or not, cannot be answered clearly from the results: With the average depth being just over the double of the surface roughness (20μm), most of the flaws are not really cracks, but certainly the maximum depth of 120μm indicates a small crack."

Second, even assuming a pre-existing crack, the size of the initial crack can not be easily decided because there is too much randomness in the size of the discontinuities. This large randomness in the initial crack size becomes an important source of uncertainty in the fatigue strength, especially in the long-life regime, and this uncertainty forces designers to assume bigger initial crack sizes which are greater than the average value in reality.

Third, recalling the 120μm maximum defect (crack) size of Smith and Smith's investigation [16], note that the size of the plastic zone near its crack tip is large enough to violate the basic assumptions of the LEFM in the calculation of the cyclic stress intensity factor at the crack tip in the early growth stage. Although this point remains controversial, this stage is the major portion of the fatigue crack growth in the long-life regime [20,21,22]. This crack tip plasticity contributes to the so-called "anomalities of short crack behavior" which are crack growth below threshold, anomously high crack growth rates near threshold, and decreasing growth rate with increasing crack length. Recent studies [23,24,25] showed that for mild steel, cracks which are smaller than .25 to 1 mm can not be physically represented as having a driving force due to the cyclic stress intensity factor (ΔK). Also Nowak [25] and Schjive [26] showed that the

early growth (short crack) behavior involved microstructural behavior at the crack tip (or notch tip) as well as the macroscopic elastic stress field.

Recently, there has been an effort to account for the early growth behavior of the short crack in early growth stage using a modified fracture mechanics approach [27] using ΔK_{eff} or ΔJ_{eff}. This approach continues the use of fracture mechanics load parameters and accounts for the crack closure effects, however this approach still assumes that the weld discontinuity is a pre-existing "short crack". Whether this approach will produce a more useful design method to assess the early growth behavior remains to be seen.

Thus, the use of linear elastic fracture mechanics and the neglect of the initiation and early growth period, which is generally the dominant portion of total fatigue life in the long-life regime fatigue behavior, can give over-conservative life predictions in the long-life regime.

1.3.3 Alternate Approach: Local-Strain Approach

There is growing evidence [20,21,22] that fatigue crack initiation and early growth behavior are dominant in the long-life regime (See Fig. 4). Lawrence et.al [28,29,4,1,20] have proposed a model (the Total Life Model) to assess the fatigue crack initiation and early growth from notches in weldments. This approach is a variation of the local-strain approach based on the strain-life relationship [30]. Since the crack size cannot be a significant contributor to the damage until the crack grows to a dominant size relative to the plastic zone size, the local-strain approach uses the local stress amplitude (σ_a) as a load parameter which represents the damage at the notch tip.

1.4 Scope of This Study

In this study, a probabilistic long-life regime weldment fatigue design method based on the local-strain approach will be presented. This method herein termed the Weldment Fatigue Crack Initiation Model (WFCIM) assesses the physical and statistical behavior of fatigue crack initiation and early growth in weldments.

The physical factors (fatigue variables) which influence the fatigue crack initiation and early growth behavior in weldments will be analyzed, and their statistical distribution will be estimated based on laboratory data.

A Monte Carlo simulation of weldment fatigue strength based on the statistical regularity of the fatigue variables will be used to estimate the average weldment fatigue strength and its uncertainty in the long-life regime. The fatigue behavior of three different kinds of weldments will be simulated: load-carrying cruciform weldments, non-load-carrying cruciform weldments and butt weldments. The simulated fatigue strength and uncertainty for each weldment will be compared with fatigue test data.

The simulated mean fatigue strength and uncertainty will be used to estimate a probability based fatigue design strength, and will be compared with prevailing fatigue design criteria.

The Monte Carlo simulation will be used to factorize the total uncertainty of fatigue strength into the contribution of each physical factors of weldments such as: material properties, welding distortion, geometric variation, residual stress and mean stress.

2. LONG-LIFE REGIME WELDMENTS FATIGUE DESIGN BASED ON TOTAL LIFE MODEL

2.1 Weldment Fatigue Crack Initiation Model (WFCIM)

As implied by its name, the Total Life Model developed by Lawrence et.al. [28] considers both: (1) the fatigue crack initiation and early growth life (N_I) which is based on the strain-life relation,

$$\varepsilon_a^T = \frac{\sigma_f'}{E} (2N_I)^b + \varepsilon_f' (2N_I)^c \qquad (8)$$

where ε_a^T = Total Strain Amplitude

σ_f' = Fatigue Strength Coefficient

ε_f' = Fatigue Ductility Coefficient

b = Fatigue Strength Exponent

c = Fatigue Ductility Exponent

E = Young's Modulus;

and, (2) the fatigue crack propagation life (N_p) which is based on fracture mechanics (Eq. 7). The total fatigue life (N_T) is:

$$N_T = N_I + N_p \qquad (9)$$

Since the initiation and early growth of fatigue cracks is thought to become the controlling portion of the fatigue life in the long- life regime [20,21,22], the fatigue resistance of weldment to the crack initiation and early growth under constant amplitude loading in the long-life regime was modeled by Lawrence et al [28] using Basquin-Morrow equation [30]:

$$\sigma_a = \sigma_f' (1 - \sigma_m / \sigma_f') (2 N_I)^b \qquad (10)$$

The Basquin-Morrow equation can be modified to deal with the combined axial and bending load conditions;

$$\sigma_a = (K^A_{fmax}\, S^A_a + K^B_{fmax}\, S^B_a) = \sigma'_f(1 - \sigma_m / \sigma'_f)(2\, N_I)^b \qquad (11)$$

where σ_a - Total Stress Amplitude

σ_m = Local Mean stress

K^A_{fmax} = Axial Fatigue Notch Factor

K^B_{fmax} = Bending Fatigue Notch Factor

S^A_a = Nominal Axial Stress amplitude

S^B_a - Induced Bending Stress Amplitude

Equation 11 takes into account material fatigue properties, residual stresses, variations in local geometry, and stresses induced by welding distortion.

An empirical expression for the fatigue strength for weldments subjected to both axial or bending loads has been suggested by Lawrence and Chang [31] based on Eq. 11. Weldments are generally subjected to both axial and bending loads, the latter of which often result from the straightening of weld distortions under load. Thus, the combined effects of axial and bending loads must be considered in the estimation of weldment fatigue strength.

In the long-life-regime, the local stress-strain response to the applied remote stress amplitude (S_a) and the nominal mean stress (S_m) can be assumed to be elastic. Thus, the local mean stress (σ_m) and stress amplitude (σ_a) at the notch-root can be expressed as:

$$\sigma_m = \sigma_r + (K^A_{fmax} S^A_m + K^B_{fmax} S^B_m)$$

$$= \sigma_r + \frac{1 + R}{1 - R}(K^A_{fmax} S^A_a + K^B_{fmax} S^B_a) \qquad (12)$$

$$\text{since} \quad S_m = (\frac{1 + R}{1 - R}) S_a$$

where σ_r is the notch-root residual stress and R is the stress ratio. From Basquin's relationship (Eq.11) and Eq. 12.

$$\sigma_a = (K^A_{fmax} S^A_a + K^B_{fmax} S^B_a)$$

$$= [\sigma'_f - \sigma_r - \frac{1 + R}{1 - R} (K^A_{fmax} S^A_a + K^B_{fmax} S^B_a)](2N_I)^b \qquad (13)$$

Rearranging Eq. 13, the total fatigue strength of a weldment at long-life-regime is:

$$S^T_a = \frac{(\sigma'_f - \sigma_r) (2N_I)^b}{K^{eff}_{fmax} [1 + \frac{1 + R}{1 - R} (2N_I)^b]} \qquad (14)$$

where $K^{eff}_{fmax} = (1 - x) K^A_{fmax} + x K^B_{fmax}$

$x = S^B_a / S^T_a$

$S^T_a = S^A_a + S^B_a$

or when the bending components are unwillingly induced by welding distortion, the nominal axial fatigue strength is:

$$S^A_a = \sigma'_f \frac{1}{K^A_{fmax}} \frac{1 - x}{1+x(X-1)} (1- \frac{\sigma_r}{\sigma'_f}) \frac{1}{[1+ \frac{1 + R}{1 - R}(2N_I)^b]} (2N_I)^b \qquad (15)$$

where X = Ratio of K^B_{fmax} to K^A_{fmax}

A comparison of fatigue strength predictions made using Eq. 14 and experimental data for both as-welded and post-weld treated steel weldments [31] is given in Fig. 5.

Based on this empirical expression of weldments fatigue strength in Eq.14, Lawrence and Yung [32] developed a deterministic fatigue design expression for weldments. Figure 6 shows a graphical method to determine fatigue strength at 2 million cycles of fatigue life for the A-36 as-welded weldments in several configurations. This design method can be a good guideline of the mean fatigue strength at the high cycle region around 2 million cycles of fatigue life as expected with the prediction in Fig. 5.

2.2 Extension of WFCIM to the Probabilistic Weldment Fatigue Design Method

There are five "factors" which together with the magnitude of the applied fluctuating stresses, determine the fatigue crack initiation and early growth behavior in weldments in Eq. 15, the WFCIM:

(1) the mechanical properties of the material in which fatigue crack initiation and early growth take place (P);

(2) the severity of the discontinuity or notch which is an inherent property of the geometry of the joint (G);

(3) the self-induced stress components caused by the distortion occurred during welding (B);

(4) the notch-root residual stresses which result from fabrication and subsequent use of the weldments (RS);

and (5) Applied mean stresses at the crack initiation and early growth sites (MS).

The effects of these five "factors" on the fatigue strength of a given weldments can be factorized in a rewritten Basquin equation:

$$S_a^A = P \quad G \quad B \quad RS \quad MS \quad (2N_I)^b \tag{16}$$

where $P = \sigma_f'$; Effects of Material Properties

$G = \dfrac{1}{K_{fmax}^A}$; Geometry and Notch Effects

$B = \dfrac{1 - x}{1 + x\,(X - 1)}$; Effects of Induced-Stress by Welding Distortion

$RS = \left(1 - \dfrac{\sigma_r}{\sigma_f'}\right)$; Residual Stress Effects

$MS = 1/\left[1 + \dfrac{1 + R}{1 - R}(2N_I)^b\right]$; Applied Mean Stress Effects

A deterministic value of fatigue strength results from deterministic values of the five "factors" (fatigue variables) in Eq. 16. If we permit these variables to vary randomly (with a certain statistical regularity), the resulting fatigue strength estimates using Eq. 16 will be a stochastic fatigue strength with a certain probability distribution function.

The fatigue variables on the right side of Eq.16 can be divided into deterministic variables or desirable design quantities ($2N_I$, R) and random variables (K_{fmax}^A, σ_f, σ_r, b, X, x). The design fatigue strength (S_a^A) then becomes a random variable which is depend on the random variation of those variables. The randomness of the fatigue strength can be obtained using a Monte Carlo simulation technique which estimates the fatigue strength and its distribution through a series of fatigue strength estimates calculated

from values of the fatigue variables generated using random numbers and the appropriate probability function for each variable.

Monte Carlo Simulation Procedure: Figure 7 is a schematic description of the Monte Carlo simulation procedure. The statistical distribution of each fatigue variable was determined from the laboratory data. However, if direct measurements were unavailable, analytical and empirical relationships of fatigue variables with other measurable data were used. Each fatigue variable was fitted with an appropriate analytical probability distribution functions and related statistical estimators. The following chapter will discuss statistical modeling of the fatigue variables of weldments.

A Monte Carlo simulation of Eq. 16 was performed to obtain the statistical distribution of axial fatigue strength (S_a^A), which is a design parameter for a given fatigue life. An IBM- PC/AT was used for the simulation and an IMSL [33] statistical package and Fortran 77 language was used to construct a simulation software (Appendix A.). For each fatigue variables, 1000 random data were generated.

3. STATISTICAL MODELING OF FATIGUE VARIABLES

3.1 Fatigue Variables for Material Property Factor (P)

To the degree that the Basquin-Morrow Equation (Eq. 10) describes the fatigue crack initiation and early growth phenomenon in the high cycle region, the material parameters σ_f' (fatigue strength coefficient) and b (fatigue strength exponent) are the fatigue properties which describe that process. Since σ_f' and b are essentially the intercept and slope of fatigue data in the S-N diagram, they are stochastic variables with a strong statistical dependence; that is, while σ_f' and b are stochastic variables, they are not statistically independent. Therefore, in stochastic modeling, only one of these two parameters is treated as a random variable. For this study, the fatigue strength coefficient (σ_f') was considered to be a random variable; whereas, the exponent (b) was considered as a deterministic variable.

Mean values of fatigue Properties: Due to the costly and time-consuming testing required to determine the strain-controlled fatigue properties (σ_f' and b), especially in for the heat affected zone (HAZ), average relationships between fatigue strength properties and the hardness (DPH) and monotonic strength properties such as ultimate tensile strength (S_u) have been established [31, 34, 35, 36]. Recently McMahon [37] summarized these relationships for steels:

For hot rolled and quenched & tempered steel,

$$\sigma_f' = .95\ S_u + 400 \qquad (17)$$
$$= 3.35\ DPH + 400$$
$$b = -1/6 \log (2.1 + 917/S_u)$$
$$= -1/6 \log (2.1 + 266/DPH)$$

where σ_f' and S_u have units in MPa.

Knowing the mean values of ultimate tensile strength (S_u) or hardness (DPH) at the fatigue crack initiation sites, one can estimate the average values of fatigue properties using Eqs. 17 for steels.

For weldments, since most fatigue cracks initiate at the weld metal or HAZ whose post-weld ultimate tensile strength is not known or altered by the welding procedure, the average value of measured hardness (DPH) can be used to estimate the average ultimate tensile strength and, accordingly, the fatigue properties. When the measured hardness is not available, the ultimate tensile strength of base metal can be used to estimate the average ultimate tensile strength of grain-coarsened HAZ using the empirical relationship [31]:

$$(S_u)_{HAZ} = 1.5\ (S_u)_{B.M.} \qquad (18)$$

Variation of fatigue strength Coefficient: Since the data for the fatigue strength coefficient (σ_f') of crack initiation sites in weldments, especially in HAZ, was neither available in sufficient quantity to permit estimation of its statistical uncertainty nor easy to generate, two different approaches were taken to estimate the uncertainty of fatigue strength coefficient: one was based on the uncertainty of ultimate tensile strength (S_u), and the other was based on the uncertainty of hardness (DPH).

Since the relationship between ultimate tensile strength (S_u) and fatigue strength coefficient (σ_f') in Eq. 17 was determined by regression

analysis, the standard deviation of fatigue strength coefficient (s_σ) can be estimated with the standard deviation of ultimate tensile strength (s_{Su}) as [5]:

$$s_\sigma = .95\ s_{Su}\ /\rho \tag{19}$$

where ρ is the correlation coefficient between σ_f' (MPa) and S_u which quantities are assumed to be jointly normally distributed in the regression analysis. McMahon [37] reported ρ =.8 for Eq. 17.

Data sets of the material properties (S_u and S_y) for hot-rolled steel sheets [38] and line pipe material [39] were statistically tested, and their statistics are shown in Table 1. Each data set represented materials from number of different heats of steel having the same material specification. The two data sets showed 3.4 ksi (24 MPa) and 4.2 ksi (29 MPa) standard deviation values for their ultimate tensile strength (s_{Su}), respectively. Assuming these typical values of standard deviation in ultimate tensile strength (s_{Su}) as typical variations of ultimate tensile strength of fatigue crack initiation site, one can estimate the standard deviation of fatigue strength coefficient (s_σ) using Eq. 19.

Since the fatigue crack initiation behavior occurs in a very small volume of material within 1 mm^3, the hardness (DPH) for the possible crack initiation sites were measured, and the measured hardness data were statistically tested to estimate the uncertainty of material properties in microstructural level. Then the standard deviation values of hardness (s_{DPH}) at the crack initiation site were used to estimate the standard deviation of the fatigue strength coefficient (σ_f') using the relationship between s_σ and s_{DPH} similar to the relationship between s_σ and s_{Su} in Eq. 17:

$$s_\sigma = 3.35\ s_{DPH}\ /\ \rho \tag{20}$$

where ρ = 0.8.

The statistics of measured hardness (DPH) at the crack initiation sites (HAZ and weld metal) and base metal of 12.7 mm plate thickness ASTM A-36 steel weldments are given in Table C1. The base metal had a standard deviation of 11.1, the weld metal had a standard deviation of 15.4, and the grain-coarsened HAZ had a standard deviation of 15.2.

The approach based on DPH resulted in about two times larger s_σ than that based on S_u. It is still in question which approach (based on uncertainty of ultimate strength or uncertainty of hardness) properly represents the uncertainty of fatigue strength coefficient. However, the approach based on the uncertainty of ultimate tensile strength was used in the simulation for present study because it seemed more reasonable to estimate the statistical behavior of a bulk material property (σ_f') based on a statistical behavior of another bulk material property (S_u) rather than based on a point to point material property variation at the notch-root (in a small volume at the microstructural level).

Therefore in this study, Eq.17 and a standard deviation of 29 MPa for ultimate tensile strength was used to estimate the standard deviation of fatigue strength coefficient (s_σ). Of two typical values of standard deviation in Table 1 (24 and 29 MPa), the larger value (29 MPa) was used since the larger will cause more uncertainty in fatigue strength and accordingly, a more conservative fatigue design strength.

3.2 Fatigue Variables for Geometry and Notch Factor (G)

The stress concentrations inherent in weldments result from the overall configuration of the members and the local geometric discontinuities caused by the weld. Lawrence et. al. [28] have developed the concept of the

"worst-case-notch" for weld discontinuities which results from a radius giving the highest possible value of the fatigue notch factor ($K_{f\ max}$). Peterson [40] proposed a relationship between the fatigue notch factor (K_f) and the theoretical elastic stress concentration factor.

$$K_f = 1 + \frac{K_t - 1}{1 + a/r} \tag{21}$$

where r is notch-root radius, and 'a' (Peterson's constant) can be related to the material strength as:

$$a = .025 \left(2070 / S_u \right)^{1.8} \tag{22}$$

where 'a' is in mm, and S_u is in MPa.

We can write the elastic stress concentration factor as:

$$K_t = 1 + \alpha(t/r)^{.5}, \tag{23}$$

where α is a nondimensional geometric coefficient, and t is the plate thickness in mm, the worst-case-notch concept is that "K_{fmax}" is the maximum value of K_f which occurs for a given geometry when r = a ($dK_f/dr = 0$):

Thus,

$$K_{fmax} = 1 + 0.00325\ \alpha \left(S_u \right)^{0.9}\ t^{0.5} \tag{24}$$

The variation of fatigue notch severity, K_{fmax}, depends on the variation of the nondimensional geometric coefficient (α), specimen plate thickness (t) and material property (S_u). The nondimensional geometric coefficient α is a function of the loading condition and gross, measurable, geometric parameters such as flank angle (θ), leg size (L), or IJP size (c); See Fig.8.

The analytical and numerical relationships between α and the raw geometric parameters in different loading conditions are summarized for several weld joints in Reference [32], and some of the relationship used in

this study are shown in Fig 8. For this study, data of the raw geometrical parameters measured from test specimens and their analytical relationships were used to generate the data of α, and the data set of α was statistically tested. The statistics of ultimate tensile strength estimated in Section 3.1 were used to determine the material effects on the fatigue notch severity. The probability distribution of fatigue notch severity was obtained through random simulation of Eq. 24 using appropriate probability distribution functions for α and S_u. The statistical distribution of the random variable representing the geometry and notch factor (G; reciprocal of worst-case fatigue notch factor) was obtained through Eq. 16.

3.3 Fatigue Variables for Welding Distortion Factor (B)

Fabrication distortions affect weldment fatigue process in two ways: they induce a component of cyclic stress amplitude, and they cause specimen gripping mean stresses. For constant amplitude loading for which the applied stress amplitude and mean stress level are constant, the variation in the induced stress amplitude and gripping mean stress depends solely on the variation in the amount of distortion, represented by B in Eq. 16.

The amount of welding distortion depends on many variables such as the type of welding process, type of pre- and post-weld treatment, welding heat input, welding sequence, geometry of preparation, and, of course workmanship [41]. Since the complex nature of the fabrication distortions does not permit any general analytical relationships among those distortion variables, we should use measurements of distortion or induced stress components from a sample group of production weldments for the estimation of the effect of welding distortion.

Lawrence et. al. [42,28] recognized the large effect of the induced-stress by welding distortions on weldment fatigue behavior, and a parameter, bending factor (x) was defined:

$$x = \frac{\text{Induced Bending Stress Amplitude}}{\text{Total Remote Stress Amplitude}} \tag{25}$$

where the nominal stress amplitude is axial. The bending factor (x) can be obtained through strain gauge measurements during the testing. Accordingly the welding distortion effect can be represented as in Eq. 16:

$$B = \frac{1 - x}{1 + x \left(\frac{K^B_{fmax}}{K^A_{fmax}} - 1 \right)}$$

The statistical regularity of distortion effects (B) can be estimated using the data for the bending factor (x) together with the statistical distribution of K^A_{fmax} and K^B_{fmax}. When for data of bending factor (x) are not available, the data for the angular distortion (d) can be utilized to obtain the bending factor by the relationship between induced bending stress and distortion amount defined by Burk [42] as(see Fig. 9):

For the fixed end condition,

$$S^B = d \left(\frac{3 S^A E}{4} \right)^{.5} \tanh \left[\frac{L_G}{2t} \left(\frac{3 S^A}{E} \right)^{.5} \right] \tag{26}$$

where S^B = Induced Bending Stress Level

S^A = Applied Nominal Axial Stress level

E = Young's Modulus

L_G = Gripping Distance

t = Thickness of Loading Plate

d = Angular Distortion in Radian

3.4 Fatigue Variables for Residual Stress Factor (RS)

Lawrence [43] showed that the notch-root residual stress is a significant part of the mean stress effects on the fatigue strength of as-welded specimens through the set-up cycle analysis. Although the residual stresses may vary along the possible fatigue crack initiation sites, a conservative estimate is that the maximum notch-root residual stress at the fatigue initiation site will be about the same value of the yield stress of the base material (S_y). Therefore the residual stress effects term (RS) in Eq. 16:

$$RS = (1 - \frac{S_y}{\sigma_f'}) \tag{27}$$

The statistical distribution of the yield strength for hot-rolled steel sheets and pipe materials are listed in Table 1. Each data set represents materials from number of different heats for the same material specification. Both data sets gave about 4 ksi (28 Mpa) standard deviation for the yield strength. For the simulations in this study, 4 ksi (28 MPa) was assumed as a typical standard deviation value for the maximum tensile residual stress.

3.5 Fatigue Variables Representing Applied Mean Stress Factor (MS)

The term MS in Eq. 16 represents the applied mean stress effects and depends on R, N_I, and b. For constant amplitude loading, R is a controllable variable; and it can be treated as a deterministic variable. Also, b can be treated as a deterministic variable if we impose a randomness on σ_f', as explained in Section 1. When we also consider N_I as a

deterministic design value in Eq. 16, the applied mean stress effects term (MS) becomes a deterministic variable.

For the variable load history, the R ratio is not controlled, indeed, it is difficult to represent the local mean stress behavior with R ratio which is a remote loading parameter. Therefore, instead of using R in Eq. 16, we propose using a parameter which describes the real notch-root mean stress (σ_m), the fatigue strength:

$$S_a^A = \sigma_f' \frac{1}{K_{fmax}^A} \frac{1 - x}{1+x(X-1)} \left(1 - \frac{\sigma_m}{\sigma_f'}\right) (2N_I)^b \tag{28}$$

$$= \quad P \quad G \quad B \quad LS \quad (2 N_I)^b$$

where $\sigma_m = \sigma_r + \sigma_m^A + \sigma_m^B$

$$= \quad \sigma_r \quad + \quad (K_{fmax}^A \, S_m^A + K_{fmax}^B \, S_m^B)$$

then the term LS = $(1 - \sigma_m/\sigma_f')$ represents the notch-root real mean stress including applied mean stress, induced gripping mean stress and residual stress effects, and the term B represents the bending stress amplitude induced due to fabrication distortion. The statistical distribution of this term can be obtained by knowing the statistical regularity of the variables σ_r, K_{fmax}^A, S_m^A, K_{fmax}^B, S_m^B and σ_f'. Therefore, the statistical regularities of S_m^A and S_m^B should be determined, together with the statistical regularities of K_{fmax}^A, K_{fmax}^B, σ_f' and σ_r shown in the previous sections, to define the statistical regularity of notch-root mean stress effects under variable load histories. Generally, in the laboratory specimens under the axial nominal loading history, S_m^B results from gripping bending stresses, and these stresses are easily measurable using strain gages. S_m^A represents an applied mean stress component.

4. THE MONTE CARLO SIMULATION; PROCEDURES AND RESULTS

Ten fatigue data sets for three kinds of weldments were compared with Monte Carlo computer simulations: 12.7 mm and 6.35 mm plate-thick load-carrying cruciform weldments [44]; 25 and 32 mm plate-thick non-load-carrying cruciform weldments [12,45,46]; 20 mm plate-thick butt weldments [47,48], 6 mm plate-thick butt weldments with three different applied mean stress levels [49], and single-V butt weldments with two different mean stress levels from UIUC Fatigue Data Bank [50]. Of the fatigue data sets, those for load-carrying cruciform weldments were generated by author and the others were from literatures.

Considering the availability of the statistics of fatigue variable data, one can group above eleven simulations into four different types:

Type I: For this type of simulation, the statistics of fatigue variables were estimated based on the fatigue test data set measured from the same specimens used to generate the S-N data. Also the measurements and testing were done by author. The simulations for 12.7 mm and 6.35 mm load-carrying cruciform weldments were of this type.

Type II: For this type of simulation, the statistics of fatigue variables were estimated based on the fatigue test data set measured from the same specimens used to generate the S-N data, but the measurements and testing were done by other investigators. The simulations for 20 mm butt weldments, and 25 and 32 mm non-load carrying cruciform weldments were of this type.

Type III: For this type of simulation, the statistics of fatigue variables were estimated partially based on the fatigue test data

measured from different (but similar) specimens from those used to generate S-N data. The simulations for 6 mm butt weldments were of this type.

Type IV: For this type of simulations, the statistics of fatigue variable were estimated totally based on the data set of fatigue variables from the other sources and best guesses. The simulations for the single-V butt weldments from UIUC Fatigue Data Bank were of this type.

Generally, simulated fatigue strength fitted the lognormal distribution, and the mean fatigue strength (mean of log ΔS) and mean $\pm 2s$ fatigue strength scatter band (mean of log $\Delta S \pm$ two-standard deviation of logΔS) were estimated and compared with the experimental S-N data in a log-log graph.

4.1 Simulation for Load-Carrying Cruciform Weldments: (Type I simulation)

Load-carrying, fillet-welded cruciform Weldments were fabricated and tested using ship block load history [44]: see Appendix B.3. The fatigue variable data such as geometric parameters, material property and induced stresses were measured and their statistics were used in simulation. Details of test procedure and results are given in Appendix B.

Simulation Procedure: The statistics of the fatigue variables used for the simulation of fatigue strength against both IJP and toe failures for 12.7 mm and 6.35 mm plate-thickness specimens are given in Tables 2 and 3, respectively. The statistics were estimated from the fatigue test results

in Tables B-1, B-2 and B-3. Details of statistical analysis of fatigue variables are given in Appendix C.1.

Equation 28 was employed instead of Eq. 16 for the simulation because of the variable load history used. The applied mean stress (S_m^A) was taken as zero, and only the fatigue test data with zero applied mean stress were compared with the simulation.

Simulation Results: The statistics of the simulated fatigue strength for 12.7 mm specimens at 10^6 cycles are given in Table 4. The mean S-N curve and mean $\pm$ $2s_{\log\Delta S}$ S-N scatter band are compared with the S-N fatigue test data in Fig. 10. The S-N fatigue test data in Figs. 10 and 11 reflect the equivalent constant amplitude stress range [44] (ΔS_e = 86.9 MPa) for the total testing cycles to failure (5047 cycles times blocks to failure) of "ship block load history" (see Appendix B.4).

The predicted mean fatigue strength for IJP failure was lower than that for toe failure because the stress concentration was higher. The simulated mean fatigue strength for toe failure agreed reasonably well with the test data, but the simulated mean fatigue strength for IJP failure was conservative. This conservatism may result from the fact that the WFCIM neglects the propagation life.

The predicted total uncertainties in fatigue strength (Ω_S) for toe and the IJP failure were .232 and .177, respectively; see Table 4. The greater uncertainty in fatigue strength for toe failure is due to a large variation of induced bending stress components due to distortion (especially by gripping mean stress) which affects more the fatigue strength of the toe. Therefore, in spite of the large difference between the mean fatigue strength against toe and IJP failures, the mean - $2s_{\log\Delta S}$ S-N curve were

nearly the same because of the larger scatter of fatigue strength for toe failure. Consequently, severe distortion can cause the toe to be a more critical crack initiation site than the IJP despite its higher fatigue notch factor. The IJP-toe failure pattern discussed in Appendix B.4 results from this condition.

The statistics of the simulated fatigue strength for 6.35 mm specimens at 10^6 cycles are given in Table 6. The mean S-N curve and mean $\pm 2s_{\log\Delta S}$ S-N scatter band are compared with the S-N fatigue test data in Fig. 11. The total uncertainty in fatigue strength (Ω_S) at the toe and IJP was predicted to be .205 and .144; see Table 5. Similar to the 12.7 mm specimens, the larger variation in the fatigue strength for toe failure was predicted than that for IJP failure occurred due to the larger uncertainty in induced bending stress components.

4.2 Simulations for Non-Load-Carrying Cruciform Weldments

4.2.1 Fatigue Test Data from Engesvik and Moan: (Type II simulation)

Engesvik and Moan [12,46] tested non-load-carrying fillet welded cruciform weldments under constant amplitude loading (ΔS = 150 MPa, R=0), and performed a Monte Carlo simulation of the fatigue crack propagation life of these weldments based on linear elastic fracture mechanics (Eq.7) and estimates of the statistics of the related fatigue variables: see Section 1.2.2.

Simulation Procedure: The statistics of fatigue variables used in the simulation of fatigue strength is given in Table 6. The distributions of

the toe flank angle (θ) of fillet weldment and bending factor (x) was used as reported [46]. The mechanical properties of the base material reported [46] was used to estimate the average mechanical properties of crack initiation site (assumed as grain-coarsened HAZ at toe). The mean stress ratio (R) was taken as zero (a deterministic value). The notch-root stress was considered to be zero since the testpieces were stress-relieved. The dimensions of the test specimens were taken as deterministic values. More details of the statistical analysis of fatigue variables are given in Appendix C.2.

Simulation Results: The simulation results of the fatigue strength for a life of 10^6 cycles are listed in Table 7. The scatter bands of S-N data predicted by simulation results from our study and that of Engesvik and Moan are shown in Fig. 12. The solid lines in this figure represent the mean S-N curve and the mean $\pm$ $2s_{\log\Delta S}$ S-N scatter band results from our simulation. The dashed lines represent the mean S-N curve and the mean $\pm$ $2s_{\log\Delta S}$ S-N scatter band results from the simulation by Engesvik and Moan.

The predicted total uncertainty of axial fatigue strength at the toe (Ω_S) was .117; see Table 7, and the simulation by Engesvik and Moan [12] gave a similar uncertainty in fatigue strength for a given fatigue life. The scatter of S-N fatigue test data agreed well with both simulation results.

Our simulation showed a larger variation in fatigue life for a given nominal stress range than their simulation, principally because of the different S-N slopes of the two models (-1/n versus b).

4.2.2 Fatigue Test Data from Lassen and Eide: (Type II simulation)

Lassen and Eide [45] also tested non-load-carrying fillet welded cruciform joint with 25 mm thick loading plate under a constant amplitude loading (ΔS = 150 MPa, R=0.08), and studied the effects of fatigue variables upon the uncertainty of fatigue crack propagation life in weldments.

Simulation Procedure: The statistics of the fatigue variables used for the simulation is listed in Table 8. The statistical distributions of the toe flank angle (θ) of fillet weldment and bending factor (x) were used as reported [45]. The mean stress ratio (R) was taken as 0.08 (a deterministic value). The dimensions of test specimens were considered to be deterministic. All other procedures were same as those for the simulation of Engesvik and Moan test data: see Appendix C.3.

Simulation Results: The statistics of simulated fatigue strength for 10^6 cycles are given in Table 9. The mean S-N curve and related mean $\pm 2s_{\log\Delta S}$ S-N scatter band predicted by the simulation are compared with S-N fatigue test data scatter band in Fig. 13. Although the application of this probabilistic model should be restricted to the region over 10^6 cycles, the S-N fatigue test data (which are less than 10^6 cycles) agreed well with the scatter band extended to the 10^5 cycles from the simulation results. The predicted total uncertainty of axial fatigue strength (Ω_S) at the toe was 0.081.

4.3 Simulation for Butt Weldments (Nihei et. al.)

Nihei et. al. performed a large constant amplitude fatigue testing program of SMAW butt steel weldments [47,48,49], and paid careful attention to the statistical aspects of fatigue parameters including toe angle and radius, welding distortion, as well as other geometric parameters.

4.3.1 JIS-SM50B 20 mm Thick Butt Weldments: (Type II simulation)

Simulation Procedure: The statistics of the fatigue variables used for the simulation of the fatigue strength for the 20 mm SM50B butt weldments are given in Table 10. The statistical estimators were based mainly upon the reported test results [47,48]. The statistical distributions of toe flank angle (Θ) and angular distortion (d/2) and bead width (W_B) were reported in [41]. The deterministic values of applied mean stress ratio (R) and specimen width (W) were used as reported [48]. The mechanical properties of the base material reported [48] were used as the mean values to estimate the mean values of mechanical properties of the grain-coarsened HAZ. Details of the statistical analysis of fatigue variables are given in Appendix C.3.

Simulation Results: The statistics of the simulated fatigue strength (S_a^A) for 10^6 cycles are given in Table 11. The mean S-N curve and $\pm 2s_{\log\Delta S}$ S-N scatter band from the Type II simulation are compared with the fatigue test data [48] in Fig. 14.

The predicted total uncertainty in fatigue strength (Ω_S) of the toe was 0.077. The simulation results agree well with the test data beyond lives of 10^6 cycles as can be seen in Fig. 14. The conservative predictions at

shorter lives probably results from the importance of propagation life in this life region.

4.3.2 JIS-SM50A 6 mm Thick Butt Weldments: (Type III simulation)

Simulation Procedure: The statistics of the fatigue variables used in the simulation for the SM50A 6 mm butt weldments are given in Table 12. Basically the same procedures as for the JIS-SM50B 20mm butt weldment were used for the statistical analysis of fatigue variables; however, the statistical data for the angular distortion (d) and toe flank angle (θ) were not available for the 6mm butt welded specimens. The toe flank angle and the distortion are strongly dependent on the welding parameters, especially on the heat input and welding sequence. Therefore, the statistics of the 9 mm butt weldments [47] were used for the simulation since their welding parameters were nearly similar to the 6 mm butt weldments (see Table C14 in Appendix C.5 for a comparison).

Simulation Results: Type III Simulations for three different R ratios (-1.0, -.33 and 0.0) were performed, and the results are given in Table 13. The simulated mean S-N curve and $\pm 2s_{\log\Delta S}$ S-N scatter band are compared with the S-N fatigue test data [49] in Figs 15, 16, and 17.

The total uncertainty in fatigue strength (Ω_S) at the toe with R=-1 was predicted as .067. The simulation results for other two different R ratio (0.0, -.33) had about same values of uncertainty since R was deterministic in each case.

The simulation for R=-1 agreed well with the test data beyond 10^6 cycles as seen in Fig. 14. The simulation for higher stress ratios, R=-.33

and 0.0 (Figs. 16 and 17), gave conservative predictions, indicating that higher mean stresses reduce the portion of crack initiation life, and that the total life in this region is largely fatigue crack propagation.

4.4 Simulation for Single-V Butt Weldments from UIUC Fatigue Data Bank:(Type IV simulation)

Constant amplitude S-N fatigue test data for as-welded (not specified for any special post-weld treatments) mild steel single-V butt weldments from UIUC Fatigue Data Bank [50] was compared with simulated mean fatigue strength and its uncertainty. Since most of the specimens were not specified for its mechanical and chemical specification, the specimens with yield strength between 30 to 48 ksi were considered as mild steel specimens. Also, this study aimed at the fatigue design in the long-life regime, only the data over $5x10^5$ cycles were used in simulation. A total of two hundreds specimens were compared with simulation results (135 specimens with R=0, 65 specimens with R=-1): see Table 14 and Fig. 18.

Simulation Procedure: The statistics of fatigue variables used in the simulation are given in Table 15. Two simulations for two different R ratios (R= 0, -1) were performed using Eq. 16. Of fatigue variables for the simulation, only the material properties (S_u and S_y) of base material for each specimen were known. The statistics of other fatigue variables for these specimens were estimated based on the data from other sources and best guesses. For both simulation R ratio was considered as a deterministic value. Details of the simulation procedure were given in Appendix C.6.

Simulation Results: The Type IV simulation results for both R ratios are given in Table 16. The simulated mean S-N curve and $\pm$ 2 $s_{\log\Delta S}$ S-N scatter band are compared with the S-N fatigue test data in Figs 19 and 20.

The predicted total uncertainty in fatigue strength (Ω_S) was 0.324 for R=0, and .296 for R=-1. The simulation results for both simulation (R=0 and R=-1) agreed well with the test data as can be seen in Figs. 19 and 20.

5. DISCUSSION

5.1 Origins of the Uncertainty in Weldment Fatigue Strength

The Basquin-Morrow equation written in the form of Eq. 16 has the form of a continued product and provides a stochastic model for the uncertainty of fatigue strength. According to Ang's uncertainty analysis based on the first order approximation of mean and variance, the uncertainty as measured by the coefficient of variation (COV) of fatigue strength (Ω_S) is given by [5]:

$$\Omega_S^2 \approx \Omega_f^2 + \Omega_P^2 + \Omega_G^2 + \Omega_B^2 + \Omega_{RS}^2 + \Omega_{MS}^2 \tag{29}$$

where Ω_P :COV of the factor P, a random variable representing the effects of material properties.

Ω_G :COV of the factor G, a random variable representing the effects of geometry and notch.

Ω_B :COV of the factor B, a random variable representing the effects of self-induced stress components by welding distortion.

Ω_{RS} :COV of the factor RS, a random variable representing the effects of notch-root residual stress.

Ω_{MS} :COV of the factor MS, a random variable representing the effects of applied mean stress.

Ω_f :Uncertainty due to the prediction error of WFCIM.

The magnitude of Ω_P results from the uncertainty in the fatigue behavior of a notch-root material properties (σ_f' and b). Because of the

difficulty in obtaining the material properties for the weld HAZ, we used the variation of ultimate tensile strength to estimate the variation in fatigue property at the crack initiation sites. The uncertainty of the material property factor (P) resulting from simulations includes not only the variation in material properties (σ_f') mentioned above, but also the uncertainty implicit in the stochastic nature of the relationship between σ_f' and S_u (Eq.17).

The magnitude of Ω_f describes the error in the WFCIM due to its assumption of pure elastic behavior. For this study, the Ω_f was taken as zero for the long-life regime where purely elastic notch-root behavior can be assumed.

The uncertainty of each "factor" (P, G, B, RS or LS) was estimated by the simulation for the weldments considered in this study. Equation 29 permits one to assess the contribution of each factor to the total uncertainty in fatigue strength. By knowing the relative importance of uncertainty in each factor, we can decide the merit of any fatigue strength improvement strategy: reducing the variation in weld geometry or fabrication distortion, for example.

Load-Carrying Cruciform Weldments: The uncertainties in each factor (P, G, B and LS) for the two different crack initiation sites (IJP and toe) of the 12.7 mm specimens are listed in Table 17.

For both IJP and toe failures, the uncertainty in local mean stress factor (Ω_{LS}) was a major contributor to the total uncertainty in fatigue strength. The main source of the uncertainty of the local mean stress factor was the gripping mean stress (S_m^B) induced by distortion. The larger uncertainty in local mean stress effects (Ω_{LS}) for the toe failure than for

IJP failure indicates the larger effects of gripping mean stress at the toe, which is a bending stress component and has maximum value at the surface (toe). The IJP failure had less uncertainty in geometry and notch effects (Ω_G) than the toe failure, and it indicated that the IJP size, whose variation affects more on the fatigue notch factor of IJP, had less variation than the leg sizes of the weld whose variation affects more the fatigue notch factor of toe than IJP. For the toe failure, the uncertainty in distortion factor (only due to the induced stress amplitude) (Ω_B) was significant due to the nature of induced bending stress components. The uncertainty in material effects (Ω_P) was almost same for the toe and the IJP failures and was not so significant.

The total uncertainty in fatigue strength was factorized into the uncertainties in each factors (P, G, B, and LS) using Eq. 29. The square of uncertainty value (Ω^2) in each factor was compared in Fig. 21 to show the relative significance of the uncertainties in each factor upon the total uncertainty of fatigue strength. The percentages of the square of total uncertainty in fatigue strength for toe failure due to each factor were ranked as follows; Ω^2_{LS} = 80%, Ω^2_G = 11%, Ω^2_B = 7% and Ω^2_P = 2%. Similarly, the percentages of the square of total uncertainty in fatigue strength for IJP failure were ranked as; Ω^2_{LS} = 87%, Ω^2_G = 6%, Ω^2_B = 4% and Ω^2_P = 3% (Fig. 21).

The uncertainties in each factor of the 6.35 mm specimens are listed in Table 18. Similar results were observed upon factorizing the total uncertainty into the uncertainties of each factors; see Fig. 21.

Non-Load-Carrying Cruciform Weldments (Engesvik and Moan): The uncertainties in each factors (P, G, B and RS) are given in Table 19.

The uncertainties in both the distortion factor (Ω_B) and the geometry and notch factor (Ω_G) were the main source of the total uncertainty in fatigue strength. The uncertainty in applied mean stress factor (Ω_{MS}) was zero since the MS term was considered to be a deterministic variable. The uncertainty in notch-root residual stress factor (Ω_{RS}) was also considered zero since the specimens were all stress-relieved.

In our simulation, the distortion factor (B) was the biggest contributor to the uncertainty in fatigue behavior; whereas, Engesvik and Moan did not consider the distortion factor. Their simulation results [12] showed that the toe radius (r) has the biggest influence on the uncertainty of fatigue behavior; whereas, we did not consider the toe radius to be a variable (we consider the worst-case radius which is determined by variation of S_u). Both simulation results showed the importance of variation in toe flank angle (θ) on the total uncertainty.

The square of uncertainty value (Ω^2) in each factor was compared in Fig. 22 to show the relative significance of the uncertainties in each factors upon the total uncertainty of fatigue strength. The percentages of the square of total uncertainty due to each factor were ranked as follows; $\Omega_B^2 = 55\%$, $\Omega_G^2 = 34\%$ and $\Omega_P^2 = 11\%$

Non-Load-Carrying Cruciform Weldments (Lassen and Eide): The uncertainty of each factor (P, G and B) is given in Table 20.

The uncertainty in the geometry and notch factor (Ω_G) was the main source of the total uncertainty in fatigue strength; whereas, the distortion factor (Ω_B) was not significant. The uncertainties in applied mean stress factor (Ω_{MS}) and notch-root residual stress factor (Ω_{RS}) were also

considered zero same as the case in the simulation of fatigue data from Engesvik and Moan.

The square of uncertainty value (Ω^2) in each factor was compared in Fig. 22 to show the relative significance of the uncertainties in each factors upon the total uncertainty of fatigue strength. The percentages of the square of total uncertainty due to each factor were ranked as follows; Ω_G^2 = 79%, Ω_P^2 = 13% and Ω_B^2 = 8%.

SM50B 20 mm Thick Butt Weldments (Nihei et. al.): The uncertainty values in each factors (P, G, B MS and RS) are given in Table 23.

The uncertainties in the geometry and notch factor (Ω_G) and the distortion factor (Ω_B) were smaller than other simulations, resulting less total uncertainty of fatigue strength. There was no dominant source of uncertainty of these weldments. The uncertainty in applied mean stress factor (Ω_{MS}) was zero since we considered the MS term to be a deterministic variable.

The square of uncertainty value (Ω^2) in each factor was compared in Fig. 22, the percentages of the square of total uncertainty due to each factor were ranked as follows; Ω_{RS}^2 = 35%, Ω_G^2 = 27%, Ω_B^2 =20% and Ω_P^2 = 18%.

SM50A 6 mm Thick Butt Weldments (Nihei et. al.): The uncertainties in each factors (P, G, B, MS and RS) from the simulation with R=0 are given in Table 21.

As with the 20 mm butt weldments, there was no dominant source of the uncertainty in the fatigue strength. The uncertainty of applied mean stress was zero since we considered the MS term to be a deterministic variable.

Similar results for were obtained for the simulation with different R ratios.

The square of uncertainty value (Ω^2) in each factor was compared in Fig. 22 to show the relative significance of the uncertainties in each factors upon the total uncertainty of fatigue strength with R=0. The percentages of the square of total uncertainty due to each factor were ranked as follows; Ω^2_{RS} = 38% Ω^2_P = 22%, Ω^2_B = 22% and Ω^2_G = 18%.

Single-V Butt Welds from UIUC Fatigue Data Bank: The uncertainties in each factors (P, G, B, MS and RS) from the simulation with R=0 are given in Table 22.

The uncertainty in distortion factor (Ω_B) was a main source of the uncertainty in the fatigue strength, and the uncertainty in geometry and notch factor (Ω_G) was significant. The uncertainty of applied mean stress was zero since we considered the MS term to be a deterministic variable.

The square of uncertainty value (Ω^2) in each factor was compared in Fig. 23 to show the relative significance of the uncertainties in each factors upon the total uncertainty of fatigue strength. The percentages of the square of total uncertainty due to each factor were ranked as; Ω^2_B = 84%, Ω^2_G = 10%, Ω^2_P = 4% and Ω^2_{RS} = 2%.

Summary: Of three different kinds of weldments with the Type I and II simulations, the load-carrying cruciform weldments had the largest uncertainty due to the induced bending stress components. The fabrication process of these weldments were most prone to welding distortion or misalignment because of the separate pieces of loading plates welded in horizontal position; whereas, the non-load-carrying cruciform weldments are

fabricated from a one-piece loading plate. The butt weldments were fabricated from two pieces but welded in the flat position.

The importance of the uncertainty due to induced bending stress indicates that controlling this source of uncertainty during design and fabrication could reduce the total uncertainty in fatigue strength and hence permit higher design stresses.

The uncertainty in geometry and notch factor (G) for toe of the load-carrying cruciform weldments was similar to that of the non-load-carrying cruciform weldments; whereas, the uncertainty of geometry and notch factor for the butt weldments (Type II simulation) was smaller.

Generally, the main sources of the total uncertainty were the variation in the induced bending stress components due to fabrication distortions represented by the factors B or LS, and the geometric variation represented by the G factor. The uncertainties of the material property (P) and the residual stress (RS) (assumed as the uncertainty of base metal yield strength) were relatively smaller than others except for Type IV simulation, since those weldments were fabricated from steels having the same material specification, and the uncertainty in the material properties estimated for those were almost a minimum value.

5.2 The Use of the WFCIM as a Probability-Based Fatigue Design Method

The fatigue design strength, $(S_a^A)_D$, for a certain probability of failure can be estimated from the simulation results; the mean and total uncertainty values of the fatigue strength.

Assuming that the fatigue strength varies with lognormal distribution (accordingly, log S_a^A has a normal distribution), and the estimated mean (m_S)

and variance (s_S^2) of fatigue strength equal to the population mean (Ω_S) and variance (σ_S^2) of fatigue strength, we can determine the fatigue strength with a certain probability of failure (P_F) using standard normal probability function (Φ);

$$P_F = p(S_a^A < (S_a^A)_D) = p(\log S_a^A < \log (S_a^A)_D)$$
$$= p(Y < \log (S_a^A)_D) \qquad (30)$$
$$= p\left(\frac{Y - \mu_Y}{\sigma_Y} < \frac{\log (S_a^A)_D - \mu_Y}{\sigma_Y}\right)$$

$$P_F = \Phi\left[\frac{\log (S_a^A)_D - \mu_Y}{\sigma_Y}\right] \qquad (31)$$

where $Y = \log S_a^A$, $\Omega_S = s_S/m_S$

$\mu_Y = \log m_S - .5 \log(1 + \Omega_S^2)$

$\sigma_Y^2 = .434 \log(1 + \Omega_S^2)$

Then the fatigue design strength can be obtained:

$$\log (S_a^A)_D = \Phi^{-1}(P_F)\ \sigma_Y + \mu_Y$$

or,

$$(S_a^A)_D = 10^{(\Phi^{-1}(P_F)\ \sigma_Y + \mu_Y)} \qquad (32)$$

In this study, the (mean - $2\sigma_Y$) fatigue strength ($\Phi^{-1}(P_F) = -2$) was taken as the fatigue design strength $(S_a^A)_D$ using Eq. 33, and it represents 97.7 % of probability of survival, or 2.3 % of probability of failure.

The simulation results in Chapter 4 were used to estimate the (mean-$2\sigma_Y$) fatigue design strength for respective weldments, and resulting fatigue design strength were compared with (mean - $2\sigma_Y$) design values from The Welding Institute (TWI) [51]. For a direct comparison in the log-log S-N

curve, the fatigue design strength, $(S_a^A)_D$, was converted into the fatigue design stress range, ΔS_D ($\Delta S_D = 2\ (S_a^A)_D$).

Load-Carrying Cruciform Weldments: The simulated distribution of fatigue strength (S_a^A) 12.7 mm and 6.35 mm load-carrying cruciform weldments in Table 9 and 10 were used to determine the fatigue design strength using Eqs. 31 and 32. Since both of the possible crack initiation sites (IJP and toe) were involved in the final failure of the specimens, the smaller of the two fatigue design strengths (that were for IJP failure or for toe failure) was taken as the fatigue design strength of the weldments. The fatigue strength for IJP failure for 12.7 mm weldments, and that for toe failure for 6.35mm weldments was taken as the fatigue design strength for respective weldments. Both predicted fatigue design strength gave "safe" design values, that is, none of the fatigue test data appeared below the design curves, in Figs. 10 and 11.

The fatigue design strength of 12.7 mm and 6.35 mm were compared with the Class W (mean - $2\sigma_Y$) design strength from TWI design criteria in 24. The three design curves showed almost same design values. The simulated design curve for 12.7 mm specimens intersects with the TWI curve around 3.5×10^6 cycles, and the predicted design curve for 6.35 mm specimens intersects around 5×10^5 cycles. Although the simulated design value had avoided systematic error by considering fatigue variables which were not considered in the TWI design criteria, the large uncertainty assuming mainly from the gripping mean stress caused quite conservative design value for this group of specimens.

The conservatism of the TWI design curve beyond 10^7 cycles was a result

of extrapolating intermediate weldment component S-N data into the long life region.

Non-Load-Carrying Cruciform Weldments: The simulated distribution of fatigue strength (S_a^A) for 32 mm and 25 mm non-load-carrying cruciform weldments in Tables 7 and 9 were used to determine the fatigue design strength using Eqs. 31 and 32. The predicted fatigue design strength for both weldments showed "safe" design values, comparing with fatigue test data in Figs. 12 and 13.

The simulated (mean - $2\sigma_Y$) design curves were compared with the Class F2 (mean - $2\sigma_Y$) design curve from TWI design criteria in Fig. 25. The design curves intersect around 2 to 5 x 10^5 cycles. The conservatism of TWI design curve in the long life region might result from the systematic errors which were reduced for the simulated design curves. The use of extended S-N curve caused a conservatism of the TWI design curve in the long life regime.

Butt Weldments: The simulated distribution of fatigue strength (S_a^A) of 20 mm (Table 11), and 6 mm with three different R ratios (Table 13) and single-V butt weldments with two different R ratios (Table 15) were used to determine the fatigue design strength using Eqs. 31 and 32 The resulting (mean - $2\sigma_Y$) design curves were compared with TWI Class D (mean - $2\sigma_Y$) design curve in Fig. 26.

As expected, the simulated design curves for the single-V butt weldments from UIUC fatigue data bank showed similar design values with the TWI design Curve. The other simulated design curves had higher design values since the systematic errors were reduced for respective group of

weldments by considering the specimen size and mean stress during the simulation.

Since all the simulated design curves showed "safe" values in comparison with the fatigue test data, one can easily see the unnecessary conservatism of the design curves based on the S-N data gathered without consideration of the systematic variation of important fatigue variables (TWI design curve, single V-Butt weldments from UIUC fatigue data bank).

Summary: The predicted fatigue design strength showed "safe" design values for all the simulated weldments.

The simulations for non-load-carrying weldments and the butt weldments for which the Type II and Type III simulations were performed, permit apparently higher fatigue design strength than the TWI design Curves because of consideration of systematic variations of the important fatigue variables (thickness, mean stress, material property).

The fatigue design strength predicted by the Type IV simulation using the conservative assumptions forced by the variety of weldments included in the fatigue data bank S-N test data showed similar design values to the comparable TWI design curve.

The use of extrapolated S-N relationship based on the S-N component test data in the intermediate range for the long-life region in TWI design criteria could be another reason of conservatism in the long life region.

To estimate a probability-based fatigue design strength, the Monte Carlo simulation method described is a potential substitute for the time consuming and costly S-N component testing procedure. The information required by the simulation method are easy and inexpensive to collect.

5.3 Improvement of Weldment Fatigue Design Strength through Reductions in Uncertainty

For the same mean fatigue strength, a larger uncertainty will force a lower fatigue design strength. Munse suggested the reliability factor (R_F) to represent the effect of uncertainty of fatigue strength (scatter of S-N data) upon the reduction of fatigue design strength [9]: see Fig. 27,

$$R_F = \Delta S_D \; / \; \Delta S \tag{33}$$

where ΔS_D is a constant amplitude fatigue design stress range for a desired reliability, and S is the stress range (actually, the median stress range for lognormal distribution of ΔS) for a given design life from a mean S-N relationship.

The effects of the uncertainty of each fatigue variables upon reliability factor (R_F) were studied to show the uncertainty effects on the fatigue design strength. The mean and uncertainty of fatigue strength can be obtained from the simulation; and thus, the reliability factor can be obtained using Eqs. 33 and 34. The simulation results for 12.7 mm load-carrying cruciform weldments for toe failure and 32 mm non-load-carrying weldments were used for this study since they showed a relatively larger uncertainty.

12.7 mm Load-Carrying Cruciform Weldments with Toe Failure: The variation of R_F for the variation of the uncertainty in each fatigue variables were shown in Fig. 27. The horizontal line indicates the initial reliability factor of this group of specimens, and it was 0.63. Each curve shows the effect of changing the uncertainty of one fatigue variables upon the

reliability factor. The uncertainty value for each fatigue variable was varied from zero to 1.5 times of the current uncertainty amount, but for the fatigue variables which had higher initial values, the curve stopped at the uncertainty value of 1.2.

Since the gripping mean stress was the main source of the total uncertainty of fatigue strength, reducing the uncertainty in the gripping mean stress could increase the reliability factor as much as 24%. The initial uncertainties of the other fatigue variables were not so significant, but one can see the possible rapid reduction of reliability factor by increasing the uncertainty of those variables, especially the material properties and the fatigue notch factor.

32 mm Non-Load-Carrying Cruciform Weldments: The horizontal broken line in Fig. 28 indicated the reliability factor of this group of specimens, and it was 0.79. As with the previous example, the distortion factor was the dominant source of the total uncertainty in fatigue strength, and reducing the uncertainty in the bending factor (x) could increase the reliability factor as much as 10%. The reliability factor could be increased as much as 3% by reducing the uncertainty in geometry. The uncertainties of the material property (σ_f') was not so significant but one can see possible rapid decrease of fatigue design strength by increasing the uncertainty in material properties, by use of unsorted or unspecified material, for example.

Summary: The experience with the above two weldments indicates that the fatigue design strength could be most effectively improved by removing or reducing the dominant source of uncertainty. Also it indicates that an

effort to uniformly reduce the initially insignificant sources of uncertainty will not be so effective in improving the fatigue design strength. However, an increase of an initially insignificant source of uncertainty could cause a rapid further reduction in the fatigue design strength.

By knowing the source and influence of the uncertainty of each fatigue variable on the fatigue design strength, designers can decide the economic merits of a improvement techniques.

6. CONCLUSION AND SUMMARY

(1) A Monte Carlo simulation of the fatigue strength based on the Basquin-Morrow equation and based on the observed statistical regularity of the fatigue variables estimated from laboratory data was used to predict both the mean and the uncertainty of weldment fatigue strength.

(2) The predicted uncertainty agreed well with the scatter of component fatigue test data at long lives ($>10^6$ cycles). The predicted mean strength was generally lower than the experimental results probably as a result of the conservative assumptions adopted for the simulations: the neglect of effects of fatigue crack propagation as well as the pure elastic notch-root behavior and maximum tensile residual stress at the notch-root.

(3) The main origin of the uncertainty in this study was the uncertainty resulting from the bending stresses induced by welding distortion, and the uncertainty resulting from variations in geometry.

(4) The comparison of the predicted fatigue design strength with a design criteria from The Welding Institute showed that a Monte Carlo simulation of fatigue strength based on measured data of the fatigue variables can substitute for or at least augment fatigue data banks and serve as a basis of a component design in the long life regime.

(5) The suggested probabilistic design method would permit designers to decide the economic merits of reducing the variation in a particular fatigue variable such as fabrication distortion, weld geometry or material properties, by identifying the origin and magnitude of the uncertainty resulting from each.

7. FURTHER SUGGESTED STUDY

The accuracy of the simulation results largely depend upon the accuracy of estimation of statistical regularity of fatigue variables which is depend upon the size of data. A systematic study of variation in fatigue variables to build up the data base is therefore suggested.

A study of the stochastic or analytical relationship between the uncertainties of fatigue variables and fabrication conditions (welding process, welding parameter, fabrication environment and workmanship) would be helpful to make this model more useful in design situations.

To extend this model to the region less than 10^6 cycles, combining WFCIM with a propagation model is desirable. The comparison in this study with the simulation results of Engesvik and Moan showed quite promising, and suggests that combining both models could lead to a hybrid Initiation-Propagation model which would predict the fatigue strength and its scatter in the intermediate as well as the long life region.

The Monte Carlo simulation method should be extended to the variable load history design of weldments in conjunction with the Munse Fatigue Design Procedure (MFDP). Since the MFDP uses the linear damage rule, a study of the uncertainty caused by the linear damage rule and its verification through systematic testing program is necessary.

Table 1

Typical Statistics of Material Property for Steel Specimens From Number of Different Heats but with Same Specification

	High-Form Hot-Rolled Sheet [38]		Hot-Rolled Line Pipe Material [39]	
No. of Heats	10		44	
No. of Specimens	24		44	
	S_u	S_y	S_u	Sy
Standard Deviation	24 MPa (3.4 ksi)	27 MPa (3.9 ksi)	29 MPa (4.2 ksi)	28 MPa (4.0 ksi)
Coefficient of Variation	5 %	7 %	5.5 %	5%

Table 2

Statistical Estimators of Fatigue Variables Used in Simulation of Fatigue Strength for 12.7 mm Load-Carrying Cruciform Weldments

Fatigue Variables	IJP			TOE		
	m*1	s*2	p(x)*3	m	s	p(x)
Fatigue Strength Coefficient (σ_f',MPa)	1051.	34	Normal	1032.	34	Normal
Fatigue Strength Exponent (b)	-.08835	-	D*4	-.08912	-	D
Ultimate Tensile Strength (S_u, MPa)	713	29	Normal	692	29	Normal
Axial Fatigue Notch Factor (K_{fmax}^A)	4.829	.219	Normal	3.363	.277	Normal
Bending Fatigue Notch Factor (K_{fmax}^B)	1.407	.196	Normal	1.898	.041	Normal
Bending Factor (x)	.114	.0899	Normal	.114	.0899	Normal
Gripping Mean Stress (S_m^B,MPa)	75.7	65.4	Lognormal	75.7	65.4	Lognormal
Applied Mean Stress (S_m^A,MPa)	0.0	-	D	0.0	-	D
Residual Stress (σ_r,MPa)	310.	28	Normal	310.	28	Normal

*1: Estimated Mean
*2: Estimated Standard Deviation
*3: Probability Distribution Function Used in Simulation
*4: Deterministic Variable

Table 3

Statistical Estimators of Fatigue Variables Used in Simulation of Fatigue Strength for 6.35 mm Load-Carrying Cruciform Weldments

Fatigue Variables	IJP			TOE		
	m*1	s*2	p(x)*3	m	s	p(x)
Fatigue Strength Coefficient (σ_f',MPa)	1166.	34	Normal	1035.	34	Normal
Fatigue Strength Exponent (b)	-.08427	-	D*4	-.08902	-	D
Ultimate Tensile Strength (S_u, MPa)	832	29	Normal	695	29	Normal
Axial Fatigue Notch Factor (K_{fmax}^A)	4.296	.218	Normal	2.829	.296	Normal
Bending Fatigue Notch Factor (K_{fmax}^B)	1.420	.254	Normal	1.639	.032	Normal
Bending Factor (x)	.133	.0895	Normal	.133	.0895	Normal
Gripping Mean Stress (S_m^B,MPa)	84.4	48.2	Lognormal	84.4	48.2	Lognormal
Applied Mean Stress (S_m^A,MPa)	0.0	-	D	0.0	-	D
Residual Stress (σ_r,MPa)	331	28	Normal	331	28	Normal

*1: Estimated Mean
*2: Estimated Standard Deviation
*3: Probability Distribution Function Used in Simulation
*4: Deterministic Variable

Table 4

Statistics of Simulated Fatigue Strength for 12.7 mm Thick Load-Carrying Cruciform weldments at 10^6 Cycles of Fatigue Life

	AXIAL FATIGUE STRENGTH FOR IJP S_a^A (MPa)	AXIAL FATIGUE STRENGTH FOR TOE S_a^A (MPa)
Size of Simulation	1000	1000
Min.	0.86	0.52
Max.	53.2	79.0
m*1	35.1	44.3
s*2	6.2	10.3
COV*3	.177	.232

*1: Estimated Mean
*2: Estimated Standard Deviation
*3: Coefficient of Variation

Table 5

Statistics of Simulated Fatigue Strength for 6.35 mm Thick Load-Carrying Cruciform weldments at 10^6 Cycles of Fatigue Life

	AXIAL FATIGUE STRENGTH FOR IJP S_a^A (MPa)	AXIAL FATIGUE STRENGTH FOR TOE S_a^A (MPa)
Size of Simulation	1000	1000
Min.	5.0	.12
Max.	65.1	96.8
m*1	46.5	50.7
s*2	6.68	10.4
COV*3	.144	.205

*1: Estimated Mean
*2: Estimated Standard Deviation
*3: Coefficient of Variation

Table 6

Statistical Estimators of fatigue variables used in Simulation of Fatigue Strength of 32 mm Thick Non-Load-Carrying Cruciform Joint of Marine Structural Steel

Fatigue Variables	m*1	s*2	p(x)*3
Ultimate Tensile Strength (S_u, MPa)	630	29	Normal
Fatigue strength Coefficient (σ_f',MPa)	999	34	Normal
Fatigue Strength Exponent (b)	-.09182	-	D*4
Toe Flank Angle (θ, Degree)	30.	9.0	Lognormal
Applied Mean Stress Ratio (R)	0.0	-	D
Bending Factor (x)	.0894	.1060	Lognormal
Residual Stress (σ_r,MPa)	0.0*5	-	D

*1: Estimated Mean
*2: Estimated Standard Deviation
*3: Probability Distribution Function Used in Simulation
*4: Deterministic Variable
*5: Stress Relieved Specimens

Table 7

Statistics of Simulated Fatigue Strength for 32 mm Non-Load-Carrying Cruciform Weldments for 10^6 Cycles of Fatigue Life

	S_a^A, MPa
Size of Simulation	1000
Min.	5.15
Max.	87.5
m*1	68.3
s*2	8.00
COV*3	.117

*1: Estimated Mean
*2: Estimated Standard Deviation
*3: Coefficient of Variation

Table 8

Statistical Estimators of Fatigue Variables Used in Simulation of Fatigue Strength of 25 mm Thick Non-Load-Carrying Cruciform Weldments

FATIGUE VARIABLES	m*1	s*2	p(x)*3
Ultimate Tensile Strength	765	29	Normal
Fatigue strength Coefficient (σ_f',MPa)	1127.	34	Normal
Fatigue Strength Exponent (b)	-.08639	-	D*4
Toe Flank Angle (Θ, Degree)	58	9	Lognormal
Applied Mean Stress Ratio (R)	0.08	-	D
Bending Factor (x)	.0415	.0305	Lognormal
Residual Stress (σ_r,MPa)	0.0*5	-	D

*1: Estimated Mean
*2: Estimated Standard Deviation
*3: Probability Distribution Function Used in Simulation
*4: Deterministic Variable
*5: Stress Relieved Specimens

Table 9

Statistics of Simulation Results of Fatigue Strength
for 25 mm Non-Load-Carrying Cruciform Weldments
for 10^6 Cycles of Fatigue Life

	S_a^A, MPa
Size of Simulation	1000
Min.	33.4
Max.	82.2
m*1	66.2
s*2	5.35
COV*3	.081

*1: Estimated Mean
*2: Estimated Standard Deviation
*3: Coefficient of Variation

Table 10

Statistical Estimators of Fatigue Variable used in Simulating Fatigue Strength of 20 mm JIS SM50B Butt Welded Joint

Fatigue Variables	m*1	s*2	p(x)*3
Ultimate Tensile Strength (DPH)	801	29	Normal
Fatigue Strength Coefficient (σ_f',MPa)	1161	34	Normal
Fatigue strength Exponent (b)	-.08520	-	D*4
Toe Flank Angle (θ, degree)	41.1	5.7	Lognormal
Angular Distortion (d/2, Radian)	.00921	.00583	Normal
Bead Width (W_B, mm)	18.28	1.56	Normal
Specimen Width (W_S, mm)	25.0	-	D
Applied Mean Stress Ratio (R)	0.0	-	D
Maximum Tensile Residual Stress (σ_r,MPa)	397	28	Normal

*1: Estimated Mean
*2: Estimated Standard Deviation
*3: Probability Distribution Function Used in Simulation
*4: Deterministic Variable

Table 11

Statistics of Simulation Results of Fatigue Strength for 20 mm Butt Welded Joint at 10^6 Cycles

	S_a^A, MPa
Size of Simulation	1000
Min.	50.2
Max.	81.5
m*1	64.2
s*2	4.93
COV*3	.077

*1: Estimated Mean
*2: Estimated Standard Deviation
*3: Coefficient of Variation

Table 12

Statistical Estimators of Fatigue Variables Used in Simulation of Fatigue Strength of 6 mm JIS SM50A Butt Welded Joint

Fatigue Variables	m*1	s*2	p(x)*3
Ultimate Tensile Strength (S_u, MPa)	837	29	Normal
Fatigue Strength Coefficient (σ_f',MPa)	1195.	34	Normal
Fatigue Strength Exponent (b)	-.08409	-	D*4
Toe Flank Angle (θ, Degree)	34.5	5.2	Lognormal
Angular Distortion (d/2, Radian)	.00368	.00184	Normal
Specimens Width (W, mm)	25	-	D
BEAD WIDTH (W_B, mm)	6	-	D
Applied Mean Stress Ratio (R)	-1.0 -.33 0.0	- - -	D
Maximum Tensile Residual Stress (σ_r,MPa)	357.	28	Normal

*1: Estimated Mean
*2: Estimated Standard Deviation
*3: Probability Distribution Function Used in Simulation
*4: Deterministic Variable

Table 13

Statistics of Simulation Results of Axial Fatigue Strength for 6 mm Butt Welded Joint at 10^6 Cycles

	R = -1.0	R = -.33	R = 0.0
	S_a^A, MPa	S_a^A, MPa	S_a^A, MPa
Size of Simulation	1000	1000	1000
Min.	103.6	90.2	80.0
Max.	156.9	136.6	121.1
m*1	127.6	111.1	98.5
s*2	8.55	7.45	6.6
COV*3	.0670	.0670	.0670

*1: Estimated Mean
*2: Estimated Standard Deviation
*3: Coefficient of Variation

Table 14

Distribution of Material Properties for the Mild Steel (S_y=30 to 48 ksi) As-Welded*1 Single-V Butt Weldments form UIUC Fatigue Data Bank

	S_y, ksi	S_u, ksi	No. of Specimens
Specimens	30	42	21
Tested	32	58	8
with R=-1	35	61	2
	36	66	3
	38	61	3
	38	61	3
	39	71	7
	45	64	2
	48	86	3
Specimens	31	54	9
Tested	38	72	4
with R=0	33	63	35
	35	61	3
	32	58	5
	39	65	25
	34	48	2
	37	62	48
	36	66	5
	42	67	4
	38	65	4
			Total 200 Specimens
Mean	36.2(250 MPa)	61.2(422 MPa)	
Standard Deviation	4.1(28 MPa)	7.8(54 MPa)	
Coefficient of Variation	11.3 %	12.7 %	

*1: Not specified for any special post-weld treatment

Table 15

Statistical Estimators of Fatigue Variable used in Simulating Fatigue Strength of Mild Steel (S_y = 30-48 ksi) Single-V Butt Weldments from UIUC Fatigue Data Bank

Fatigue Variables	m*1	s*2	p(x)*3
Ultimate Tensile Strength (S_u, MPa)	633	54	Normal
Fatigue Strength Coefficient (σ_f',MPa)	1001	64	Normal
Fatigue strength Exponent (b)	-.09168	-	D*4
Toe Flank Angle (θ, degree)	32.2	10.5	Lognormal
Thickness (t, mm)	13	-	Uniform (6 to 20 mm)
Angular Distortion (d/2, Radian)	.00461	.00394	Normal
Applied Mean Stress Ratio (R)	0.0 -1.0	-	D
Maximum Tensile Residual Stress (σ_r,MPa)	250	28	Normal

*1: Estimated Mean
*2: Estimated Standard Deviation
*3: Probability Distribution Function Used in Simulation
*4: Deterministic Variable

Table 16

Statistics of Simulation Results of Fatigue Strength of Mild Steel (S_y = 30-48 ksi) Single-V Butt Weldments from UIUC Fatigue Data Bank

	R = -1	R = 0
	S_a^A, MPa	S_a^A, MPa
Size of Simulation	1000	1000
Min.	31.1	22.0
Max.	176.4	145.4
m*1	80.7	62.1
s*2	23.9	20.1
COV*3	.296	.324

*1: Estimated Mean
*2: Estimated Standard Deviation
*3: Coefficient of Variation

Table 17

Factorization of Uncertainty in the Fatigue Strength of 12.7 mm Load-Carrying Cruciform Weldments into the Uncertainties of Physical Factors

Physical Factor	IJP			Toe		
	COV (Ω_i)	Ω_i^2	$\Omega_i^2/\sum \Omega_i^2$	COV (Ω_i)	Ω_i^2	$\Omega_i^2/\sum \Omega_i^2$
Material Factor (P)	.0303	.000918	3 %	.0308	.000946	2 %
Geometry and Notch Factor (G)	.0435	.00189	6 %	.0801	.00641	11%
Induced Stress Amplitude Factor (B)	.0341	.00116	4 %	.0622	.00387	7 %
Local Mean Stress Factor (LS)	.1615	.02607	87%	.2123	.04507	80%

Table 18

Factorization of Uncertainty in the Fatigue Strength of 6.35 mm Load-Carrying Cruciform Weldments into the Uncertainties of Physical Factors

Physical Factor	IJP			Toe		
	COV (Ω_i)	Ω_i^2	$\Omega_i^2/\sum \Omega_i^2$	COV (Ω_i)	Ω_i^2	$\Omega_i^2/\sum \Omega_i^2$
Material Factor (P)	.0273	.000746	4 %	.0308	.000947	2 %
Geometry and Notch Factor (G)	.0488	.00238	12%	.1033	.010677	26%
Induced Stress Amplitude Factor (B)	.0402	.00162	8 %	.0658	.004328	11%
Local Mean Stress Factor (LS)	.1214	.01474	76%	.1579	.024916	61%

Table 19

Factorization of Uncertainty in the Fatigue Strength of 32 and 25 mm Non-Load-Carrying Cruciform Weldments into the Uncertainties of Physical Factors

Physical Factor	32 mm			25 mm		
	COV (Ω_i)	Ω_i^2	$\Omega_i^2/\sum \Omega_i^2$	COV (Ω_i)	Ω_i^2	$\Omega_i^2/\sum \Omega_i^2$
Material Factor (P)	.03429	.00120	11 %	.02972	.000883	13%
Geometry and Notch Factor (G)	.06240	.00389	34%	.07259	.00527	79%
Distortion Factor (B)	.07906	.00625	55%	.02283	.000521	8 %
Residual Stress Factor (RS)	.0	.0	0 %	.0	.0	0 %

Table 20

Factorization of Uncertainty in the Fatigue Strength of 6 and 20 mm Butt Weldments (R=0) into the Uncertainties of Physical Factors

Physical Factor	6 mm			20 mm		
	COV (Ω_i)	Ω_i^2	$\Omega_i^2/\sum \Omega_i^2$	COV (Ω_i)	Ω_i^2	$\Omega_i^2/\sum \Omega_i^2$
Material Factor (P)	.0285	.000814	22%	.0294	.000862	18%
Geometry and Notch Factor (G)	.0257	.000661	18%	.0358	.00128	27%
Distortion Factor (B)	.0285	.000811	22 %	.0307	.000941	20%
Residual Stress Factor (RS)	.0369	.001364	38%	.1579	.024916	35%

Table 21

Factorization of Uncertainty in the Fatigue Strength of Mild Steel Single-V Butt Weldments (R=0) into the Uncertainties of Physical Factors

Physical Factor	COV (Ω_i)	Ω_i^2	$\Omega_i^2/\sum \Omega_i^2$
Material Factor (P)	.0637	.00406	4 %
Geometry and Notch Factor (G)	.0988	.00975	10%
Distortion Factor (B)	.2848	.08111	84%
Residual Stress Factor (RS)	.0424	.00179	2 %

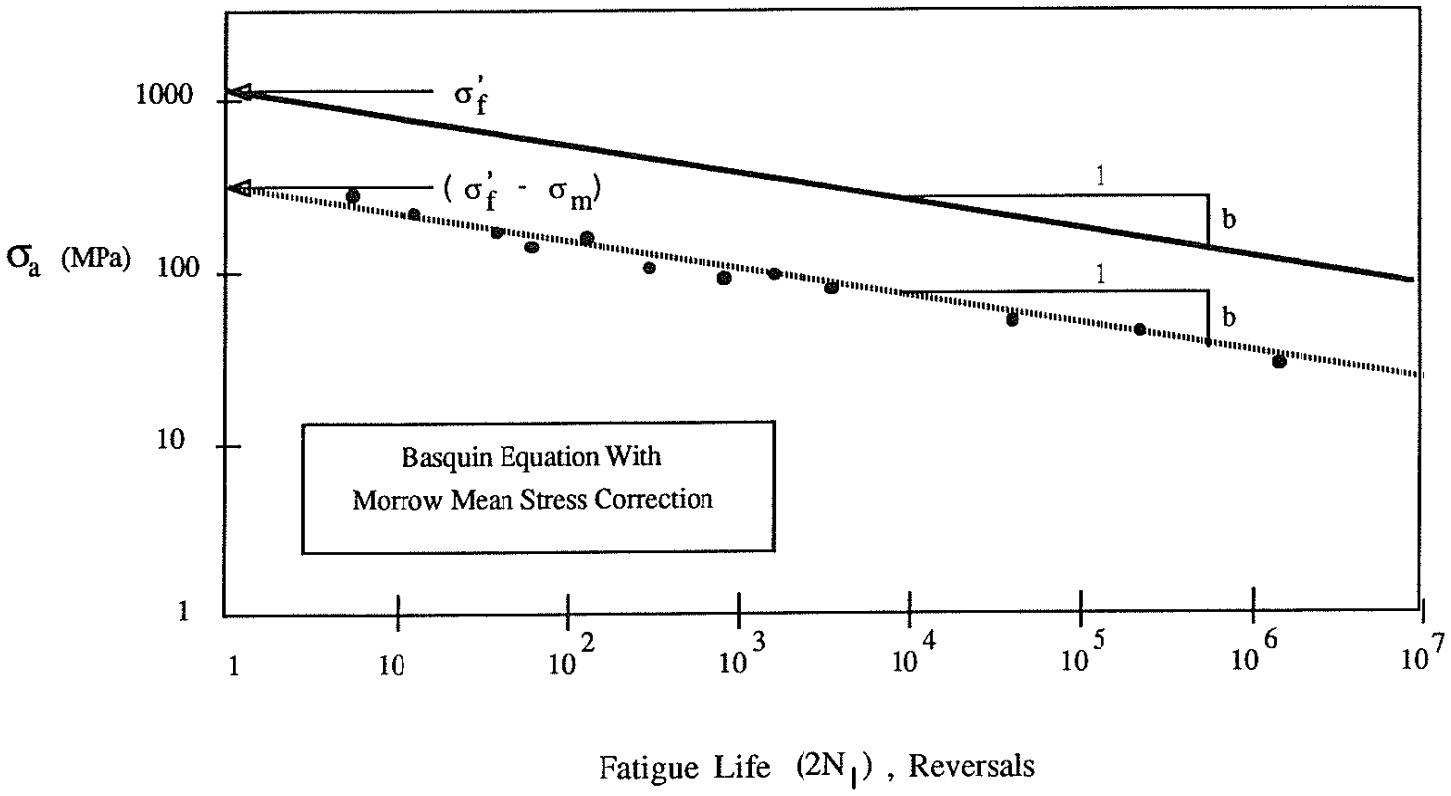

Fig. 1 Morrow mean stress correction to reduce the systematic error in the fatigue strength by considering the local mean stress effects.

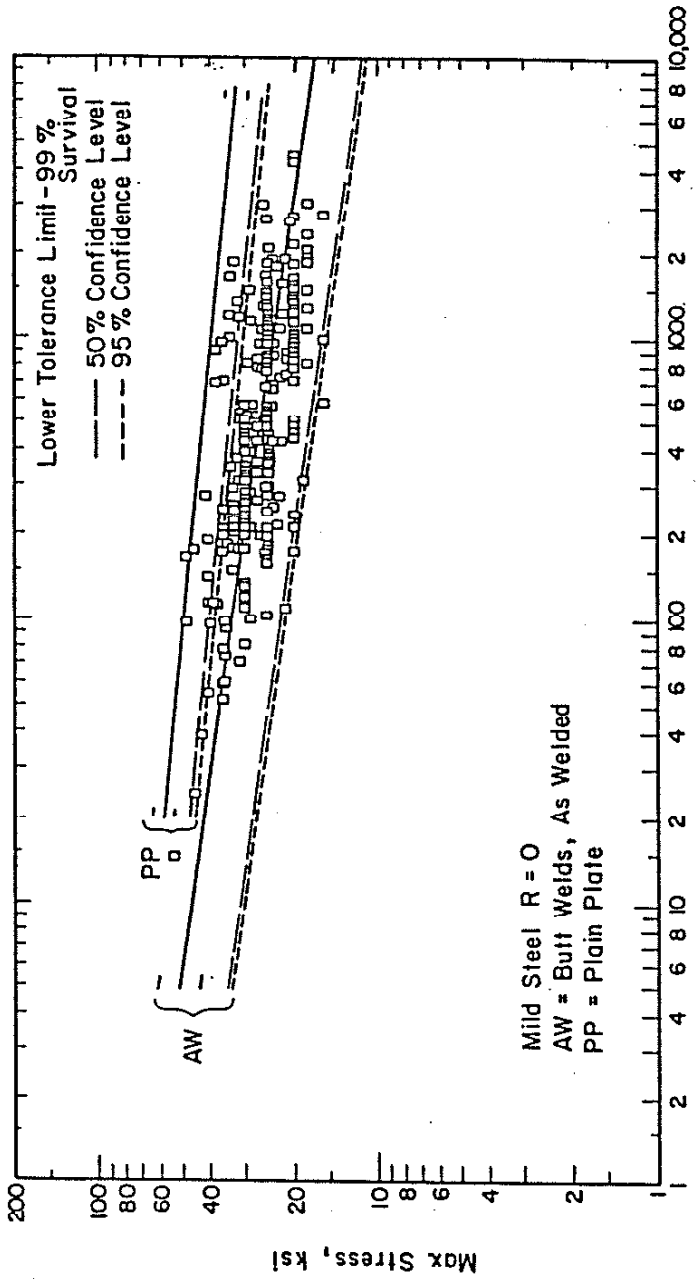

Fig. 2 A typical S-N diagram for mild steel butt weldments subjected to zero to tension loading. The fatigue resistance of as-welded butt weld is generally less than the fatigue resistance of plain plate which ia also indicated in this figure [10].

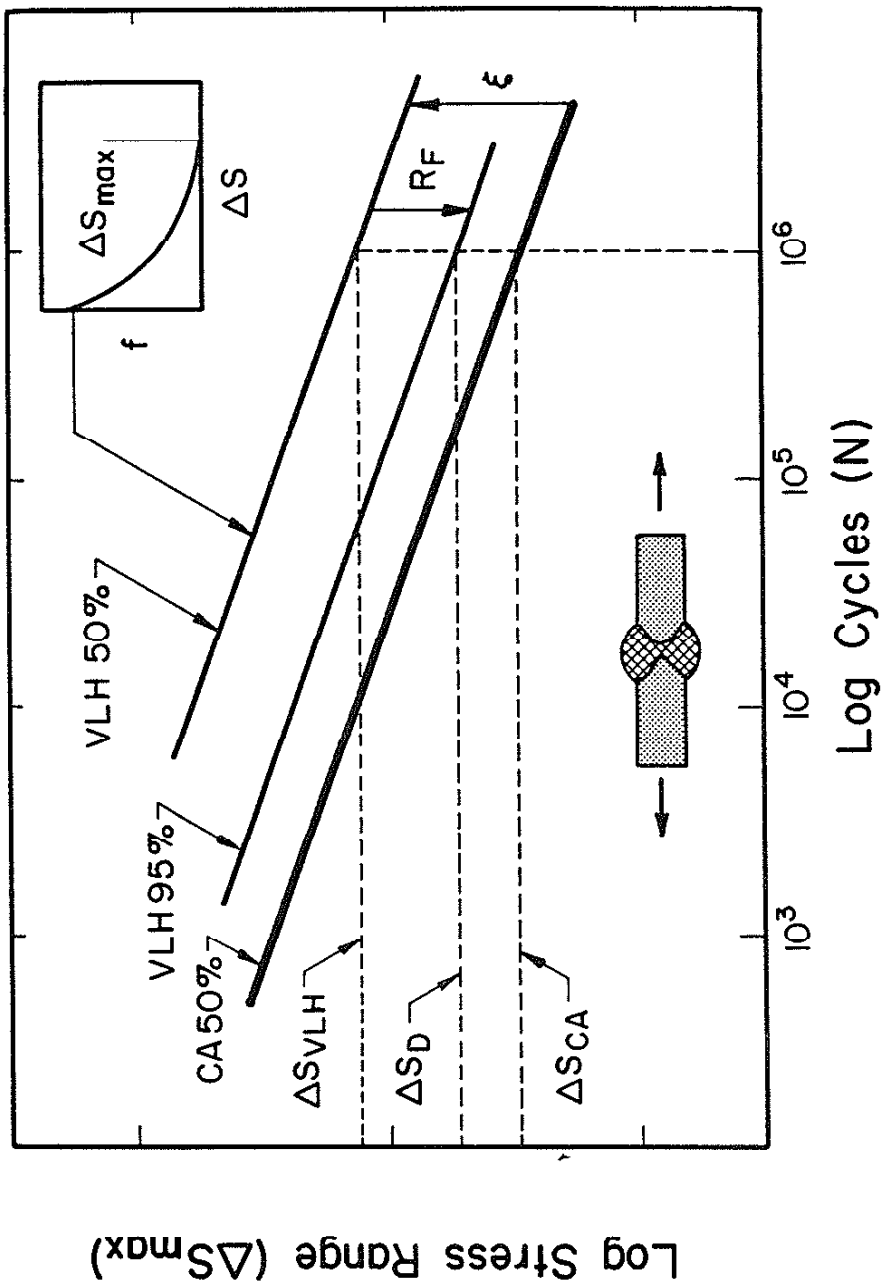

Fig. 3 Munse Fatigue Design Procedure (MFDP). The design stress range is calculated from the constant amplitude S-N diagram using the random load factor (ξ) and the reliability factor (R_F) [9].

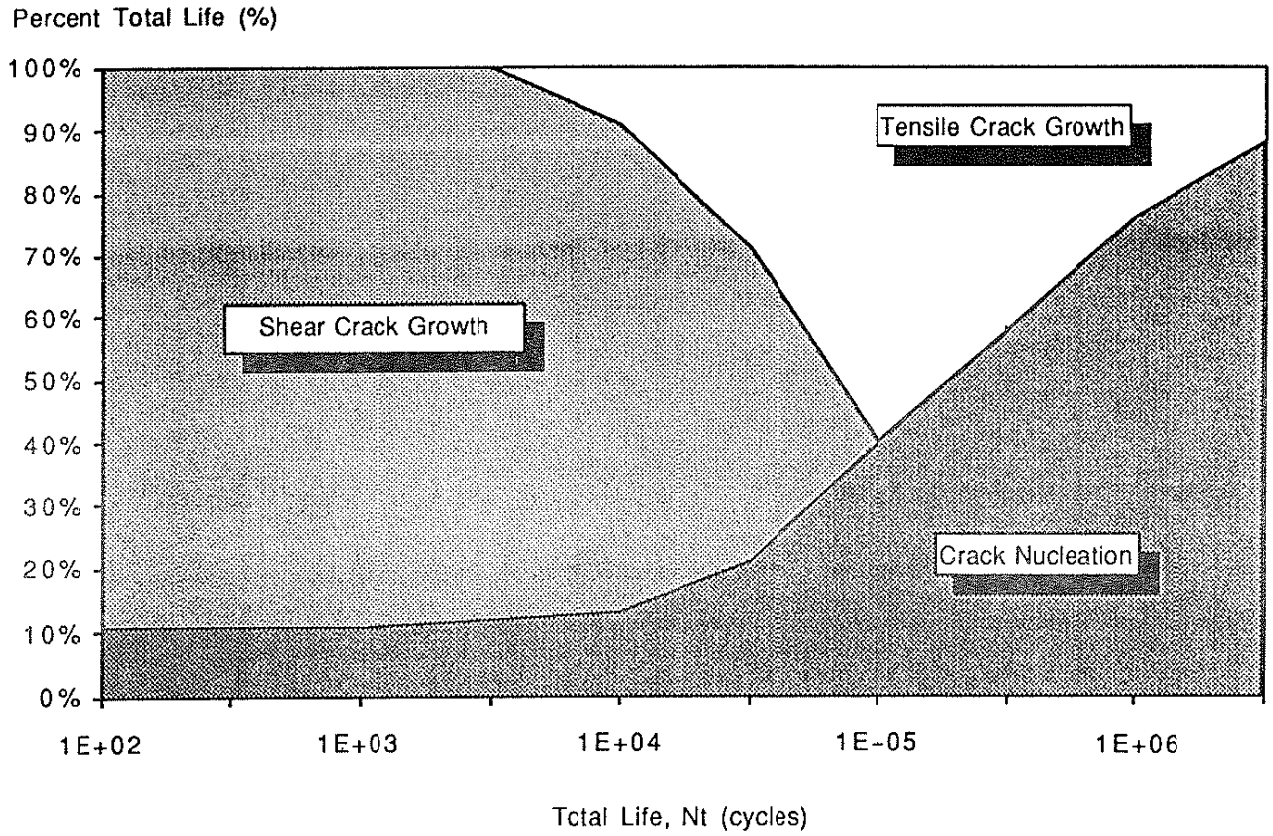

Fig. 4 Fatigue Cracking Behavior of 1045 steel in tension after Socie [21].

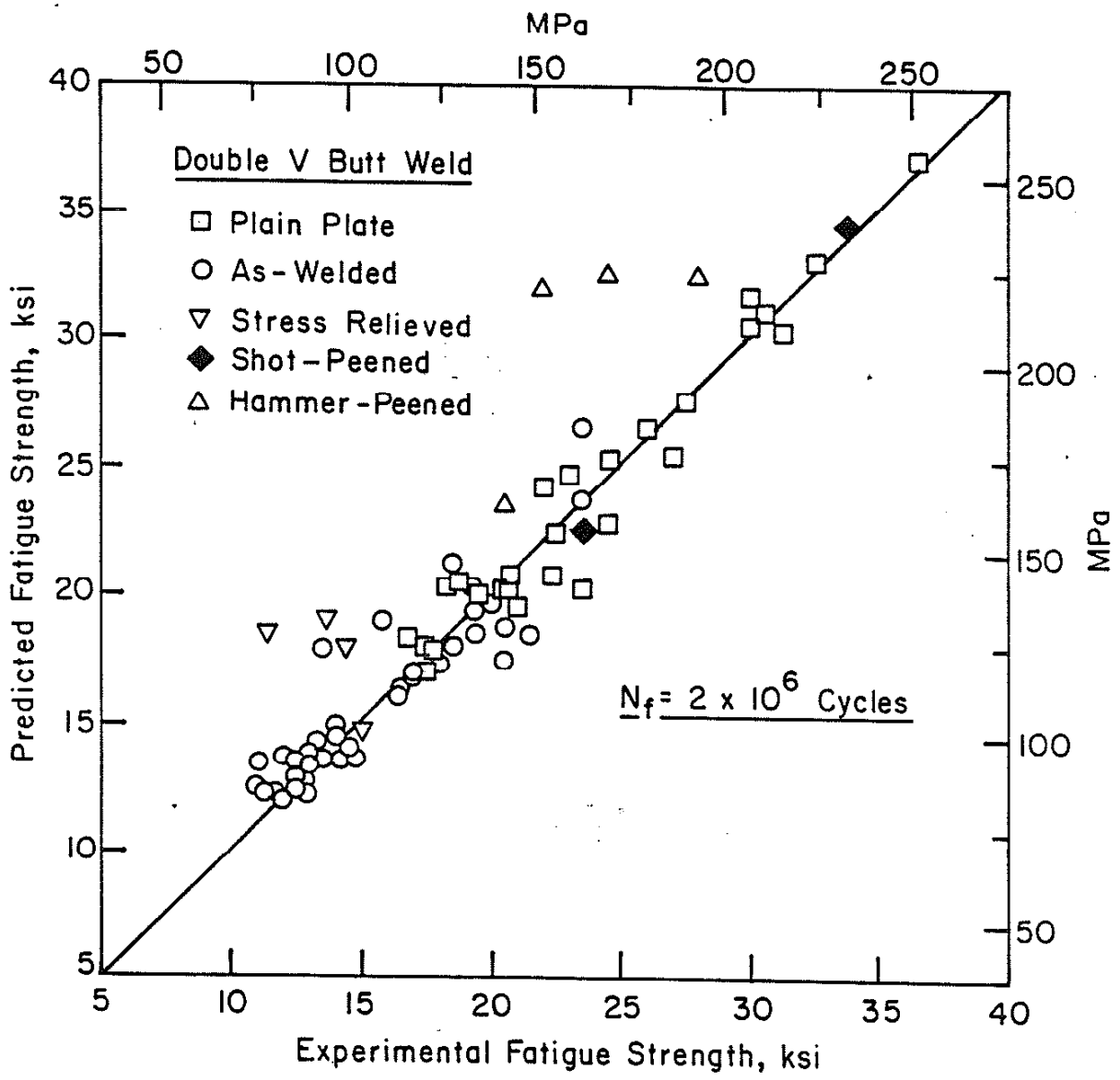

Fig. 5 Comparison of fatigue strength predicted using Eq. 14 with experimental data [31].

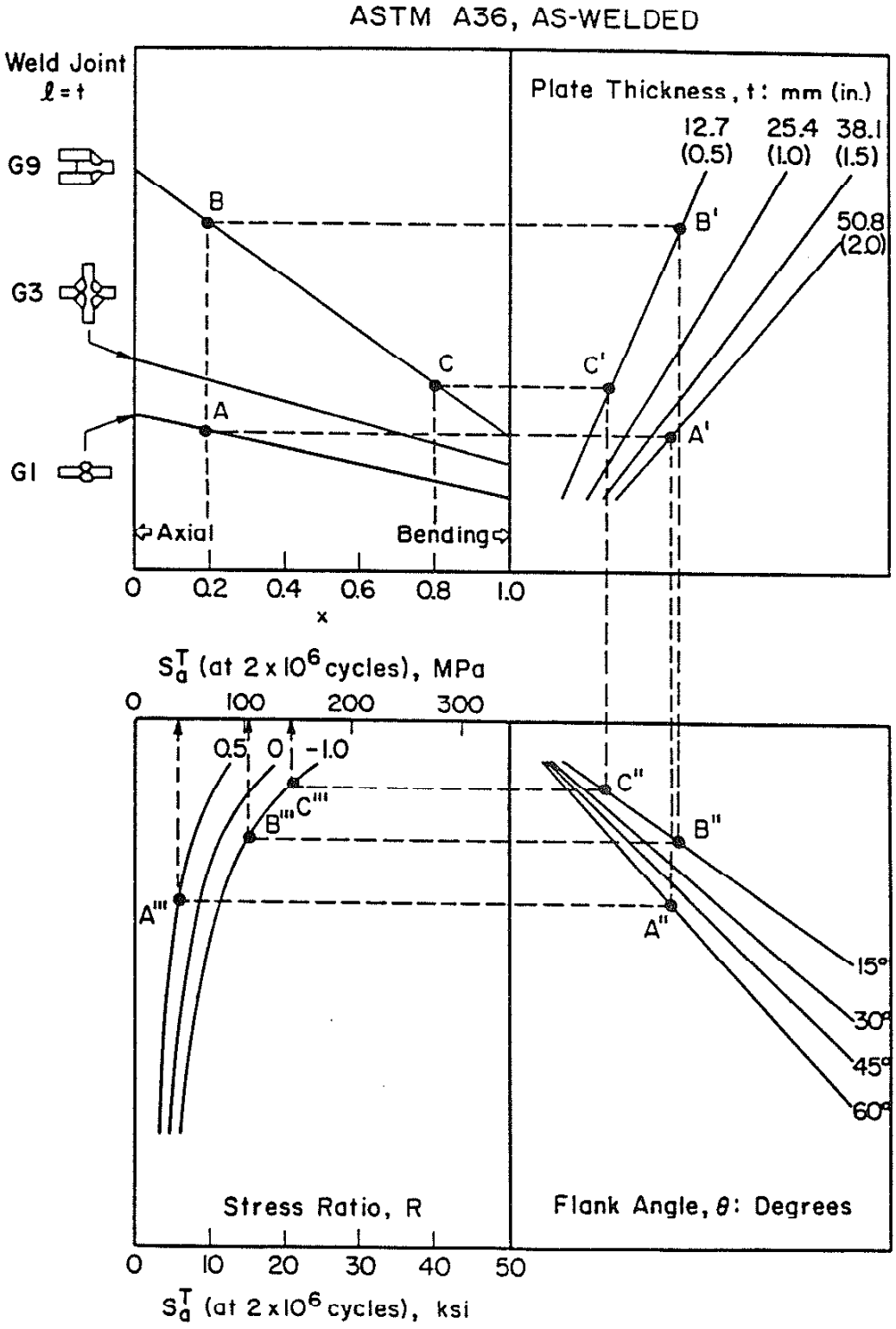

Fig. 6 Deterministic graphic guideline for the fatigue design of as-welded ASTM A-36 weldments [4].

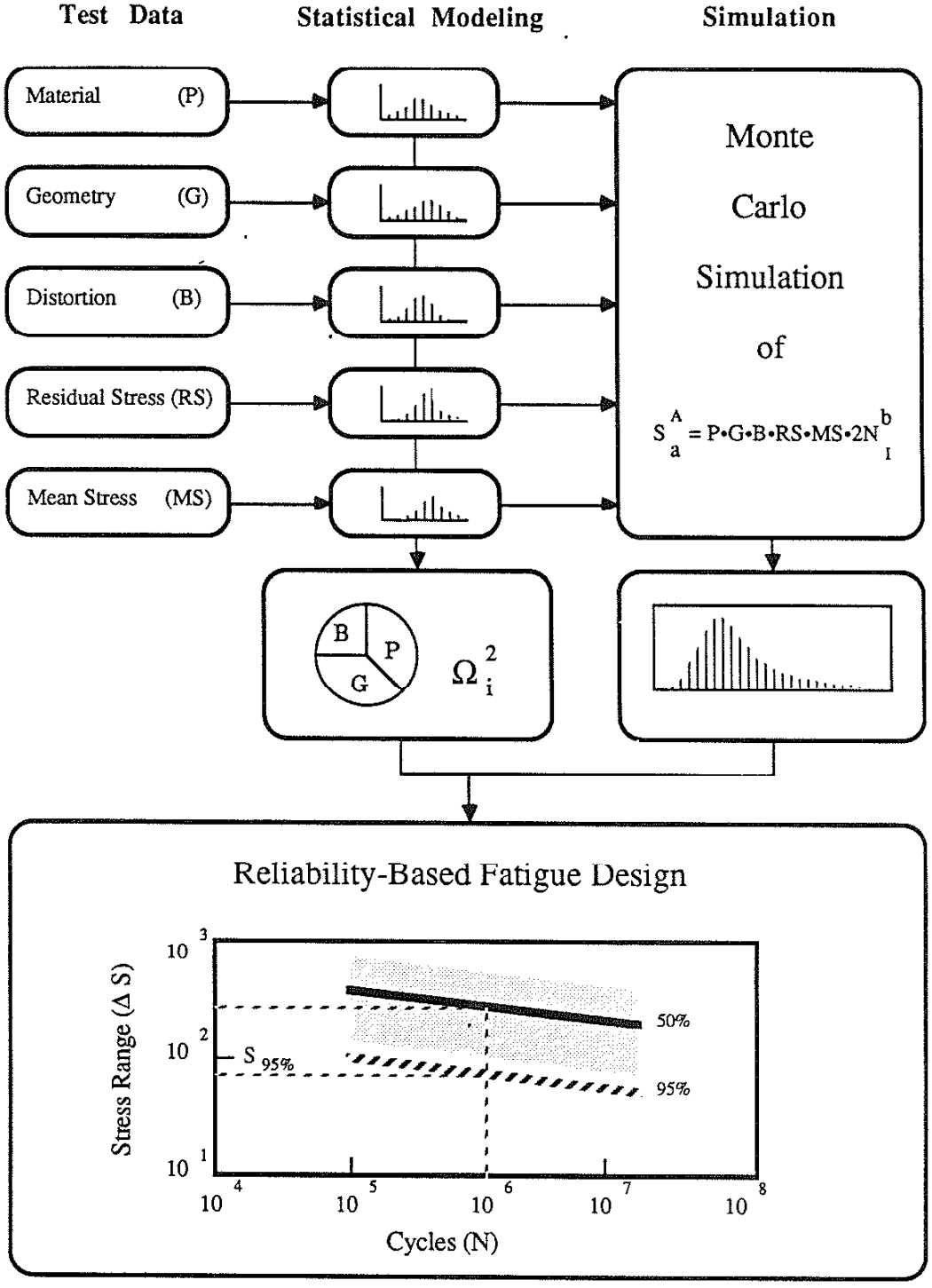

Fig. 7 Schematic description of probabilistic weldment fatigue crack initiation model (WFCIM).

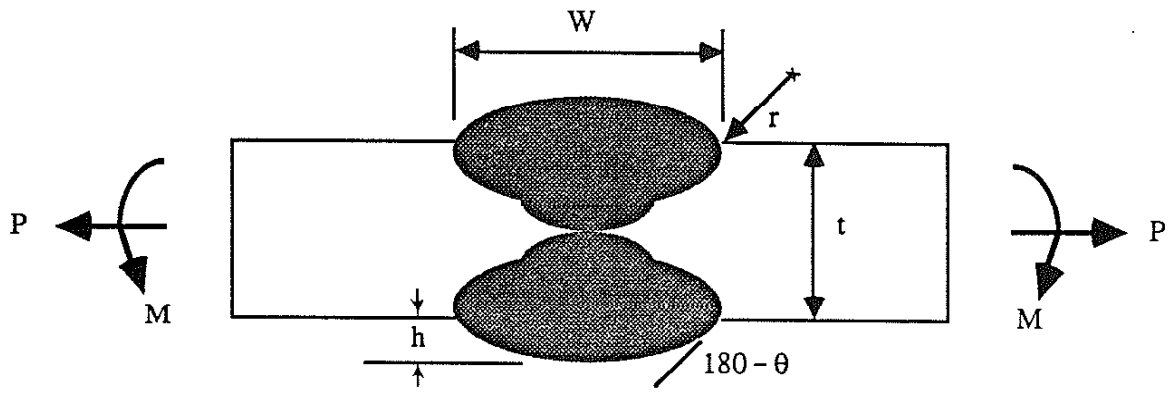

Butt Weldment	Toe	Axial	$\alpha = .27\ (\tan\theta)^{.25}$ $\beta = 1,\ \lambda = .5$	FEM
		Bending	$\alpha = .165\ (\tan\theta)^{.167}$ $\beta = 1,\ \lambda = .5$	FEM

Fig. 8 The geometry for butt and cruciform weldments and their stress concentration factors resulting from F.E.M analysis [28].

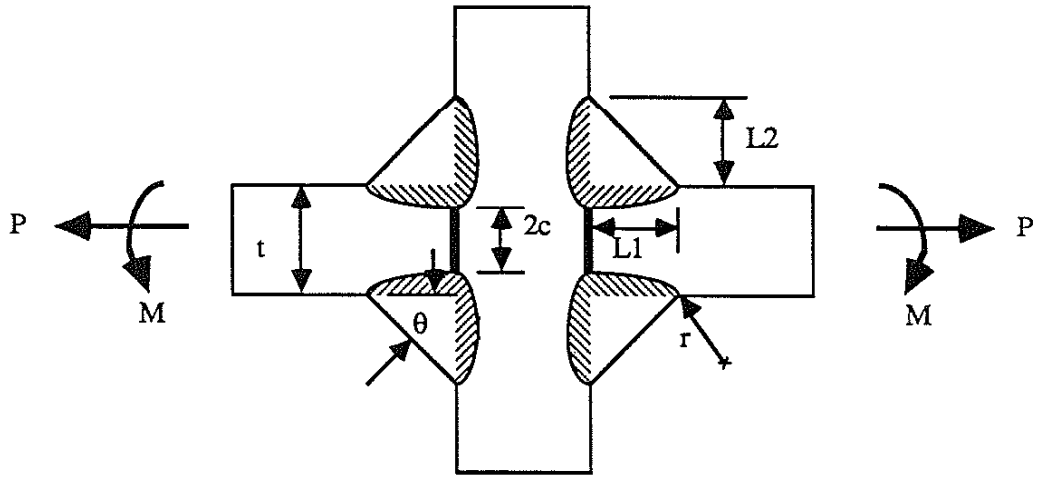

Cruciform Weldments	Toe	Axial	$\alpha = .35(\tan\theta)^{.25}[1+1.1(c/L2)^{1.65}]$ $\beta = 1,\ \lambda = .5$	FEM
		Bending	$\alpha = .21(\tan\theta)^{.167}$ $\beta = 1,\ \lambda = .5$	FEM
	IJP	Axial	$\alpha = 1.15(\tan\theta)^{-.25}(c/L2)^{.5}$ $\beta = 1,\ \lambda = .5$	FEM
		Bending	$\alpha = 3.22(c/t)^{.12}$ $\beta = 1,\ \lambda = .5$	FEM

Fig. 8 Continued.

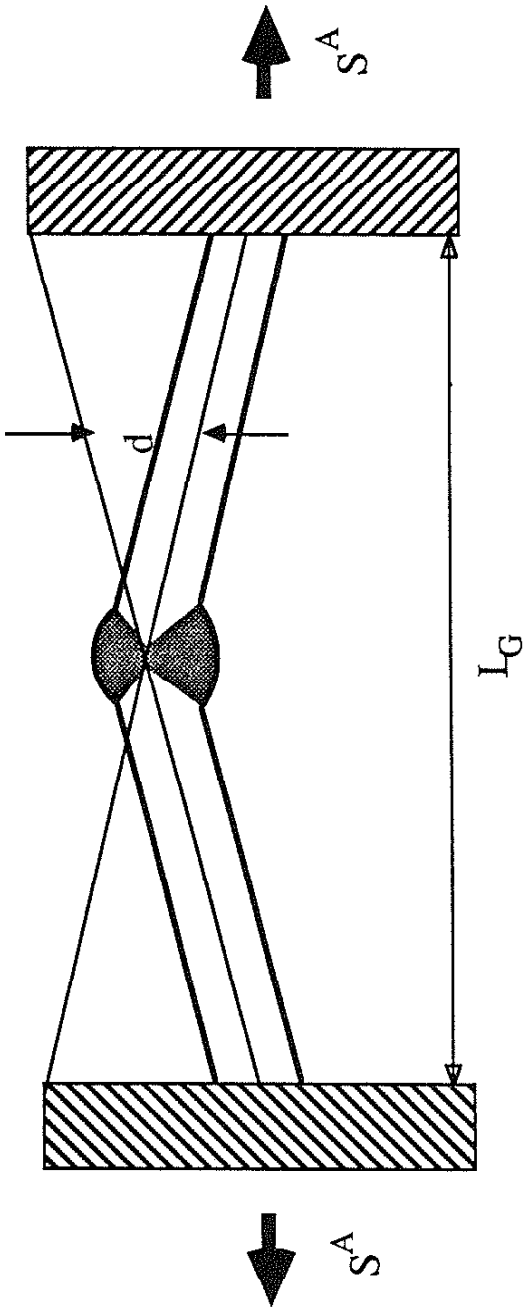

Fig. 9 Schematic description of the specimen with welding distortion for the use of Eq. 26 [42].

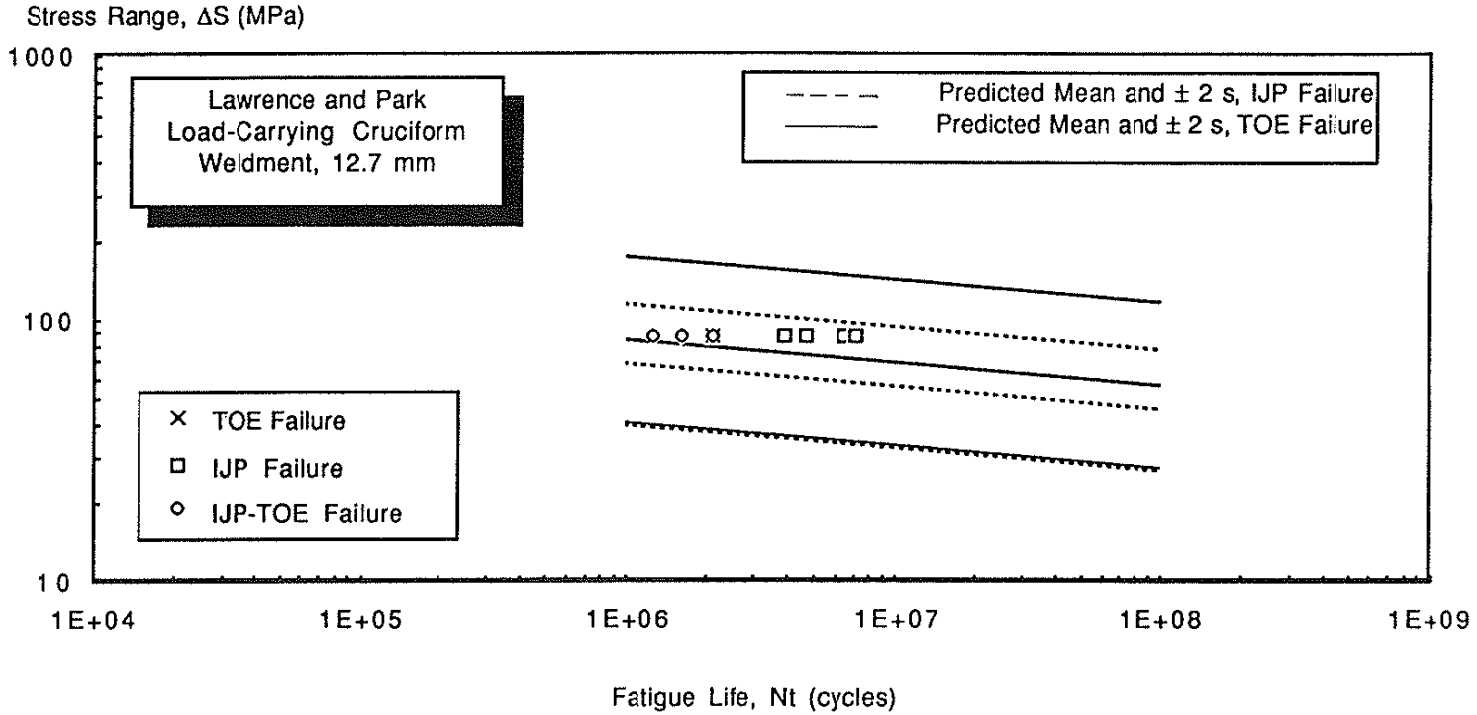

Fig. 10 Comparison of simulation results using Eq. 28 for 12.7 mm load-carrying cruciform weldments with the fatigue test data. The solid lines represents the mean (mean of logΔS), and the mean ± 2s (mean of logΔS ± 2 standard deviation of logΔS) fatigue strengths for given life.

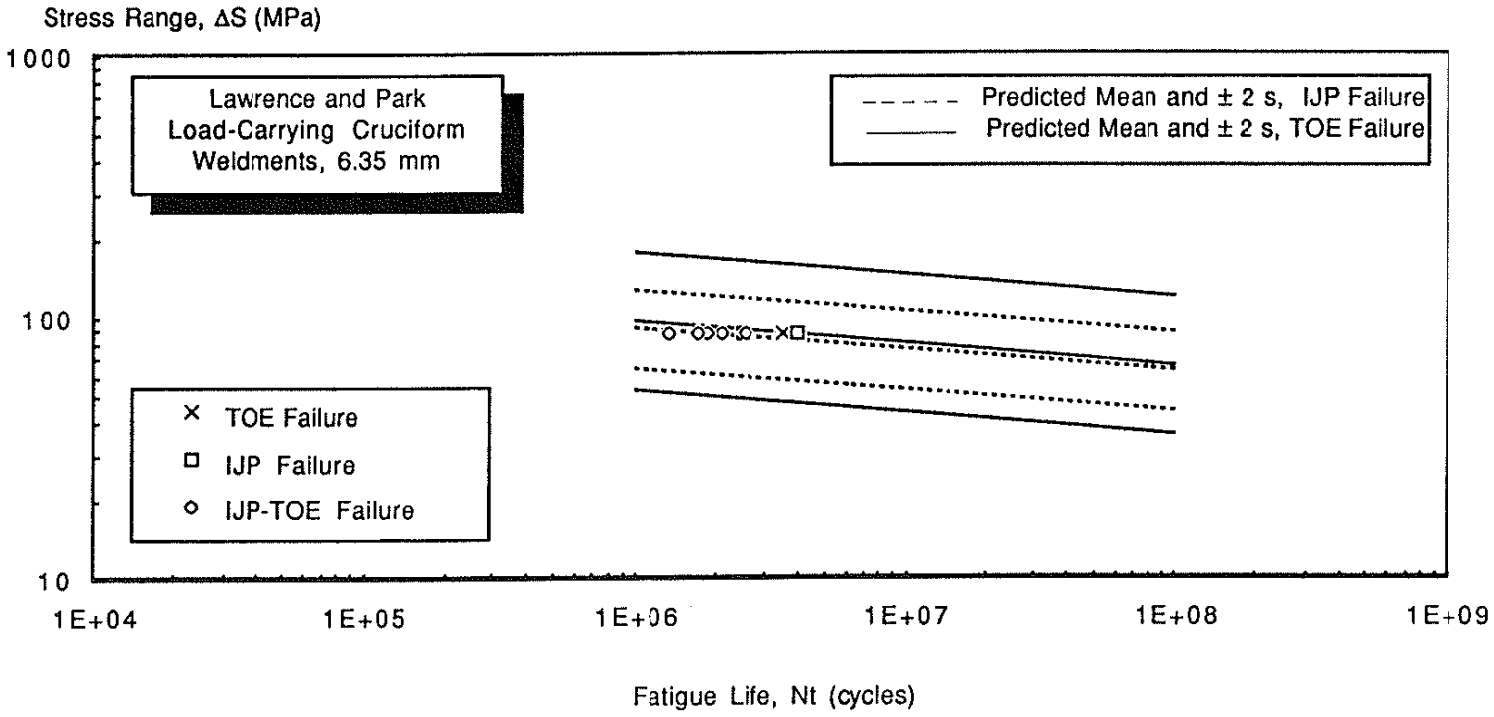

Fig. 11 Comparison of simulation results using Eq. 28 for 6.35 mm load-carrying cruciform weldments with the fatigue test data. The solid lines represents the mean (mean of logΔS), and the mean ± 2s (mean of logΔS ± 2 standard deviation of logΔS) fatigue strengths for given life.

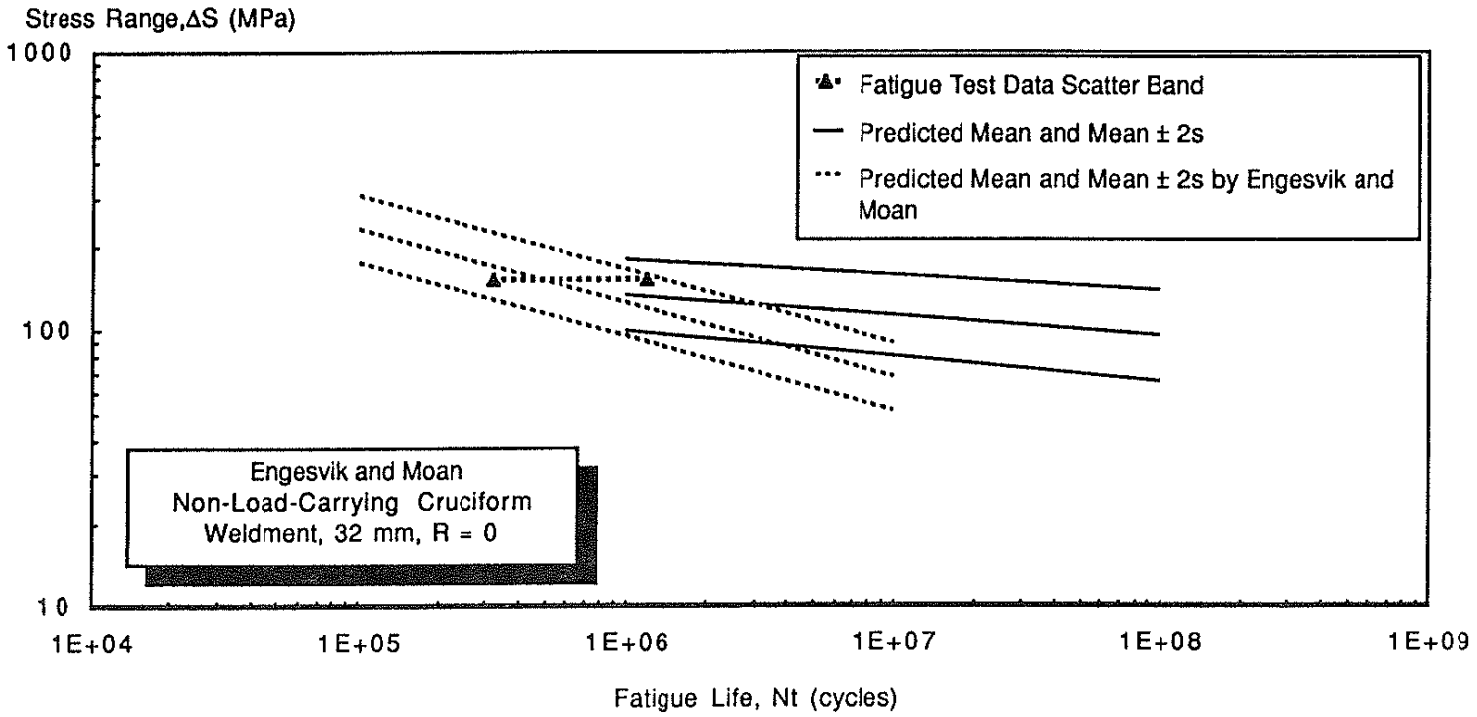

Fig. 12 Comparison of simulation results using Eq. 16 for 32 mm non-load-carrying cruciform weldments with the fatigue test data and simulation results from Engesvik and Moan. The reciprocal slope of Engesvik and Moan simulation was assumed as 3.7 which was the average value of crack propagation exponent used in their simulation. The solid lines represents the mean (mean of logΔS), and the mean ± 2s (mean of logΔS ± 2 standard deviation of logΔS) fatigue strengths for given life.

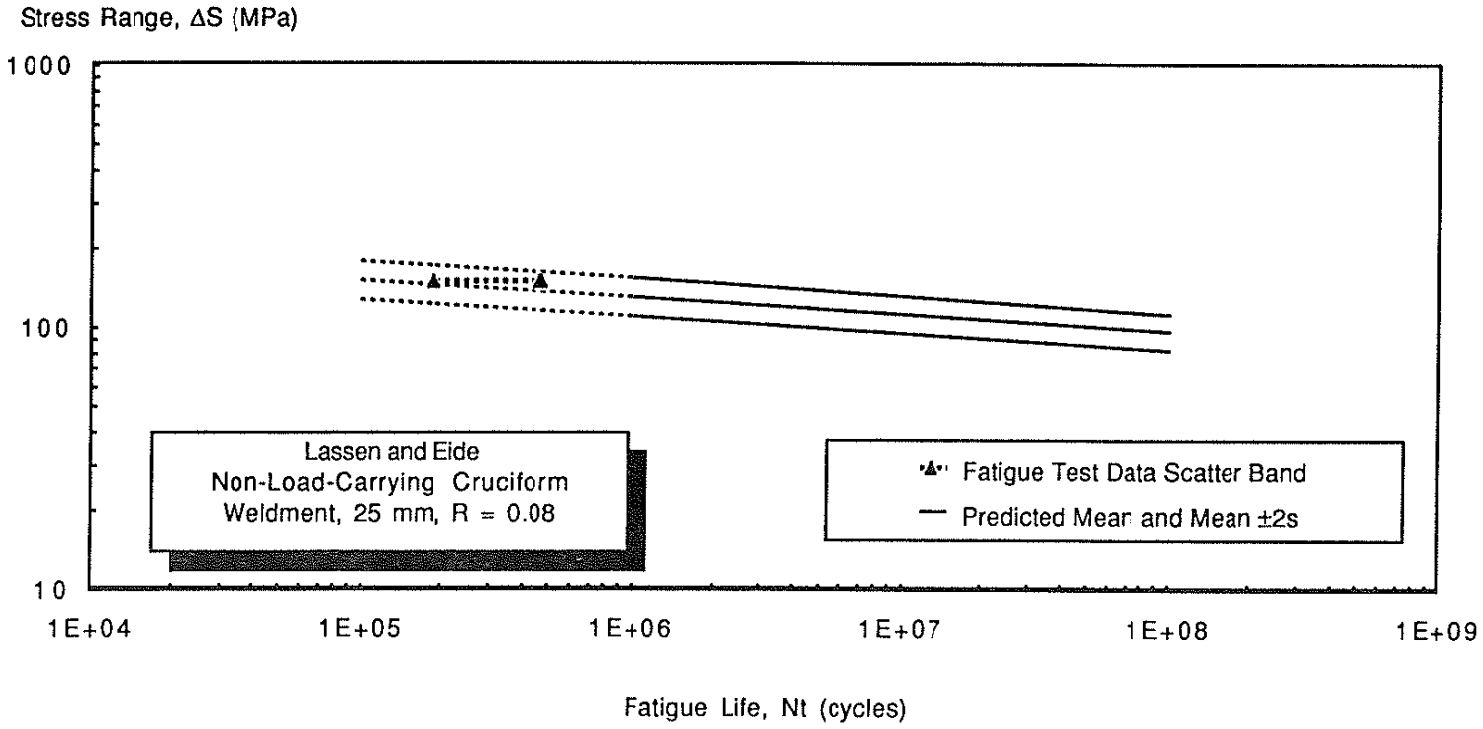

Fig. 13 Comparison of simulation results using Eq. 16 for 25 mm non-load-carrying cruciform weldments with the fatigue test data from Lassen and Eide. Since the fatigue test data were in the range less than 10^6 cycles, our simulation results were extended to the 105 cycles only for the comparison purpose. The solid lines represents the mean (mean of logΔS), and the mean $\pm$ 2s (mean of logΔS $\pm$ 2 standard deviation of logΔS) fatigue strengths for given life.

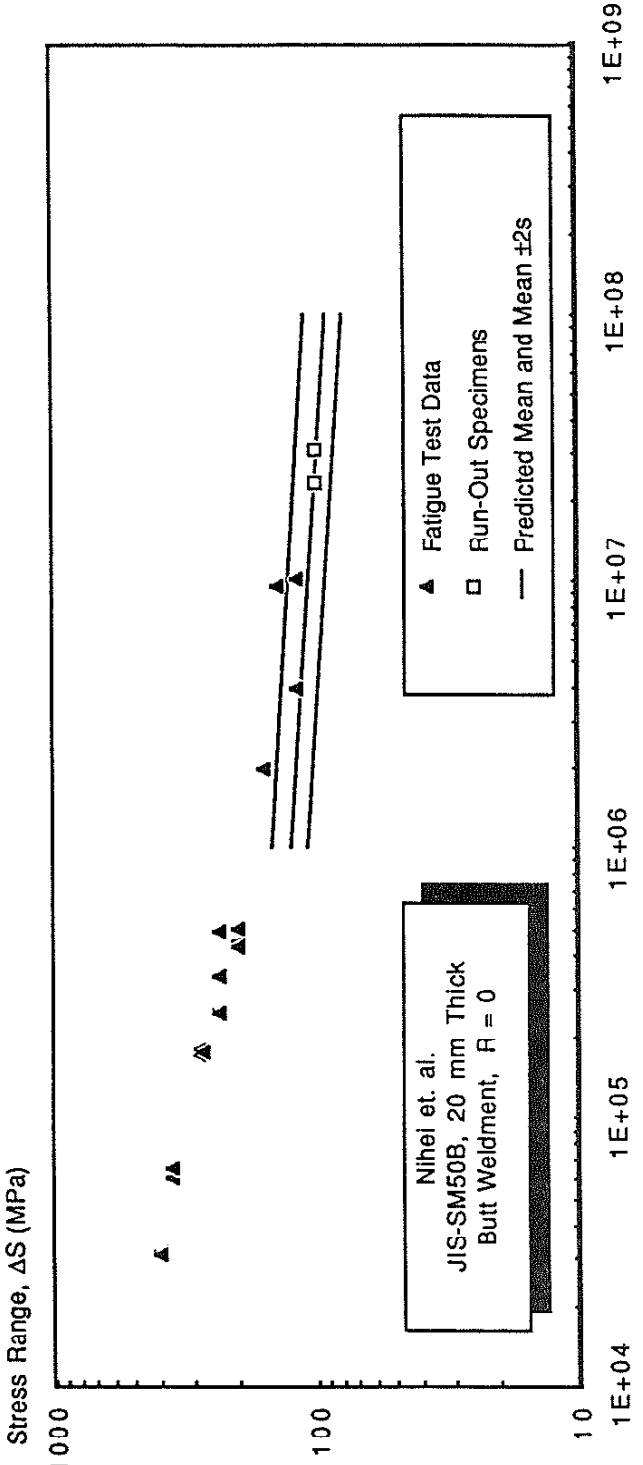

Fig. 14 Comparison of simulation results using Eq. 16 for 20 mm butt weldments with the fatigue test data from Nihei et. al.. The solid lines represents the mean (mean of logΔS), and the mean $\pm$ 2s (mean of logΔS $\pm$ 2 standard deviation of logΔS) fatigue strengths for given life.

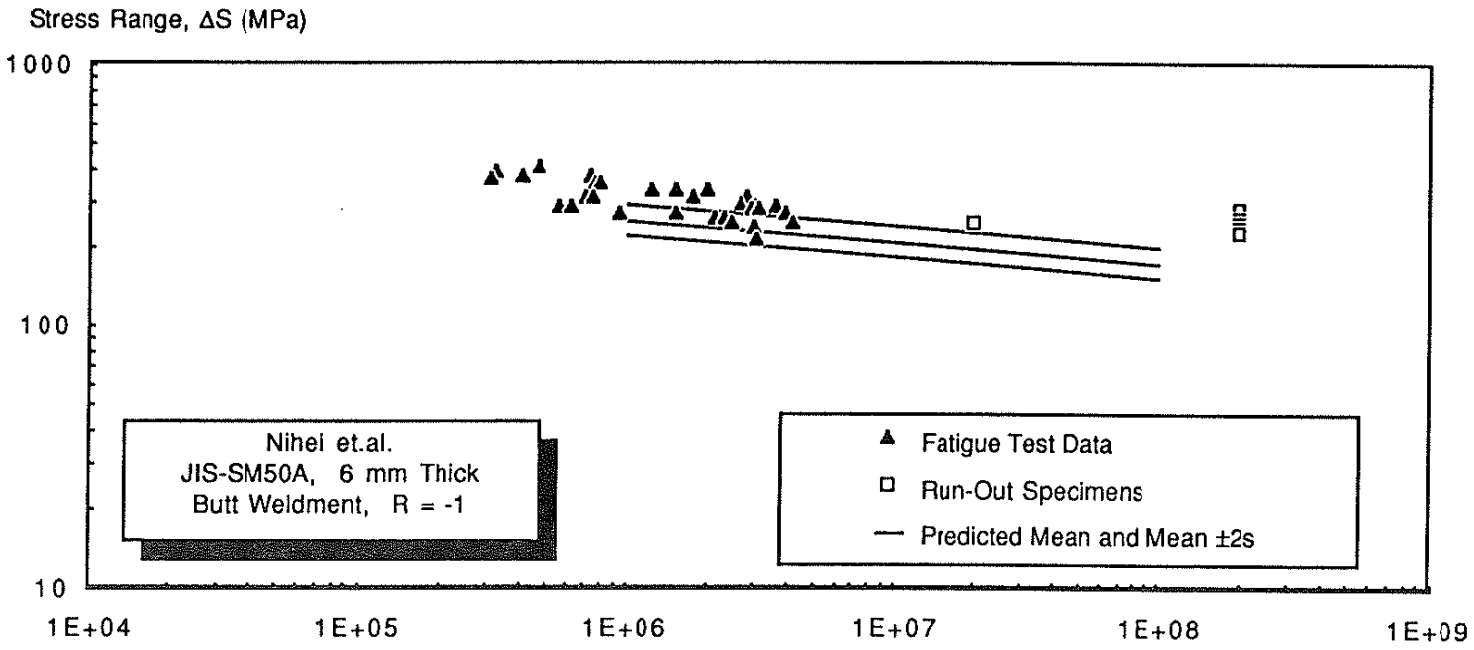

Fig. 15 Comparison of simulation results using Eq. 16 for 6 mm butt weldments (R=-1) with the fatigue test data from Nihei et. al.. The solid lines represents the mean (mean of logΔS), and the mean ± 2s (mean of logΔS ± 2 standard deviation of logΔS) fatigue strengths for given life.

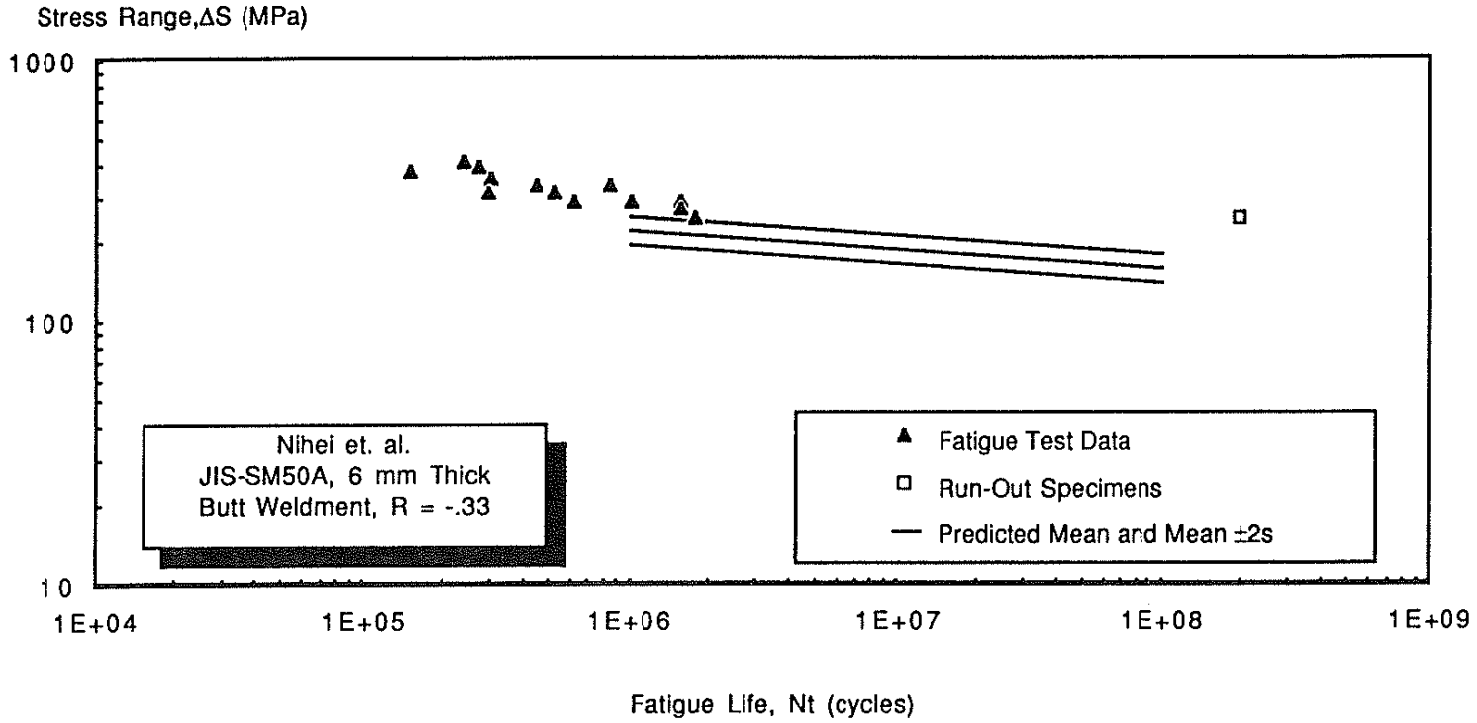

Fig. 16 Comparison of simulation results using Eq. 16 for 6 mm butt weldments (R=-.33) with the fatigue test data from Nihei et. al.. The solid lines represents the mean (mean of logΔS), and the mean $\pm$ 2s (mean of logΔS $\pm$ 2 standard deviation of logΔS) fatigue strengths for given life.

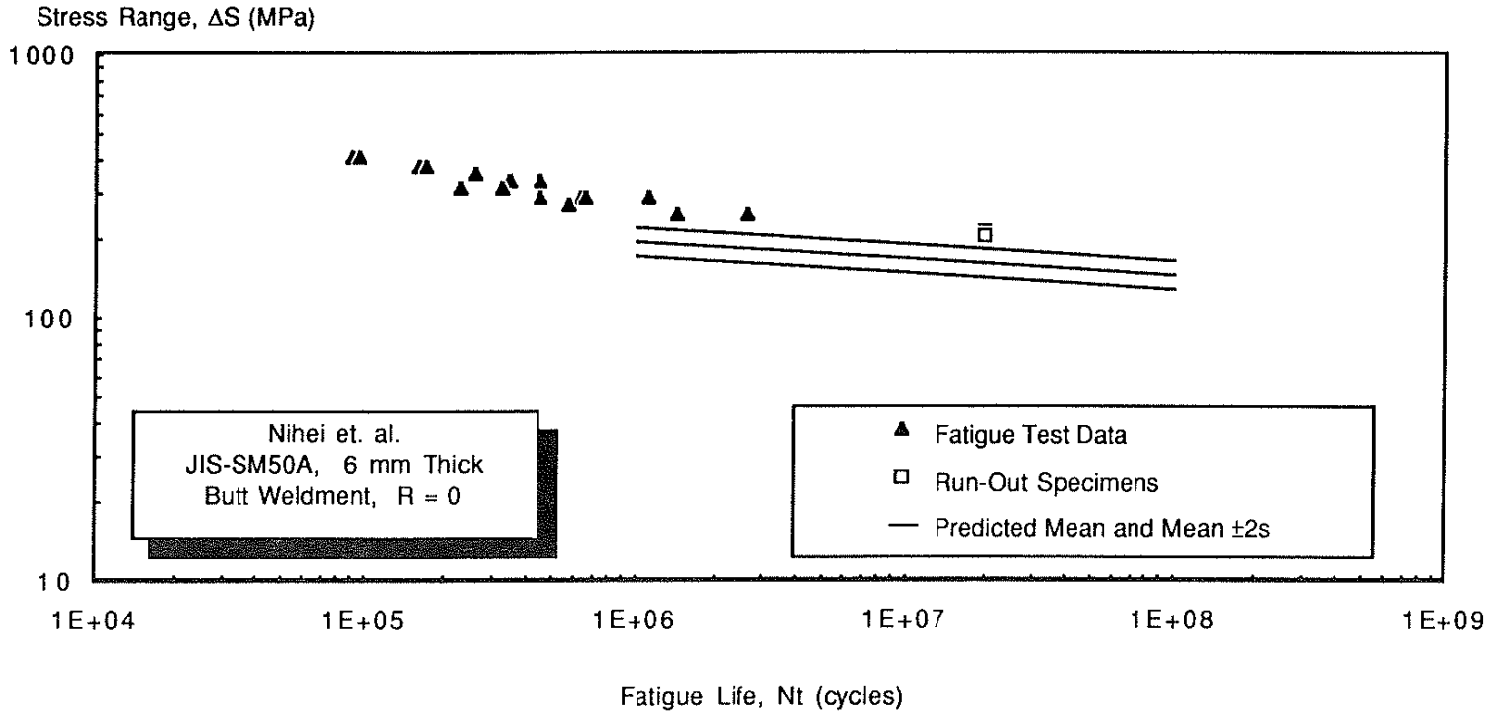

Fig. 17 Comparison of simulation results using Eq. 16 for 6 mm butt weldments (R=0) with the fatigue test data from Nihei et. al.. The solid lines represents the mean (mean of logΔS), and the mean ± 2s (mean of logΔS ± 2 standard deviation of logΔS) fatigue strengths for given life.

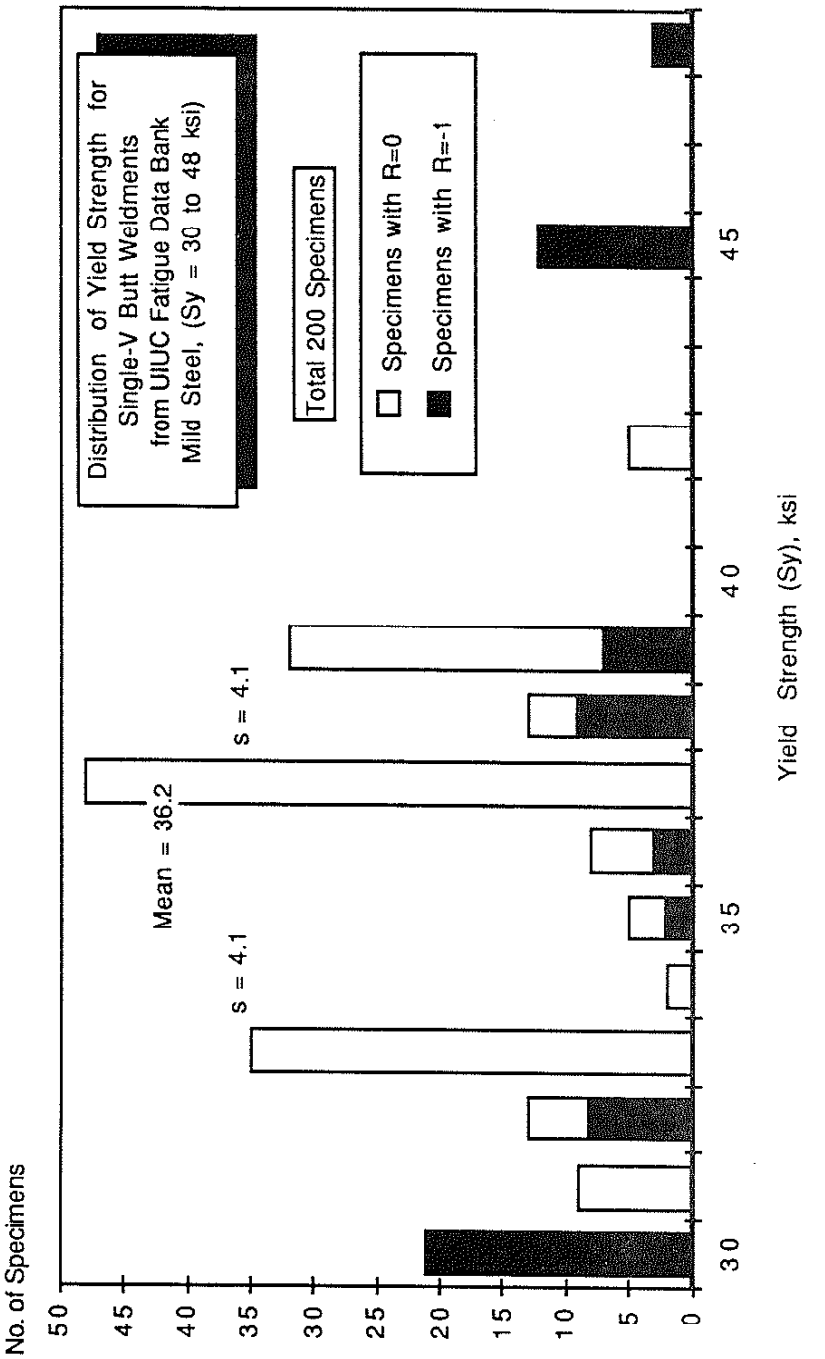

Fig. 18 Distribution of yield strength for as-welded mild steel (Sy = 30 to 48 ksi) single-V butt weldments from UIUC fatigue data bank. [50]

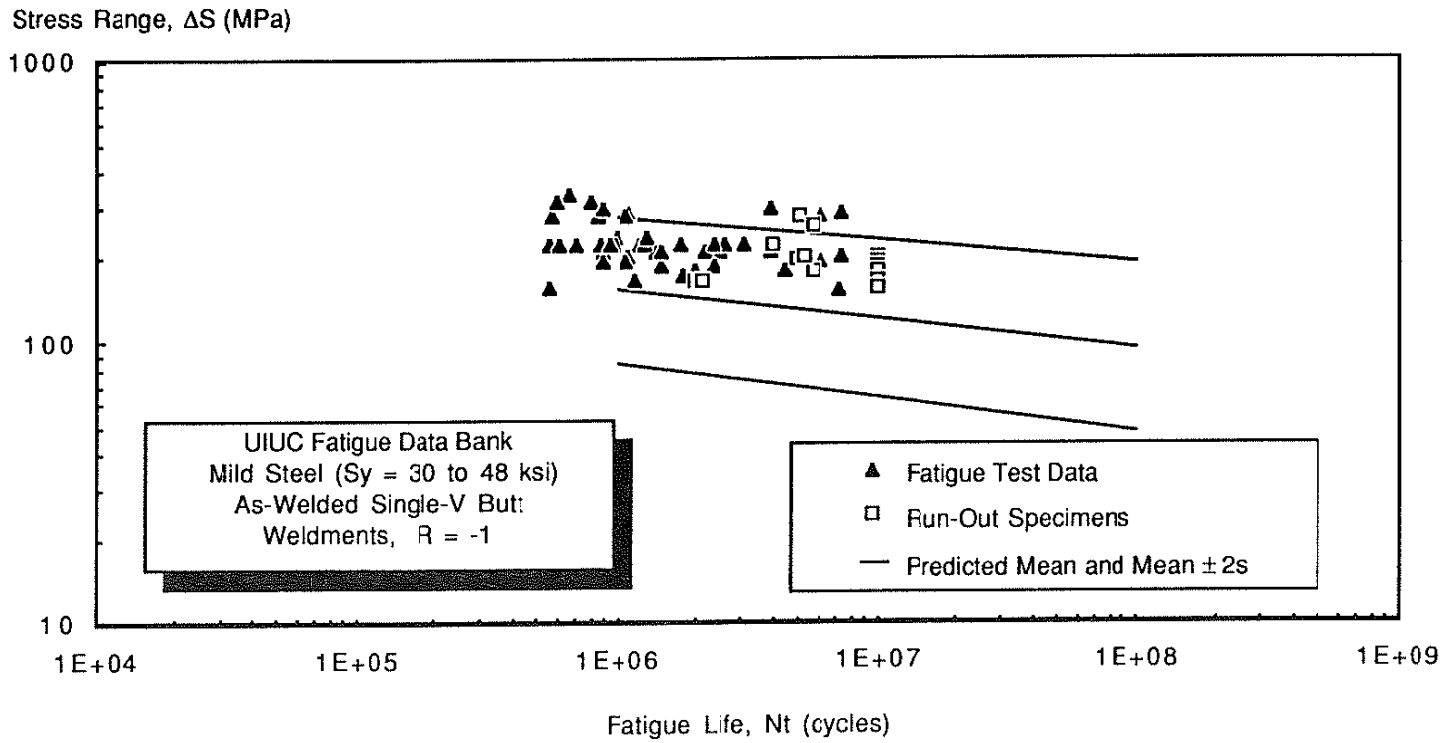

Fig. 19 Comparison of simulation results using Eq. 16 for as-welded mild steel (Sy = 30 to 48 ksi) Single-V butt weldments (R= -1) with the fatigue test data from UIUC fatigue data bank. The solid lines represents the mean (mean of logΔS), and the mean ± 2s (mean of logΔS ± 2 standard deviation of logΔS) fatigue strengths for given life.

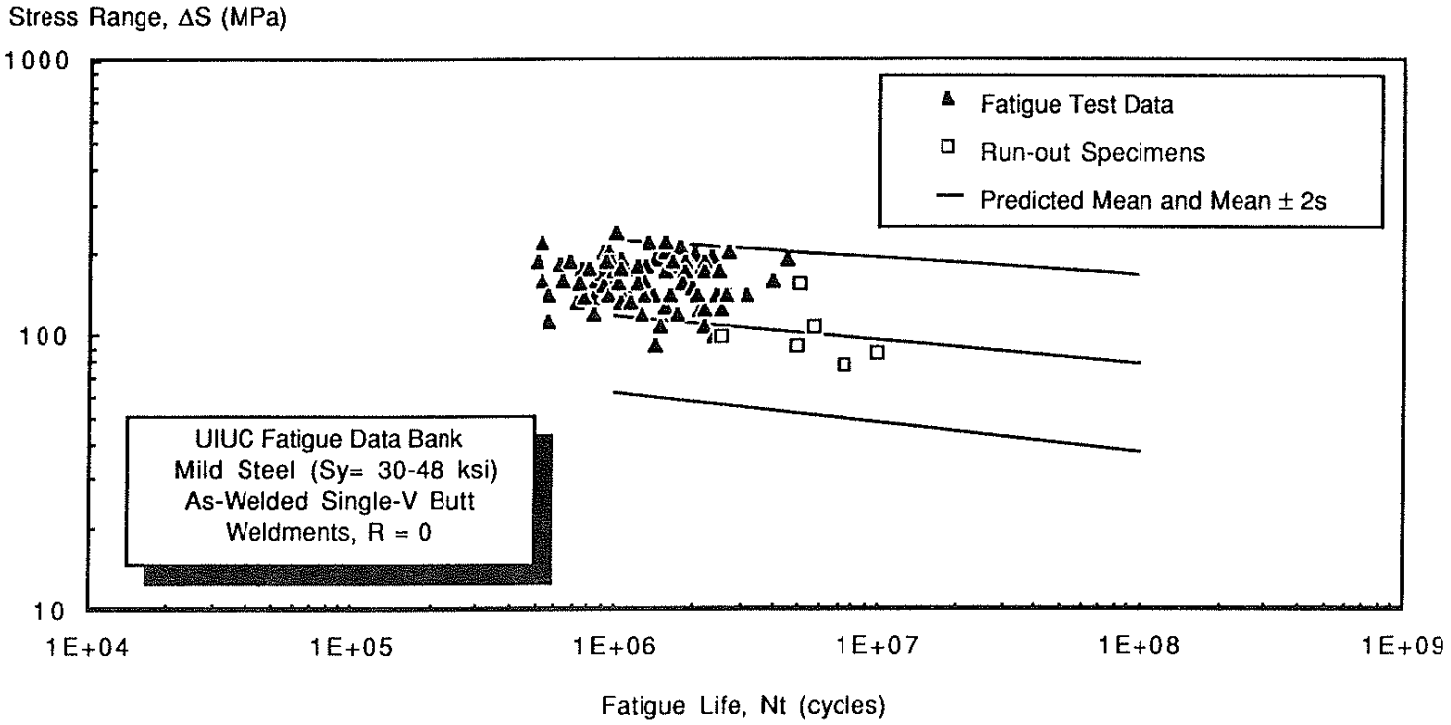

Fig. 20 Comparison of simulation results using Eq. 16 for as-welded mild steel (Sy = 30 to 48 ksi) Single-V butt weldments (R=0) with the fatigue test data from UIUC fatigue data bank. The solid lines represents the mean (mean of logΔS), and the mean ± 2s (mean of logΔS ± 2 standard deviation of logΔS) fatigue strengths for given life.

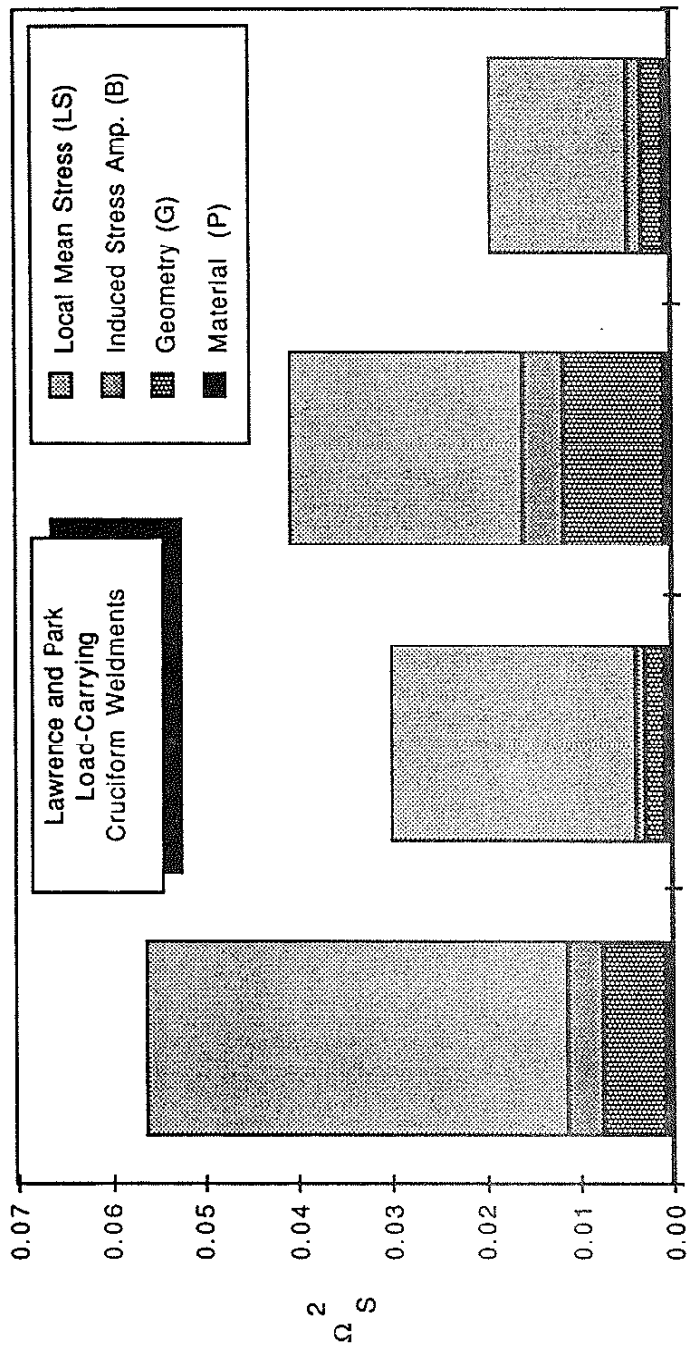

Fig. 21 Factorized square of uncertainty in each factor (P, G, B and LS) of weldment for load-carrying cruciform weldments.

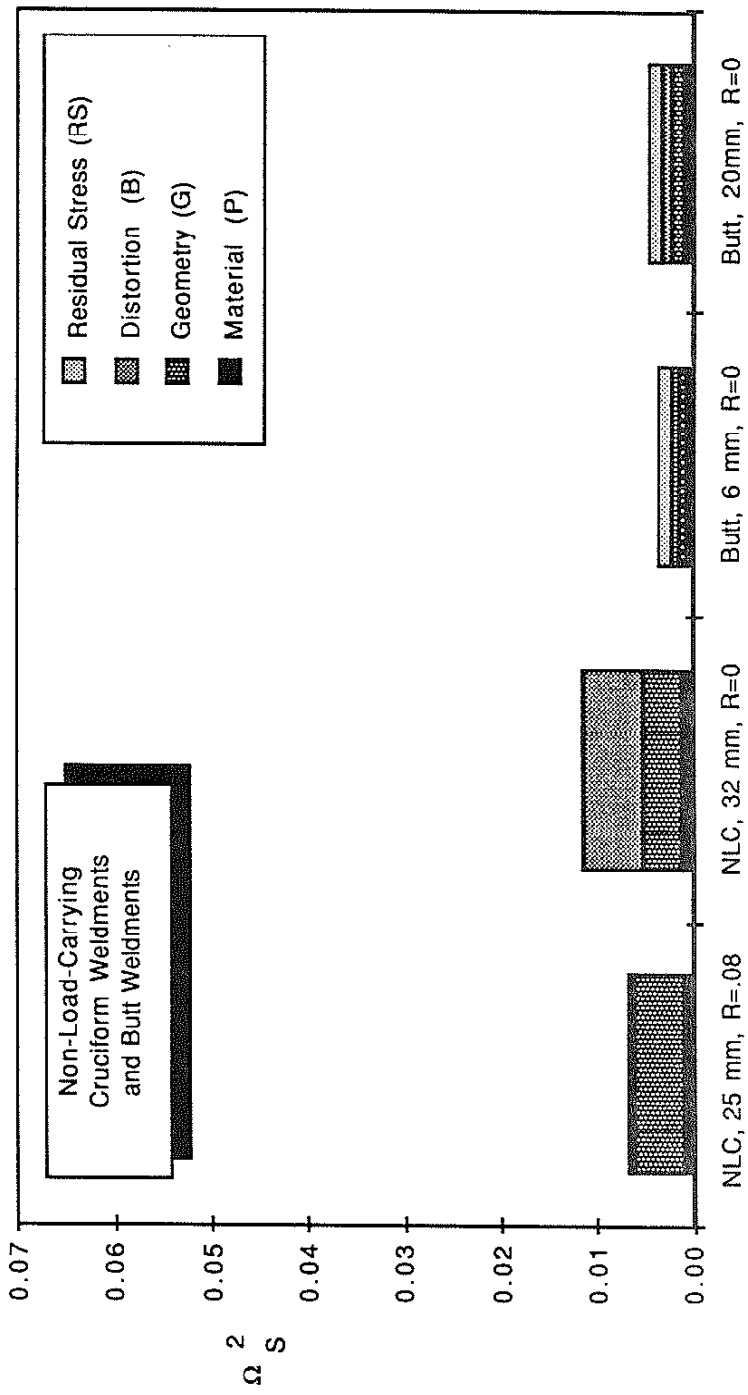

Fig. 22 Factorized square of uncertainty in each factor (P, G, B and RS) of weldment for non-load-carrying cruciform and butt weldments.

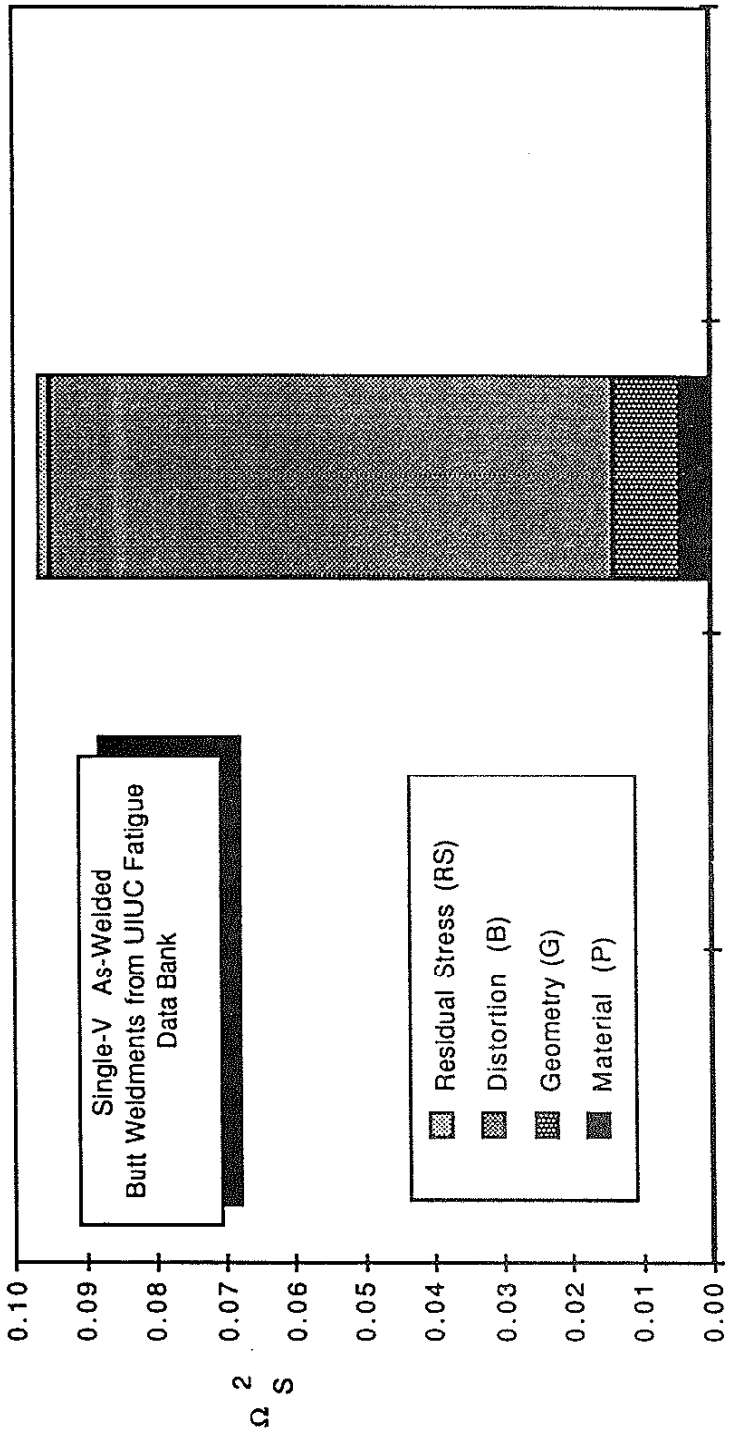

Fig. 23 Factorized square of uncertainty in each factor (P, G, B and RS) of weldment for as-welded single-V butt weldments from UIUC fatigue data bank.

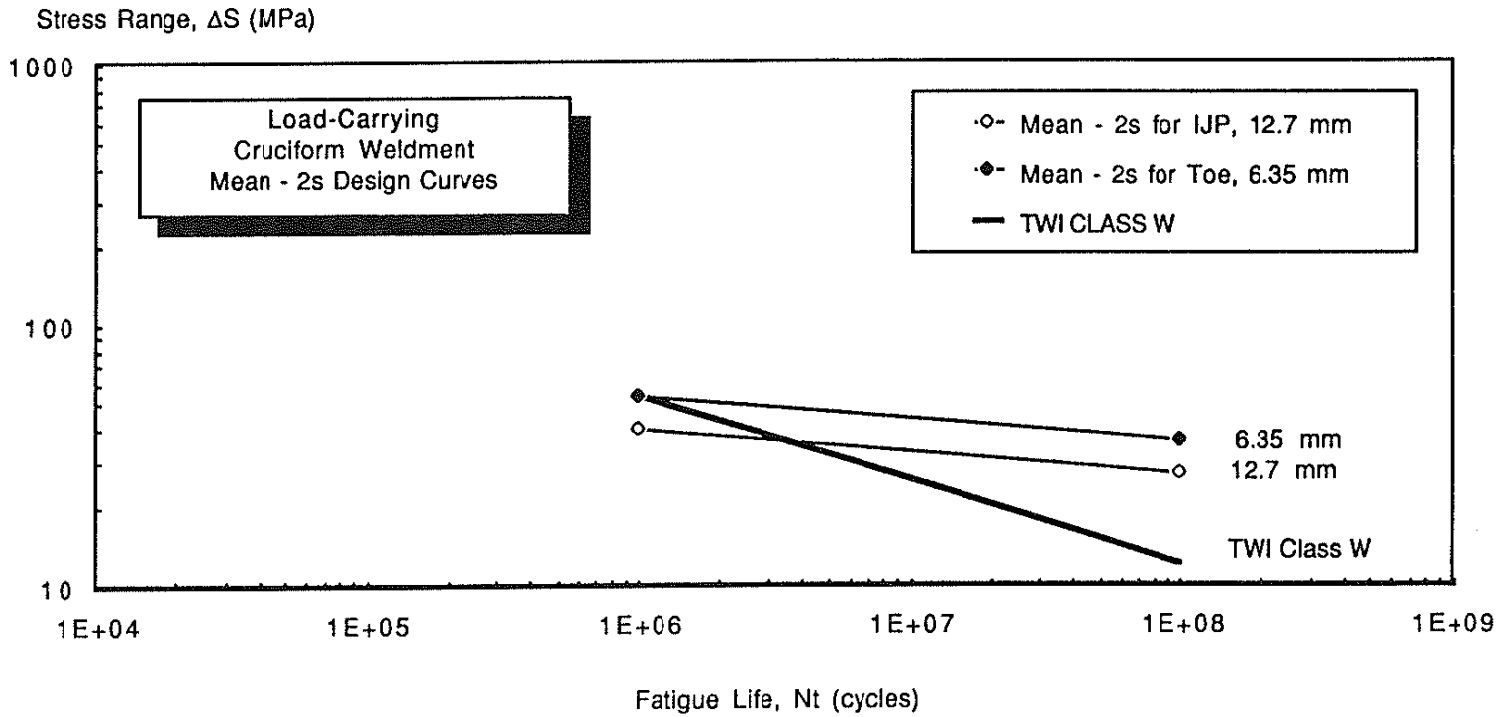

Fig. 24 Comparison of simulated (Mean - 2σ) fatigue design curves for load-carrying cruciform weldments with TWI Class W (mean-2σ) design curve.

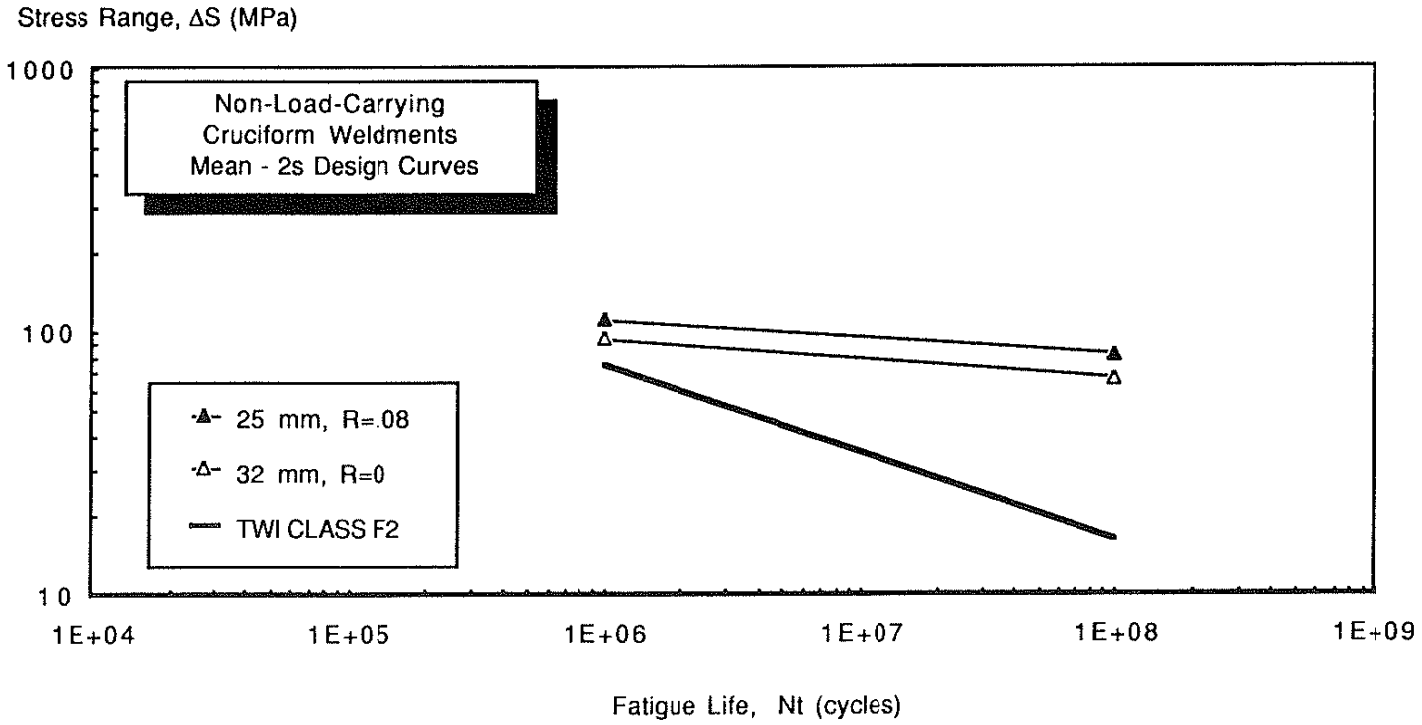

Fig. 25 Comparison of simulated (Mean - 2σ) fatigue design curves for non-load-carrying cruciform weldments with TWI Class F2 (mean-2σ) design curve.

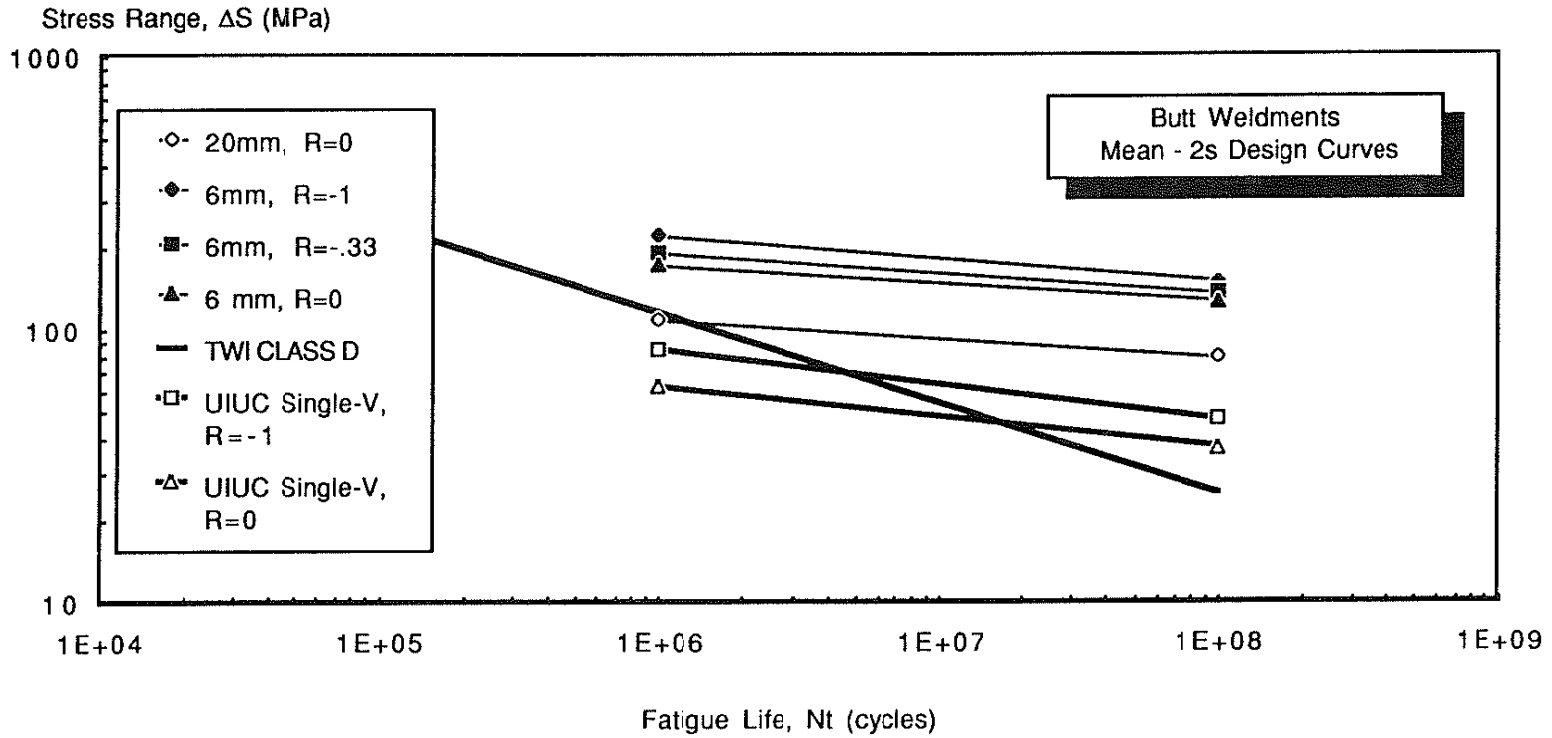

Fig. 26 Comparison of simulated (Mean - 2σ) fatigue design curves for butt weldments with TWI Class D (mean-2σ) design curve.

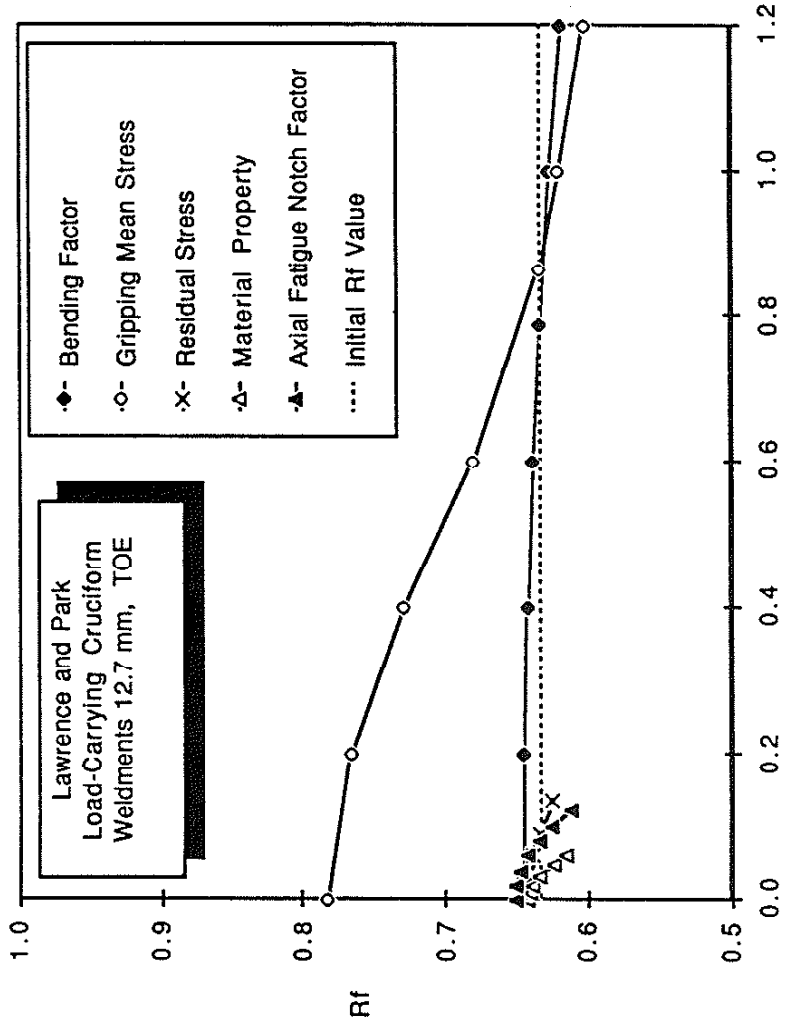

Fig. 27 Effects of uncertainty (COV) of each fatigue variable upon the reliability factor (R_F) of the fatigue strength of 12.7 mm load-carrying cruciform weldments for toe failure.

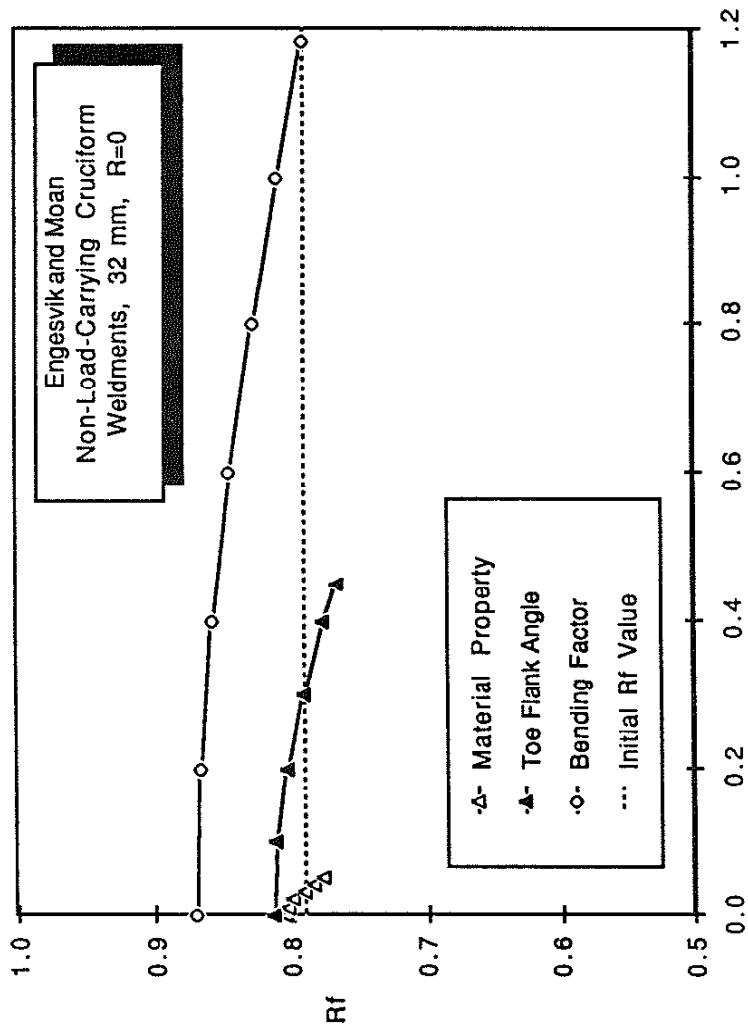

Fig. 28 Effects of uncertainty (COV) of each fatigue variable upon the reliability factor (R_F) of the fatigue strength of 32 mm non-load-carrying cruciform weldments for toe failure.

APPENDIX A. COMPTER SOFTWARE USED FOR MONTE CARLO SIMULATION

A.1 Program Listing for a Monte Carlo Simulation of Constant Amplitude Fatigue Strength.

The constant amplitude fatigue strength of Butt and non-load carrying cruciform weldments were simulated with program "CWFCIM" based on Eq.16. The output of this program can be transfered to a commercial spreadsheet program, and the statistics of the fatigue strength can be easily estimated.

```
$LARGE
      PROGRAM CWFCIM
      CHARACTER*16 FNAME1,FNAME2,FNAME3,FNAME4
      INTEGER NR,NFLAG,NDIST
      REAL R(1050),T(1050),UTS(1050),AALPHA(1050),BALPHA(1050)
      REAL THETA(1050),FKA(1050),FKB(1050),FKR(1050),FLEG(1050)
      REAL FG(1050),FT(1050),BS(1050),FBX(1050),FB(1050)
      REAL FRS(1050),FMSE1(1050),FMSE2(1050),FMSE3(1050)
      REAL FAD(1050),FRSE(1050)
      REAL SAA1(1050),SAA2(1050),SAA3(1050),GDL(1050),BEAD(1050)
      REAL C1(1050),C2(1050),C3(1050),YM,RYM,PARA1,PARA2,PARA3
      REAL FBXM,FBXS,THETAM,THETAS,BSM,BSS,FTM,FTS,UTSM,UTSS
      REAL FR,RSS,RSM,ML,SL,TM,TS,FADM,FADS,SW,BEADM,BEADS,T1
      REAL DL1,DL2,DL3,FKRSQ,ADSQ,TLAMDA,TKSAI,TMIN,TMAX
      DOUBLE PRECISION DSEED
$DEBUG
C************************************************************
C*************    OPEN   OUTPUT   FILES     ***************
C************************************************************
      WRITE(*,1010)
 1010 FORMAT(' What type of weldment?, Type 1 for Butt Weld,')
      WRITE(*,1020)
 1020 FORMAT(' Type 2 for Non-Load-Carrying Cruciform weld.')
      READ(*,*)NFLAG
      WRITE(*,1030)
 1030 FORMAT(' First Fatigue Strength Output File Name  - ',\)
      READ(*,2001) FNAME1
      OPEN(5,FILE=FNAME1,STATUS='NEW')
      WRITE(*,1040)
 1040 FORMAT(' Second Fatigue Strength Output File Name -',\)
      READ(*,2001) FNAME2
      OPEN(6,FILE=FNAME2,STATUS='NEW')
      WRITE(*,1050)
```

```
 1050 FORMAT(' Third Fatigue Strength Output File Name  -',\)
      READ(*,2001) FNAME3
      OPEN(7,FILE=FNAME3,STATUS='NEW')
      WRITE(*,1060)
 1060 FORMAT(' Factor Analysis Output File Name   ------',\)
      READ(*,2001) FNAME4
      OPEN(8,FILE=FNAME4,STATUS='NEW')
C*************************************************************
C******  INPUT DATA FOR THE RANDOM NUMBER GENERATOR *******
C*************************************************************
      WRITE(*,1070)
 1070 FORMAT(' Seed Number ?-',\)
      READ(*,*)DSEED
      WRITE(*,1080)
 1080 FORMAT(' Simulation Size (Max.=1050) ?',\)
      READ(*,*)NR
C*************************************************************
C*************   INITIALIZATION OF ARRAYS   ****************
C*************************************************************
      DO 1 I=1,NR
      AALPHA(I)=0.0
      BALPHA(I)=0.0
      THETA(I)=0.0
      FKA(I)=0.0
      FKB(I)=0.0
      FKR(I)=0.0
      T(I)=0.0
      GDL(I)=0.0
      R(I)=0.0
      FB(I)=0.0
      FG(I)=0.0
      BS(I)=0.0
      FT(I)=0.0
      FAD(I)=0.0
      FBX(I)=0.0
      FRSE(I)=0.0
      FRS(I)=0.0
      FMSE1(I)=0.0
      FMSE2(I)=0.0
      FMSE3(I)=0.0
      SAA1(I)=0.0
      SAA2(I)=0.0
      SAA3(I)=0.0
      BEAD(I)=0.0
      FLEG(I)=0.0
      C1(I)=0.0
      C2(I)=0.0
      C3(I)=0.0
   1  CONTINUE
```

```
C*************************************************************
C**********   INPUT DATA FOR THE RANDOM NUMBER    ************
C**********   GENERATION OF FATIGUE VARIABLES     ************
C*************************************************************
      WRITE(*,1090)
 1090 FORMAT(' ! Please type values for following fatigue',\)
      WRITE(*,1100)
 1100 FORMAT(' Variables. !!')
      WRITE(*,1110)
 1110 FORMAT(' M : Mean Value ')
      WRITE(*,1120)
 1120 FORMAT(' S : Standard Deviation Valuc')
      WRITE(*,1130)
 1130 FORMAT(' D : Deterministic Value')
      IF (NFLAG.EQ.2) GO TO 5010
C************   BUTT WELD GEOMETRIC COEFFICIENT   **********
      CALL GGNML(DSEED,NR,R)
      WRITE(*,1140)
 1140 FORMAT(' Flank Angle (Theta) in Degree, M & S ?',\)
      READ(*,*)THETAM,THETAS
      SL=SQRT(LOG(1+(THETAS/THETAM)**2))
      ML=LOG(THETAM)-.5*SL*SL
      DO 2 I=1,NR
      THETA(I)=EXP(R(I)*SL+ML)
      IF(THETA(I).GE.90)THETA(I)=89.
      IF(THETA(I).LE.0)THETA(I)=0.0
      THETA(I)=THETA(I)*3.14159259/180
      AALPHA(I)=.27*(TAN(THETA(I)))**.25
      BALPHA(I)=.165*(TAN(THETA(1)))**.16/
  2   CONTINUE
       IF (NFLAG.EQ.1) GO TO 5020
C*******   NON-LOAD CARRYING CRUCIFORM WELDMENTS   *********
C*******          GEOMETRIC COEFFICIENT             ********
 5010 WRITE(*,1150)
 1150 FORMAT(' What distribution for Flank Toe Angle (Theta) ?')
      WRITE(*,1160)
 1160 FORMAT(' Type  1  for Normal, 2  for Lognormal.')
      READ(*,*)NDIST
      WRITE(*,1170)
 1170 FORMAT(' Flank Angle (Theta) in Degree, M & S ?',\)
      READ(*,*)THETAM,THETAS
      IF (NDIST.EQ.2) GO TO 5030
      CALL GGNML(DSEED,NR,R)
      DO 3 I=1,NR
      THETA(I)=R(I)*THETAS+THETAM
      IF (THETA(I).LE.0.0) THETA(I)=0.0
      IF (THETA(I).GE.90) THETA(I)=89
      THETA(I)=THETA(I)*3.14159259/180
      AALPHA(I)=.35*(TAN(THETA(I)))**.25
      BALPHA(I)=.21*(TAN(THETA(I)))**.167
   3  CONTINUE
 5030 SL=SQRT(LOG(1+(THETAS/THETAM)**2))
      ML=LOG(THETAM)-.5*SL*SL
```

```
      CALL GGNML(DSEED,NR,R)
      DO 4 I=1,NR
      THETA(I)=EXP(R(I)*SL+ML)
      IF (THETA(I).LE.0.0) THETA(I)=0.0
      IF (THETA(I).GE.90) THETA(I)=89
      THETA(I)=THETA(I)*3.14159259/180
      AALPHA(I)=.35*(TAN(THETA(I)))**.25
      BALPHA(I)=.21*(TAN(THETA(I)))**.167
    4 CONTINUE
C*************    ULTIMATE TENSILE STRENGTH   ****************
 5020 CALL GGNML(DSEED,NR,R)
      WRITE(*,1180)
 1180 FORMAT(' Ultimate Tesile Strength in MPa, M & S ?',\)
      READ(*,*)UTSM,UTSS
      DO 5 I=1,NR
      UTS(I)=R(I)*UTSS+UTSM
  5   CONTINUE
C********          PLATE  -  THICKNESS             ********
      WRITE(*,1190)
 1190 FORMAT(' What distribution for thickness ?')
      WRITE(*,1200)
 1200 FORMAT(' Type 1 for normal,2 for lognormal,3 foruniform.')
      READ(*,*)NTDIST
      IF(NTDIST.NE.3)GO TO 5040
      CALL GGUBS(DSEED,NR,R)
      WRITE(*,1210)
 1210 FORMAT(' LOADING PLATE THICKNESS, Min. & Max. ?',\)
      READ(*,*)TMIN,TMAX
      DO 6 I=1,NR
      T(I)=R(I)*(TMAX-TMIN)+TMIN
  6   CONTINUE
      GO TO 5045
 5040 CALL GGNML(DSEED,NR,R)
      WRITE(*,1220)
 1220 FORMAT(' Loading Plate Thickness, M & S ?',\)
      READ(*,*)TM,TS
      IF(NTTYPE.EQ.2)GO TO 5050
      DO 7 I=1,NR
      T(I)=R(I)*TS+TM
    7 CONTINUE
      GO TO 5045
 5050 TKSAI=SQRT(LOG(1+(TS/TM)**2))
      TLAMDA=LOG(TM)-.5*TKSAI**2
      DO 8 I=1,NR
      T(I)=EXP(R(I)*TKSAI+TLAMDA)
      IF(T(I).LE.0)T(I)=ABS(T(I))
  8   CONTINUE
C********   CALCULATION OF FATIGUE NOTCH FACTOR   **********
 5045 DO 9 I=1,NR
      FKA(I)=(1.0+.00325*AALPHA(I)*(UTS(I))**0.9*T(I)**.5)
      FKB(I)=(1.0+.00325*BALPHA(I)*(UTS(I))**0.9*T(I)**.5)
      FKR(I)=FKB(I)/FKA(I)
  9   CONTINUE
```

```
C*********      MATERIAL FATIGUE STRENGTH      **************
      CALL GGNML(DSEED,NR,R)
      FTM=.95*UTSM+400
      FTS=.95*UTSS/.8
      DO 10 I=1,NR
      FT(I)=R(I)*FTS+FTM
  10  CONTINUE
C****************      B-SLOPE      ************************
      BSM=-(LOG10(2.1+917/UTSM))/6
C*********    RESIDUAL AND MEAN STRESS EFFECT    **********
      CALL GGNML(DSEED,NR,R)
      WRITE(*,1230)
 1230 FORMAT(' Maximum Tensile Residual Stress, M & S ?',\)
      READ(*,*)RSM,RSS
      DO 11 I=1,NR
      FRS(I)=R(I)*RSS+RSM
      FRSE(I)=1-FRS(I)/FT(I)
  11  CONTINUE
      WRITE(*,1240)
 1240 FORMAT(' What is the applied Mean Stress Ratio (R), D ?',\)
      READ(*,*)FR
      WRITE(*,1250)
 1250 FORMAT(' What Design Lives, give three ?')
      READ(*,*)DL1,DL2,DL3
      DO 12 I=1,NR
      FMSE1(I)=1.0/(1.0+(2*DL1)**BSM*(1.0+FR)/(1.0-FR))
      FMSE2(I)=1.0/(1.0+(2*DL2)**BSM*(1.0+FR)/(1.0-FR))
      FMSE3(I)=1.0/(1.0+(2*DL3)**BSM*(1.0+FR)/(1.0-FR))
  12  CONTINUE
C*******   BENDING FACTOR AND DISTORTION EFFECTS    *******
      WRITE(*,1260)
 1260 FORMAT(' Do you have data set for Bending Factor (x) ?')
      WRITE(*,1270)
 1270 FORMAT(' Type  1  for Yes, or  2  for No. ')
      READ(*,*) XFLAG
      IF(XFLAG.EQ.2)GO TO 5060
      CALL GGNML(DSEED,NR,R)
      WRITE(*,1280)
 1280 FORMAT(' Bending Factor (x), M & S ?')
      READ(*,*)FBXM,FBXS
      XSL=SQRT(LOG(1+(FBXS/FBXM)**2))
      XML=LOG(FBXM)-.5*XSL*XSL
      DO 13 I=1,NR
      FBX(I)=EXP(R(I)*XSL+XML)
      IF(FBX(I).LT.0)FBX(I)=ABS(FBX(I))
 13   CONTINUE
      GO TO 5065
 5060 CALL GGNML(DSEED,NR,R)
      WRITE(*,1290)
 1290 FORMAT(' Angular Distortion ( .5 d ) in Radian, M & S ?',\)
      READ(*,*)FADM,FADS
      WRITE(*,1300)
 1300 FORMAT(' How long the Gripping Distance is ?')
```

```
      WRITE(*,1310)
 1310 FORMAT(' Type 1 if less than 20 times of t, or type 2.')
      READ(*,*)NGD
      IF(NGD.EQ.2)GO TO 5070
      WRITE(*,1320)
 1320 FORMAT(' Specimen Width in mm, D ?',\)
      READ(*,*)SW
      IF (NFLAG.EQ.2) GO TO 5080
      CALL GGNML(DSEED,NR,R)
      WRITE(*,1330)
 1330 FORMAT(' Bead Width in mm, M & S ?',\)
      READ(*,*)BEADM,BEADS
      DO 14 I=1,NR
      BEAD(I)=R(I)*BEADS+BEADM
      GDL(I)=BEAD(I)+2*SW
   14  CONTINUE
      IF(NFLAG.EQ.1) GO TO 5090
 5080 CALL GGNML(DSEED,NR,R)
      WRITE(*,1340)
 1340 FORMAT(' Leg Length in mm, M & S ?',\)
      READ(*,*)FLEGM,FLEGS
      WRITE(*,1350)
 1350 FORMAT(' Attachment Plate Thickness in mm, D ?')
      READ(*,*)T1
      DO 15 I=1,NR
      FLEG(I)=R(I)*FLEGS+FLEGM
      GDL(I)=FLEG(I)*2+T1+2*SW
   15 CONTINUE
 5090 DO 16 I=1,NR
      FAD(I)=(R(I)*FADS+FADM)*2
      IF(FAD(I).LT.0)FAD(I)=ABS(FAD(I))
      FBX(I)=FAD(I)*GDL(I)/T(I)/(1+FAD(I)*.75*GDL(I)/T(I))
   16 CONTINUE
 5065 DO 17 I=1,NR
      FB(I)=(1.0-FBX(I))/(1.0+FBX(I)*(FKR(I)-1.0))
   17 CONTINUE
      GO TO 5100
 5070 DO 18 I=1,NR
      FAD(I)=(R(I)*FADS+FADM)*2
      IF(FAD(I).LT.0)FAD(I)=ABS(FAD(I))
      FG(I)=1.0/FKA(I)
      C1(I)=FG(I)*FMSE1(I)*FRSE(I)*FT(I)*(2*DL1)**BSM
      C2(I)=FG(I)*FMSE2(I)*FRSE(I)*FT(I)*(2*DL2)**BSM
      C3(I)=FG(I)*FMSE3(I)*FRSE(I)*FT(I)*(2*DL3)**BSM
   18 CONTINUE
C*************************************************************
C********   CALCULATION OF FATIGUE STRENGTH  **************
C*************************************************************
      YM=206820.
      RYM=SQRT(YM)
      DO 19 I=1,NR
      ADSQ=FAD(I)**2
      FKRSQ=FKR(I)**2
```

```
      PARA1=SQRT(.75*ADSQ*FKRSQ*YM+4*C1(I))
      PARA2=SQRT(.75*ADSQ*FKRSQ*YM+4*C2(I))
      PARA3=SQRT(.75*ADSQ*FKRSQ*YM+4*C3(I))
      SAA1(I)=C1(I)+.375*ADSQ*FKRSQ*YM-.433*FAD(I)*FKR(I)*RYM*PARA1
      SAA2(I)=C2(I)+.375*ADSQ*FKRSQ*YM-.433*FAD(I)*FKR(I)*RYM*PARA2
      SAA3(I)=C3(I)+.375*ADSQ*FKRSQ*YM-.433*FAD(I)*FKR(I)*RYM*PARA3
      FB(I)=SAA2(I)/C2(I)
 19   CONTINUE
      GO TO 5110
 5100 DO 20 I=1,NR
      FG(I)=1.0/FKA(I)
      SAA1(I)=FB(I)*FG(I)*FT(I)*FRSE(I)*FMSE1(I)*(2*DL1)**BSM
      SAA2(I)=FB(I)*FG(I)*FT(I)*FRSE(I)*FMSE2(I)*(2*DL2)**BSM
      SAA3(I)=FB(I)*FG(I)*FT(I)*FRSE(I)*FMSE3(I)*(2*DL3)**BSM
  20  CONTINUE
C*************************************************************
c**************   DATA OUTPUT COMMANDS   ******************
C*************************************************************
C
 5110 WRITE(5,1360)DSEED
      WRITE(6,1360)DSEED
      WRITE(7,1360)DSEED
      WRITE(5,1370)(SAA1(I),I=1,NR)
      WRITE(6,1370)(SAA2(I),I=1,NR)
      WRITE(7,1370)(SAA3(I),I=1,NR)
      WRITE(8,1380)(FB(I),I=1,NR)
      WRITE(8,1380)(FG(I),I=1,NR)
      WRITE(8,1380)(FT(I),I=1,NR)
      WRITE(8,1380)(FRSE(I),I=1,NR)
 2001 FORMAT(a)
 1360 FORMAT('DSEED=',E13.4,/)
 1370 FORMAT(F9.4)
 1380 FORMAT(F9.4)
      STOP
      END
```

A.2 Program Listing for a Monte Carlo Simulation of Variable Amplitude Fatigue Strength

As discussed in Section 3.5, the fatigue strength of the load-carrying cruciform weldments were simulated by the program "VWFCIM" based on Eq.28. Also the output of this program can be transferred to a commercial

spreadsheet program, and the statistics of the fatigue strength can be easily estimated.

```
$LARGE
      PROGRAM VWFCIM
      CHARACTER*16 FNAME1,FNAME2,FNAME3,FNAME4
      INTEGER NR
      REAL R(1050),FRS(1050),FKA(1050),FKB(1050),FBMS(1050)
      REAL FB(1050),FG(1050),FM(1050),FT(1050)
      REAL FBX(1050),FKR(1050),SAA1(1050),SAA2(1050)
      REAL FBXM,FBXS,FKAM,FKAS,BSM,FTM,FTS
      REAL FAMS,RSS,RSM,FKBM,FKBS,FBMSM,FBMSS,DL1,DL2
      DOUBLE PRECISION DSEED
$DEBUG
C*************************************************************
C*************    OPEN INPUT & OUTPUT FILES      **********
C*************************************************************
      WRITE(*,101)
 101  FORMAT(' INPUT DATA FILE NAME - '\)
      READ(*,201) FNAME1
 201  FORMAT(a)
      OPEN(5,FILE=FNAME1,STATUS='NEW')
      WRITE(*,102)
 102  FORMAT(' FIRST OUTPUT FILE NAME -'\)
      READ(*,201) FNAME2
      OPEN(6,FILE=FNAME2,STATUS='NEW')
      WRITE(*,103)
 103  FORMAT(' SECOND OUTPUT FILE NAME -'\)
      READ(*,201) FNAME3
      OPEN(7,FILE=FNAME3,STATUS='NEW')
      WRITE(*,104)
 104  FORMAT(' FACTOR ANALYSIS OUTPUT FILE NAME -'\)
      READ(*,201) FNAME4
      OPEN(8,FILE=FNAME4,STATUS='NEW')
C INPUT DATA FOR THE RANDOM NUMBER GENERATOR
      WRITE(*,105)
 105  FORMAT(' SEED NO. & SIMULATION SIZE ? '\)
      READ(*,*)DSEED,NR
      WRITE(5,210)DSEED,NR
 210  FORMAT(' DSEED= ',E14.5,3X,'NR= ',I6)
C*************************************************************
c*************    INITIALIZATION OF ARRAYS    *************
C*************************************************************
      DO 11 I=1,NR
      R(I)=0.0
      FB(I)=0.0
      FG(I)=0.0
      FM(I)=0.0
      FT(I)=0.0
      FBX(I)=0.0
```

```
      FKR(I)=0.0
      SAA1(I)=0.0
      SAA2(I)=0.0
      FKA(I)=0.0
      FKB(I)=0.0
      FRS(I)=0.0
      FBMS(I)=0.0
  11  CONTINUE
C*************************************************************
C**************    RANDOM NUMBER GENERATION    **************
C**************    OF FATIGUE VARIABLES        **************
C*************************************************************
CCC   GEOMETRICAL FACTOR  CCC
      CALL GGNML(DSEED,NR,R)
      WRITE(*,106)
 106  FORMAT(' MEAN & S. DEV. OF AXIAL FATIGUE NOTCH FACTOR ? '\)
      READ(*,*)FKAM,FKAS
      WRITE(5,211)FKAM,FKAS
 211  FORMAT('AXIAL FATIGUE NOTCH FACTOR, MEAN & S.DEV.= ',2F9.4)
      DO 12 I=1,NR
      FKA(I)=R(I)*FKAS+FKAM
  12  CONTINUE
CCC   MATERIAL FATIGUE STRENGTH   CCC
      CALL GGNML(DSEED,NR,R)
      WRITE(*,107)
 107  FORMAT('MEAN & S. DEV. OF FATIGUE STRENGTH COEFFICIENT? '\)
      READ(*,*)FTM,FTS
      WRITE(5,212)FTM,FTS
 212  FORMAT(' FATIGUE STRENGTH COEFF., MEAN & S.DEV.= ',2F9.4)
      DO 13 I=1,NR
      FT(I)=R(I)*FTS+FTM
  13  CONTINUE
CCC   B-SLOPE   CCC
      WRITE(*,108)
 108  FORMAT(' b-SLOPE, MEAN VALUE ONLY ? '\)
      READ(*,*)BSM
      WRITE(5,213)BSM
 213  FORMAT(' b-SLOPE, MEAN= ',F9.5)
CCC   BENDING FACTOR   CCC
      CALL GGNML(DSEED,NR,R)
      WRITE(*,109)
 109  FORMAT(' MEAN & S. DEV. OF BENDING FACTOR  ? '\)
      READ(*,*)FBXM,FBXS
      WRITE(5,214)FBXM,FBXS
 214  FORMAT(' BENDING FACTOR, MEAN & S.DEV.= ',2F9.5)
      DO 14 I=1,NR
      FBX(I)=R(I)*FBXS+FBXM
  14  CONTINUE
CCC   BENDING FATIGUE NOTCH FACTOR  CCC
      CALL GGNML(DSEED,NR,R)
      WRITE(*,110)
 110  FORMAT('MEAN & S. DEV. OF BENDING FATIGUE NOTCH FACTOR ?'\)
      READ(*,*)FKBM,FKBS
```

```
      WRITE(5,215)FKBM,FKBS
  215 FORMAT('BENDING FATIGUE NOTCH FACTOR, M. & S.DEV.=',2F9.4)
      DO 15 I=1,NR
      FKB(I)=R(I)*FKBS+FKBM
   15 CONTINUE
CCC   RATIO OF KB/KA   CCC
      DO 16 I=1,NR
      FKR(I)=FKB(I)/FKA(I)
      FB(I)=(1.0-FBX(I))/(1.0+FBX(I)*(FKR(I)-1.0))
   16 CONTINUE
C---  RESIDUAL STRESS  ---C
      CALL GGNML(DSEED,NR,R)
      WRITE(*,111)
  111 FORMAT(' MEAN & S.DEV. OF NOTCH-ROOT RESIDUAL STRESS  ? '\)
      READ(*,*)RSM,RSS
      WRITE(5,216)RSM,RSS
  216 FORMAT(' NOTCH-ROOT RESIDUAL STRESS, M. & S.DEV.= ',2F9.4)
      DO 17 I=1,NR
      FRS(I)=R(I)*RSS+RSM
   17 CONTINUE
C---  APPLIED MEAN STRESS  ---C
      WRITE(*,112)
  112 FORMAT(' DETERMINISTIC VALUE OF APPLIED MEAN STRESS  ? '\)
      READ(*,*)FAMS
      WRITE(5,217)FAMS
  217 FORMAT(' AXIAL APPLIED MEAN STRESS= ',F9.4)
C---  INDUCED MEAN STRESS  ---C
      CALL GGNML(DSEED,NR,R)
      WRITE(*,113)
  113 FORMAT(' LAMDA & KSAI OF INDUCED MEAN STRESS ? '\)
      READ(*,*)FBMSM,FBMSS
      WRITE(5,218)FBMSM,FBMSS
  218 FORMAT(' INDUCED MEAN STRESS, LAMDA & KSAI= ',2F9.4)
      DO 18 I=1,NR
      FBMS(I)=EXP(R(I)*FBMSS+FBMSM)
   18 CONTINUE
      DO 19 I=1,NR
      FM(I)=1.0-(FRS(I)+FKA(I)*FAMS+FKB(I)*FBMS(I))/FT(I)
   19 CONTINUE
C*************************************************************
C************   CALCULATION OF FATIGUE STRENGTH   *********
C*************************************************************
      WRITE(*,114)
  114 FORMAT(' DESIGN LIVES, SELECT TWO ?  '\)
      READ(*,*)DL1,DL2
      WRITE(5,219)DL1,DL2
  219 FORMAT(' DESIGN LIVES= ',2E14.5)
      DO 20 I=1,NR
      FG(I)=1.0/FKA(I)
      SAA1(I)=FT(I)*FG(I)*FB(I)*FM(I)*(2*DL1)**BSM
      SAA2(I)=SAA1(I)*(DL2/DL1)**BSM
   20 CONTINUE
```

```
C*************************************************************
c**************   DATA OUTPUT COMMANDS   ********************
C*************************************************************
      WRITE(6,203)DSEED
      WRITE(7,203)DSEED
 203  FORMAT('DSEED=',E13.4,/)
      WRITE(6,204)(SAA1(I),I=1,NR)
      WRITE(7,204)(SAA2(I),I=1,NR)
      WRITE(8,205)(FT(I),I=1,NR)
      WRITE(8,205)(FG(I),I=1,NR)
      WRITE(8,205)(FB(I),I=1,NR)
      WRITE(8,205)(FM(I),I=1,NR)
 204  FORMAT(F9.4)
 205  FORMAT(F9.4)
      STOP
      END
```

Appendix B. FATIGUE TESTING OF LOAD-CARRYING CRUCIFORM WELDMENTS

B.1 Specimen Preparation

Load-carrying cruciform weldments were fabricated from ASTM A-36 steel plates by welding in the horizontal welding position using Shielded Metal Arc Welding (SMAW) and E7018 electrodes. The welding parameters were 17 to 22 Volts, 125 to 230 Amperes; no preheat or interpass temperatures were used.

The geometry and dimensions of 12.7 mm thick test specimen are shown in Fig. B1. The specimen consists of a center plate and two loading plates welded to the center plate by wrap-around fillet welds. The 12.7 mm thick loading plates were welded to the 15.9 mm thick center plate. The leg size of the fillet weld was nominally 9.5 mm. For the 6.35 mm thick specimens, 6.35 mm thick loading plates, and 7.9 mm thick center plates were used. The fillet weld leg sizes were nominally 4.76mm to maintain similitude.

The potential sites of fatigue crack initiation are labeled in Fig. B2. Each weldment had four possible weld toe and two incomplete joint penetration (IJP) sites for fatigue crack initiation. Several test pieces were machined to eliminate the wrap-around welds as shown in Fig. B3.

B.2 Procedure of Fatigue Testing and Data Measurements

Strain gauges were mounted near the weld toes on each specimen. Gauges were mounted in pairs on either side of the specimens so that both the axial and bending components of the applied and induced stresses could be measured. Specimens were mounted in a 100 kip MTS frame and gripped using

self-aligning hydraulic grips. The stresses generated during gripping were minimized by the self-aligning feature of the grips, but stresses were induced which were measured for each specimen with the strain gauges and recorded.

A "ship block load history" was used in this study. The history was based on the distribution of scratch gauge measurement data of ship structure [52] and edited to reduce the number of small cycles. More details about the creation of "Ship Block Load History" are given in the next section.

Tests were begun by applying one cycle of the largest stress cycle in the variable ship block history. During this first cycle, the (induced) bending stresses were measured and recorded. Generally, both the (induced) static and cyclic bending stresses were quite large because this structural detail (Fig. B1) inevitably experienced welding distortions during fabrication due to the nature of the joint and because of the use of an SMAW welding procedure. The inevitable variations in geometry and the differences in resulting stress state due to the differing amounts of induced gripping (mean stress) and cyclic bending stresses requires one to think of each test as being unique despite the intended similarity of the test pieces and despite the fact that they were all subjected to identical applied stress histories.

Following the initial static application of the largest cycle of the block, the ship block load history shown in Fig. B4 was repeated until the specimen failed or until 1,500 blocks (7.6×10^6 cycles) had been applied.

The average nominal mean stress level was zero for most tests, but several specimens were tested with tensile average nominal mean stress levels which were 72.4 and 144.8 MPa. Total of twenty one specimens with

wrap-around weldments (Fig. B1) (thirteen 12.7 mm plate-thickness, eight 6.35 mm plate-thickness), and four specimens without wrap-around weldments (Fig. B3) (two 12.7 mm plate-thickness, two 6.35 mm plate-thickness) were tested.

B.3 Determination of Ship Block Load History

The Weibull distribution has been demonstrated to be an appropriate probability distribution for long-term histories through comparison with actual data such as the SL-7 container ship history [52] which is as shown in Fig. B5.

Munse [9] used the 36,011 scratch SL-7 gauge measurements or records taken over four-hour periods. Each Measurement or short history contained 1,920 cycles. The biggest "grand cycle" of each history was termed an occurrence, and the 36,011 occurrences were assembled into the histogram shown in Fig. B6 and fitted with Weibull distribution(k=1.2, w=4.674). This Weibull distribution was assumed to represent the histogram for the entire history composed of 52,000 short histories containing 1,920 cycles each, or 10^8 cycles. Using the fitted Weibull distribution, Munse estimated the maximum stress range expected during the ship life of 10^8 cycles (S_{10}-8) by assuming that the probability associated with this stress range would be $1/10^8$ cycles, that is , equal to that for the largest occurrence. From this argument and the fitted Weibull distribution, maximum stress range of 235 MPa (34.11) ksi was calculated as the maximum stress in the 20 year ship life history for the location at which the stress history was recorded.

The SL-7 history and Munse's Weibull distribution representation of it was adopted for use in this study. The next problem was to create a typical

history, that is a sequence of stress ranges which represented the typical ship experience (period of normal sea state interdispersed with storm episodes), which conformed to the overall Weibull distribution. Furthermore, to permit long-life fatigue testing, the history had to be edited to remove cycles which cause little fatigue damage but needlessly extend the required testing time. It was decided to edit the history so that one "block" would contain only 5,047 cycles and yet contain the most damaging events in a typical one month (345,600 cycles) ship history: see Fig. B4.

The first step was to decide which of the events in the SL-7 history were the most damaging and which were the least damaging and could therefore be omitted. The damage calculated for a given interval of stress range of the SL-7 history depends upon three things: the method of summing damage (linear accumulative damage or Miner's rule was used); the assessment of damage caused by a given stress range (we used the I-P model [28] rather than the extended S-N approach of Munse and this makes a big difference in what can be omitted); and the degree of stress concentration by the weld defects to be studied (we assumed a maximum fatigue notch factor ($K_{f\ max}$) typical for Detail No. 20 as $K_{f\ max} = 4.9$).

The justification for adhering to the predictions of our I-P model is that it has given reasonable estimates of weldment fatigue life under variable load histories in laboratory air
[53]. A major Difference between the I-P model and Munse's approach is the anticipated behavior of the weldments in the long life region. Fig. B7 shows the extended line assumption of the Munse Fatigue Design Procedure (MFDP). Use of the extended line exaggerates the importance of the smaller stress ranges and leads to the conclusion that they can not be deleted. The I-P model predicts that the S-N curve has a slope of about 1:10 in the long

life region and consequently, predicts a lesser importance for the smaller stress ranges: see Fig. B8.

We used the following strategy for editing the SL-7 history. If each cycle had an average period of 7.5 seconds as reported, a one month ship history would consist of 345,600 cycles [52]. Keeping only those stress ranges which contributed 92.8% of the total Damage (estimated using the I-P model and Miner's rule, see Fig. B7) leads to the elimination of stress range less than 68.9 MPa (10 ksi) and greater than 152 MPa (22 ksi). This decision would permit a reduction in length of the one month history from 345,600 (total) cycles to 5,047 cycles. Fig. B4 shows the actual "one-month history" which starts with a period of low stress range, 75.8 MPa(11 ksi), and gradually increases to a maximum of 145 MPa (21 ksi) during the central storm period after which the amplitude decreased to the original 75.8 MPa (11 ksi). At a testing frequency of 5 Hz, a block will require about 17 minutes. Since a 5,047 cycle block represents 345,600 cycles in service, 290 blocks, or 3.5 days of testing at 5 Hz or 10-15 days at lower testing frequencies are equivalent to a 10^8 cycles service history or 24 years of service. The ship block load history shown in Fig. B4 was read into the memory of a function generator which controlled a 100 kip MTS fatigue testing machine.

B.4 Fatigue Test Results

Each tested specimen was sectioned to measure the dimensions of the welds and IJP and to study the pattern of fatigue initiation and propagation; see Figs. B9 and B10. Because there was almost simultaneous

initiation and growth from both the weld toe and IJP, there were two basic patterns of failure: IJP domination and toe domination.

In the rare cases in which the induced gripping and cyclic bending stresses were small, failure initiated at the most serious stress concentrator, the IJP; and a reasonably easy-to-interpret series of events occurred: the fatigue crack initiated at both sides of the IJP and propagated to failure as shown in Fig. B9 and in Fig. 10.

When the induced bending stresses were larger, fatigue cracks initiated at both the weld toe having the greatest applied bending stress and at both the IJP notches. Because there was an interaction between the toes and the IJP resulting in a higher stress concentration at each, initiation and growth at both the toe and nearest IJP tip accelerated growth at both sites. However, continued fatigue crack growth at the active toe ultimately reduced the stresses at the nearest IJP tip causing fatigue crack growth there to cease. Because of changes in the directions of the principal stresses or the presence of the large IJP (or both) the toe crack inevidently did not progress directly across the plate thickness toward the opposing toe but curved "downward" toward the IJP and, just before intersecting the IJP, a small limit-load failure occurred linking the toe crack with the IJP. At this point, the fatigue crack growth at the opposite IJP tip was greatly accelerated; and failure occurred soon after.

The fatigue test results are listed in Tables 4 through 6. Table 4 contains the test results for the thirteen 12.7 mm thick specimens with wrap-around weldments. Table 5 contains the test results for the eight 6.35 mm thick specimens with wrap-around weldments. Table 6 contains the test results for the four specimens without wrap-around weldments. Each table contains the blocks to failure, the locations on the specimen at which

failure originated (F) or at which a fatigue crack was observed to initiate but not propagate to failure (I). As sketched in Fig. B2, this structural detail has six possible crack initiation sites : four weld toes (TOE 1-4) and two incomplete joint penetrations (IJP 1-3 and IJP 2-4). The dimensions of the weld toes and the length of the IJPs are listed for each as well as the applied mean stress, induced gripping stress and the bending factor x (the ratio of the induced cyclic bending stress range to the total cyclic stress range measured on the surface of the plate near the weld toe).

Figure B11 gives the S-N fatigue test results of the 12.7 mm and 6.35 mm thick specimens with zero average applied mean stress. The axis of stress range indicates the equivalent constant amplitude stress range (ΔS_e) which is based on the Miner's linear damage rule and S-N relationship (log C=11.57, m=4.619) for this structural detail from the University of Illinois Fatigue Data Bank [10], and the axis of life indicates the cycles to failure obtained by multiplying the blocks to failure to the 5047 cycles which is the number of cycles per block.

Table B1

Loading Conditions and Weldment Geometry for the 12.7 mm Thick Load-Carrying Cruciform Weldments Tested Using the Ship Block Load History

Spec. No.	Sites	Mean Stress (ksi)	Grip Stress (ksi)	Bending Factor	Geometry+ L1 (in.)	L2 (in.)	C (in.)	Failure Sites*	Fatigue Life (Blocks)
H-1	IJP 1-3	0.00	2.06	0.02	.304	.404	.250	F	926
	TOE 1	0.00	2.06	0.02	.304	.404	.250		
	TOE 3	0.00	-1.60	0.06	.369	.436	.250		
	IJP 2-4	0.00	0.67	0.14	.400	.408	.238		
	TOE 2	0.00	0.67	0.14	.400	.408	.238		
	TOE 4	0.00	-0.30	-0.13	.412	.445	.238		
H-2	IJP 1-3	0.00	3.70	0.14	.330	.370	.250		769
	TOE 1	0.00	3.70	0.14	.330	.370	.250		
	TOE 3	0.00	-5.4	0.02	.348	.375	.250		
	IJP 2-4	0.00	5.6	-0.25	.453	.411	.241	F	
	TOE 2	0.00	5.6	-0.25	.453	.411	.241		
	TOE 4	0.00	-5.4	-0.34	.357	.409	.241		
H-3	IJP 1-3	0.00	6.2	0.19	.365	.398	.245	F	1291
	TOE 1	0.00	-5.7	-0.10	.455	.439	.245		
	TOE 3	0.00	6.2	0.19	.365	.398	.245		
	IJP 2-4	0.00	-4.5	-0.03	.461	.425	.250		
	TOE 2	0.00	-4.5	-0.03	.461	.425	.250		
	TOE 4	0.00	5.4	-0.01	.355	.450	.250		
H-4	IJP 1-3	0.00	6.3	-0.03	.350	.434	.246		1414
	TOE 1	0.00	6.3	-0.03	.350	.434	.246		
	TOE 3	0.00	-0.2	-0.30	.342	.450	.246		
	IJP 2-4	0.00	-1.9	0.01	.375	.368	.234	F	
	TOE 2	0.00	2.1	0.06	.391	.393	.234		
	TOE 4	0.00	-1.9	0.01	.375	.368	.234		
H-5	IJP 1-3	0.00	-18.7	0.0	.367	.453	.250	I	416
	TOE 1	0.00	-18.7	0.0	.367	.453	.250		
	TOE 3	0.00	17.7	0.16	.378	.472	.250		
	IJP 2-4	0.00	-14.9	0.0	.350	.433	.250	I	
	TOE 2	0.00	-14.9	0.0	.350	.433	.250		
	TOE 4	0.00	14.8	0.13	.369	.492	.250	F	

+: See Fig. B2

*: F denotes a site causing fatigue failure.
I denotes a site initiating a fatigue crack but not involved in the final fatigue failure.

Table B1 (Continued)

Spec. No.	Sites	Mean Stress (ksi)	Grip Stress (ksi)	Bending Factor	Geometry+ L1 (in.)	L2 (in.)	C (in.)	Failure Sites*	Fatigue Life (Blocks)
H-6	IJP 1-3	0.00	29.5	0.23	.370	.413	.250		303
	TOE 1	0.00	29.5	0.23	.370	.413	.250		
	TOE 3	0.00	-28.4	-0.06	.351	.472	.250		
	IJP 2-4	0.00	-27.5	-0.01	.265	.433	.250	F	
	TOE 2	0.00	27.0	0.14	.353	.531	.250	F	
	TOE 4	0.00	-27.5	-0.01	.265	.433	.250		
H-7	IJP 1-3	10.5	-0.8	-0.08	.480	.421	.223	F	269
	TOE 1	10.5	2.3	0.15	.335	.400	.223	F	
	TOE 3	10.5	-0.8	-0.08	.480	.421	.223		
	IJP 2-4	10.5	2.0	0.12	.463	.448	.234	I	
	TOE 2	10.5	2.0	0.12	.463	.448	.234		
	TOE 4	10.5	-0.6	-0.08	.384	.450	.234		
H-8	IJP 1-3	10.5	17.1	-0.05	.405	.406	.230	I	207
	TOE 1	10.5	-14.8	0.22	.345	.446	.230		
	TOE 3	10.5	17.1	-0.05	.405	.406	.230		
	IJP 2-4	10.5	-16.3	0.07	.439	.429	.214	F	
	TOE 2	10.5	-16.3	0.07	.439	.429	.214		
	TOE 4	10.5	20.5	0.39	.353	.450	.214	F	
H-9	IJP 1-3	10.5	-2.9	0.07	.339	.483	.250	F	678
	TOE 1	10.5	5.2	-0.22	.333	.473	.250		
	TOE 3	10.5	-2.9	0.07	.339	.483	.250	F	
	IJP 2-4	10.5	-4.4	-0.07	.402	.434	.233		
	TOE 2	10.5	4.4	0.08	.378	.467	.233		
	TOE 4	10.5	-4.4	-0.07	.402	.434	.233		
H-10	IJP 1-3	10.5	-5.6	0.08	.428	.467	.234	F	211
	TOE 1	10.5	-5.6	0.08	.428	.467	.234		
	TOE 3	10.5	5.9	-0.04	.346	.483	.234	F	
	IJP 2-4	10.5	-9.3	0.01	.334	.386	.246	I	
	TOE 2	10.5	-9.3	0.01	.334	.386	.246		
	TOE 4	10.5	9.8	0.05	.360	.510	.246		

+: See Fig. B2

*: F denotes a site causing fatigue failure.
I denotes a site initiating a fatigue crack but not involved in the final fatigue failure.

Table B1 (Continued)

Spec. No.	Sites	Mean Stress (ksi)	Grip Stress (ksi)	Bending Factor	Geometry+ L1 (in.)	L2 (in.)	C (in.)	Failure Sites*	Fatigue Life (Blocks)
H-11	IJP 1-3	21.0	3.3	0.12	.355	.381	.245	F	232
	TOE 1	21.0	3.3	0.12	.355	.381	.245	F	
	TOE 3	21.0	-1.5	-0.04	.375	.387	.245		
	IJP 2-4	21.0	1.0	0.05	.365	.404	.248	I	
	TOE 2	21.0	1.0	0.05	.365	.404	.248	I	
	TOE 4	21.0	1.7	-0.09	.325	.420	.248		
H-12	IJP 1-3	21.0	-13.4	0.12	.425	.410	.244	F	184
	TOE 1	21.0	14.8	-0.07	.356	.460	.244	F	
	TOE 3	21.0	-13.4	0.12	.425	.410	.244		
	IJP 2-4	21.0	-7.87	0.14	.451	.388	.250	F	
	TOE 2	21.0	8.8	0.01	.412	.412	.250		
	TOE 4	21.0	-7.87	0.14	.451	.388	.250		
H-13	IJP 1-3	21.0	15.4	0.08	.350	.401	.233	F	173
	TOE 1	21.0	-12.9	0.17	.336	.463	.233		
	TOE 3	21.0	15.4	0.08	.350	.401	.233	I	
	IJP 2-4	21.0	-4.73	0.28	.396	.431	.232		
	TOE 2	21.0	-4.73	0.28	.396	.431	.232		
	TOE 4	21.0	8.77	0.12	.328	.459	.232		

+: See Fig. B2

*: F denotes a site causing fatigue failure.

I denotes a site initiating a fatigue crack but not involved in the final fatigue failure.

Table B2

Loading Conditions and Weldment Geometry for the 6.35 mm Thick Load-Carrying Cruciform Weldments Tested Using the Ship Block Load History

Spec. No.	Sites	Mean Stress (ksi)	Grip Stress (ksi)	Bending Factor	Geometry L1 (in.)	Geometry L2 (in.)	Geometry C (in.)	Failure Sites	Fatigue Life (Blocks)
Q-1	IJP 1-3	10.5	-12.8	0.09	.184	.188	.125	F	306
	TOE 1	10.5	15.3	0.21	.139	.234	.125	F	
	TOE 3	10.5	-12.8	0.09	.184	.188	.125		
	IJP 2-4	10.5	13.0	0.16	.182	.172	.125		
	TOE 2	10.5	13.0	0.16	.182	.172	.125		
	TOE 4	10.5	-10.6	0.17	.183	.203	.125		
Q-2	IJP 1-3	10.5	30.6	0.17	.160	.219	.177	F	292
	TOE 1	10.5	-31.0	-0.12	.213	.234	.177		
	TOE 3	10.5	30.6	0.17	.160	.219	.177	F	
	IJP 2-4	10.5	-24.8	-0.06	.150	.234	.125		
	TOE 2	10.5	-24.8	-0.06	.150	.234	.125		
	TOE 4	10.5	24.1	0.12	.159	.266	.125		
Q-3	IJP 1-3	0.0	10.2	0.13	.168	.172	.125		787
	TOE 1	0.0	10.2	0.13	.168	.172	.125		
	TOE 3	0.0	-10.3	0.12	.163	.203	.125		
	IJP 2-4	0.0	-7.4	0.00	.196	.172	.125	F	
	TOE 2	0.0	7.2	0.21	.185	.188	.125		
	TOE 4	0.0	-7.4	0.00	.196	.172	.125		
Q-4	IJP 1-3	0.0	-7.2	0.03	.168	.172	.125	F	415
	TOE 1	0.0	-7.2	0.03	.168	.172	.125		
	TOE 3	0.0	6.2	0.28	.162	.203	.125	F	
	IJP 2-4	0.0	-8.2	0.18	.192	.188	.125		
	TOE 2	0.0	-8.2	0.18	.192	.188	.125		
	TOE 4	0.0	7.1	0.32	.200	.234	.125		
Q-5	IJP 1-3	0.0	9.7	0.23	.198	.188	.125		708
	TOE 1	0.0	9.7	0.23	.198	.188	.125	F	
	TOE 3	0.0	-9.2	0.00	.163	.203	.125		
	IJP 2-4	0.0	11.4	0.12	.200	.203	.125		
	TOE 2	0.0	11.4	0.12	.200	.203	.125		
	TOE 4	0.0	-10.9	0.00	.157	.219	.125		

+: See Fig. B2

*: F denotes a site causing fatigue failure.
I denotes a site initiating a fatigue crack but not involved in the final fatigue failure.

Table B2 (Continued)

Spec. No.	Sites	Mean Stress (ksi)	Grip Stress (ksi)	Bending Factor	Geometry+ L1	L2	C (in.)	Failure Sites*	Fatigue Life (Blocks)
Q-6	IJP 1-3	0.0	13.6	0.04	.217	.219	.125		369
	TOE 1	0.0	-13.0	0.14	.153	.219	.125		
	TOE 3	0.0	13.6	0.04	.217	.219	.125		
	IJP 2-4	0.0	7.57	0.23	.199	.216	.167	F	
	TOE 2	0.0	-6.97	-0.19	.151	.250	.167		
	TOE 4	0.0	7.57	0.23	.199	.216	.167	F	
Q-7	IJP 1-3	0.0	-7.7	-0.07	.179	.177	.125		267
	TOE 1	0.0	6.8	0.10	.200	.217	.125		
	TOE 3	0.0	-7.7	-0.07	.179	.177	.125		
	IJP 2-4	0.0	10.2	0.19	.206	.177	.125	F	
	TOE 2	0.0	10.2	0.19	.206	.177	.125	F	
	TOE 4	0.0	-10.6	-0.03	.160	.177	.125		
Q-8	IJP 1-3	0.0	-8.3	-0.07	.190	.203	.125	F	506
	TOE 1	0.0	8.0	0.19	.195	.219	.125	F	
	TOE 3	0.0	-8.3	-0.07	.190	.203	.125		
	IJP 2-4	0.0	4.2	0.12	.189	.211	.125		
	TOE 2	0.0	4.2	0.12	.189	.211	.125		
	TOE 4	0.0	-4.3	0.03	.127	.203	.125		

+: See Fig. B2

*: F denotes a site causing fatigue failure.
I denotes a site initiating a fatigue crack but not involved in the final fatigue failure.

Table B3

Loading Conditions and Weld Geometry for the Cut-out Specimens of Load-Carrying Cruciform Weldments Tested using the Ship Block Load History

Spec. No.	Sites	Mean Stress (ksi)	Grip Stress (ksi)	Bending Factor (x)	Geometry L1 (in.)	L2 (in.)	C (in.)	Failure Sites	Fatigue Life (Block)
C-3	IJP 1-3	0.0	29.7	-0.18	.331	.413	.250		252
	TOE 1	0.0	-29.2	0.20	.372	.433	.250		
	TOE 3	0.0	29.7	-0.18	.331	.413	.250		
	IJP 2-4	0.0	-29.5	-0.10	.359	.453	.250	F	
	TOE 2	0.0	-29.5	-0.10	.359	.453	.250		
	TOE 4	0.0	29.6	0.21	.333	.472	.250	F	
C-4	IJP 1-3	0.0	-24.6	0.27	.383	.394	.250	F	320
	TOE 1	0.0	-24.6	0.27	.383	.394	.250		
	TOE 3	0.0	24.3	0.02	.336	.492	.250	F	
	IJP 2-4	0.0	20.2	0.30	.385	.453	.250		
	TOE 2	0.0	-20.5	-0.19	.391	.453	.250		
	TOE 4	0.0	20.2	0.30	.385	.453	.250		
C-5	IJP 1-3	0.0	-8.4	0.01	.160	.188	.125	F	338
	TOE 1	0.0	8.3	0.15	.161	.219	.125	F	
	TOE 3	0.0	-8.4	0.01	.160	.188	.125		
	IJP 2-4	0.0	7.9	0.00	.164	.203	.125		
	TOE 2	0.0	7.9	0.00	.164	.203	.125		
	TOE 4	0.0	-7.3	-0.24	.161	.203	.125		
C-6	IJP 1-3	0.0	15.0	0.17	.185	.203	.125	F	49/
	TOE 1	0.0	15.0	0.17	.185	.203	.125	I	
	TOE 3	0.0	-14.5	0.04	.188	.297	.125		
	IJP 2-4	0.0	15.7	0.15	.160	.219	.125		
	TOE 2	0.0	15.7	0.15	.160	.219	.125		
	TOE 4	0.0	-15.5	0.05	.161	.234	.125		

+: See Fig. B2

*: F denotes a site causing fatigue failure.
I denotes a site initiating a fatigue crack but not involved in the final fatigue failure.

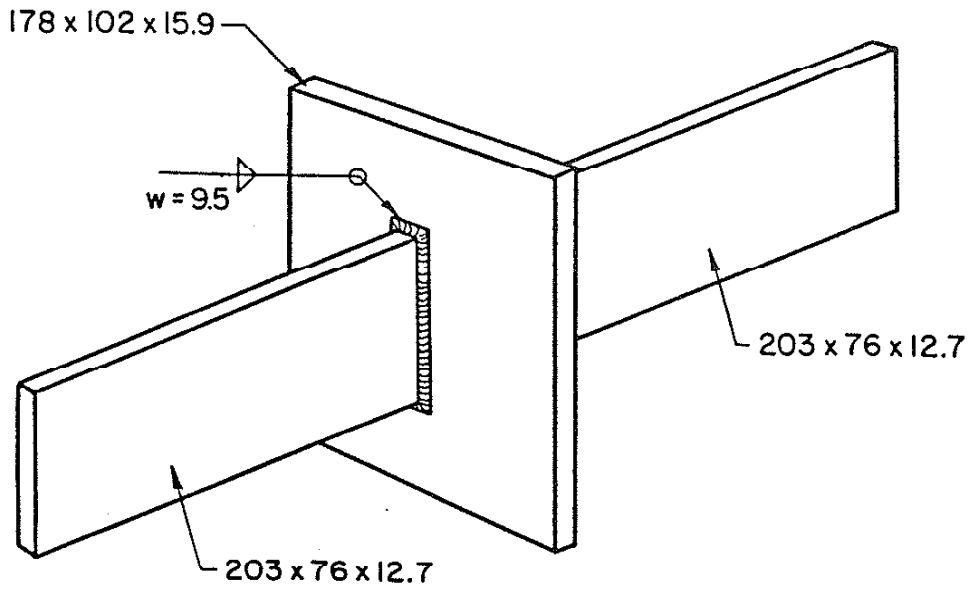

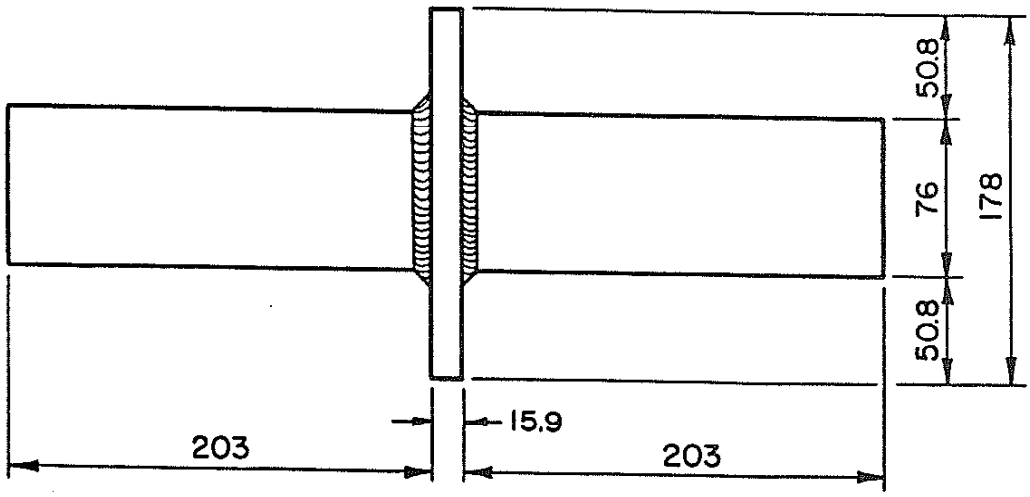

Fig. B1 Geometry and dimensions for testpieces of load-carrying cruciform weldments used in this study. (Dimensions in mm.)

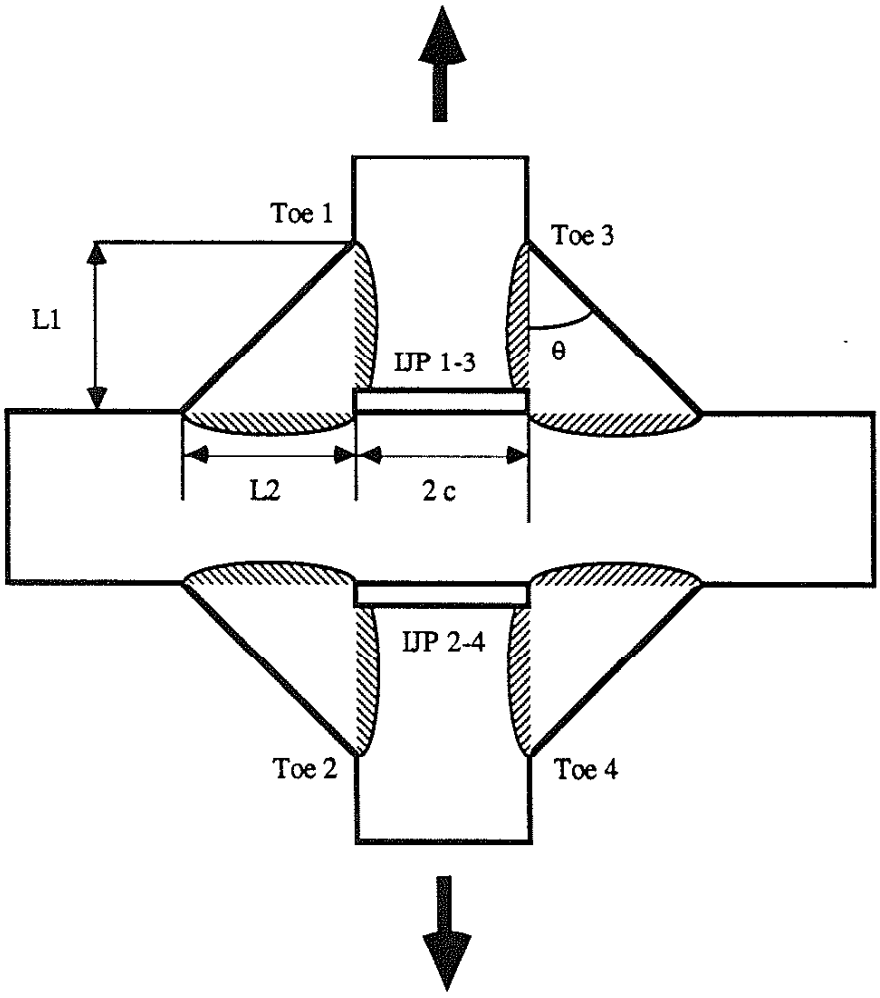

Fig. B2 Schematic description of possible crack initiation locations and geometric parameters of load-carrying cruciform weldments.

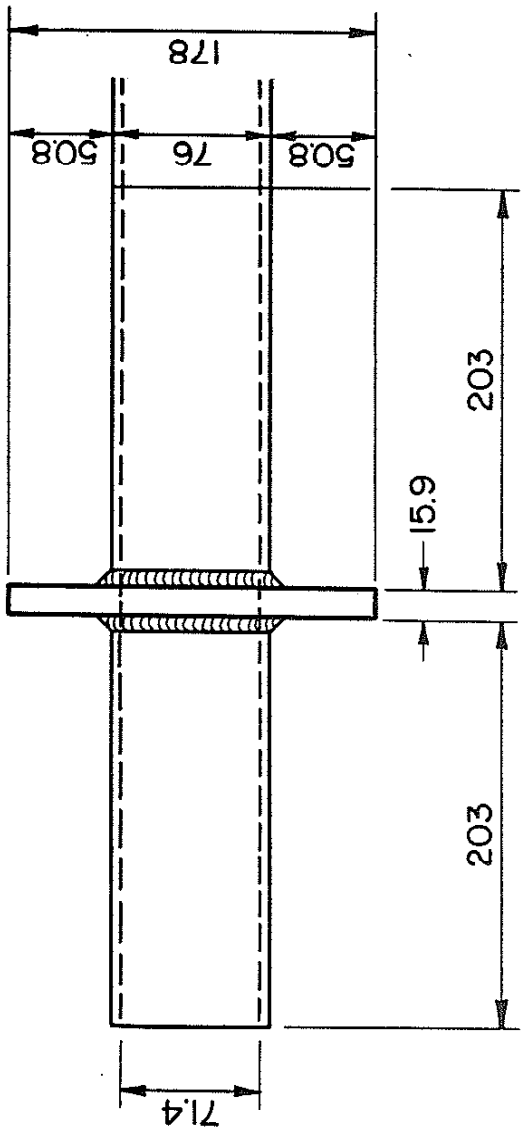

Fig. E3 Geometry and dimensions of 12.7 mm thick testpieces of load-carrying cruciform weldments without wrap-around weld.

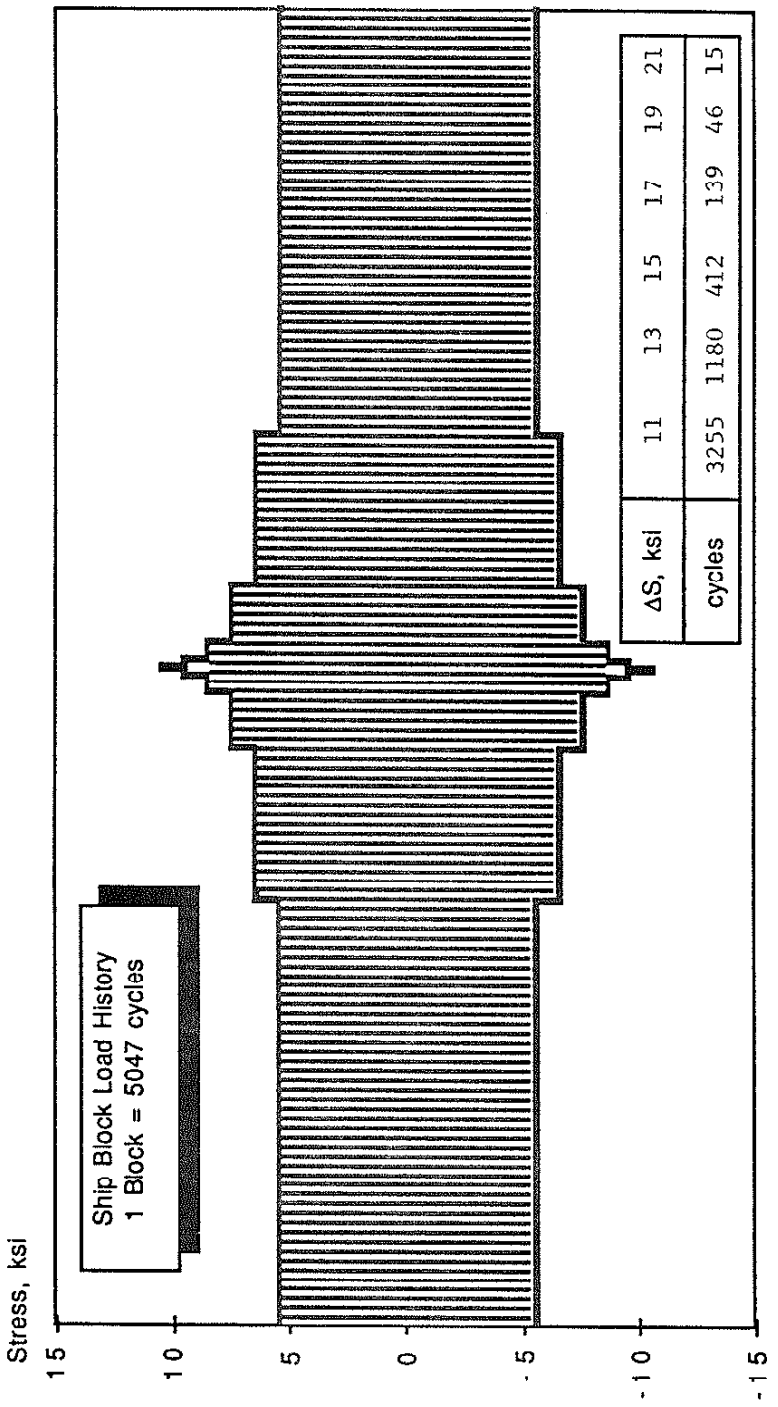

Fig. B4 Plot of one block of the constructed ship block load history having the 92.8% of the SL-7 container ship history damage. The central portion of the history represents a period of severe weather.

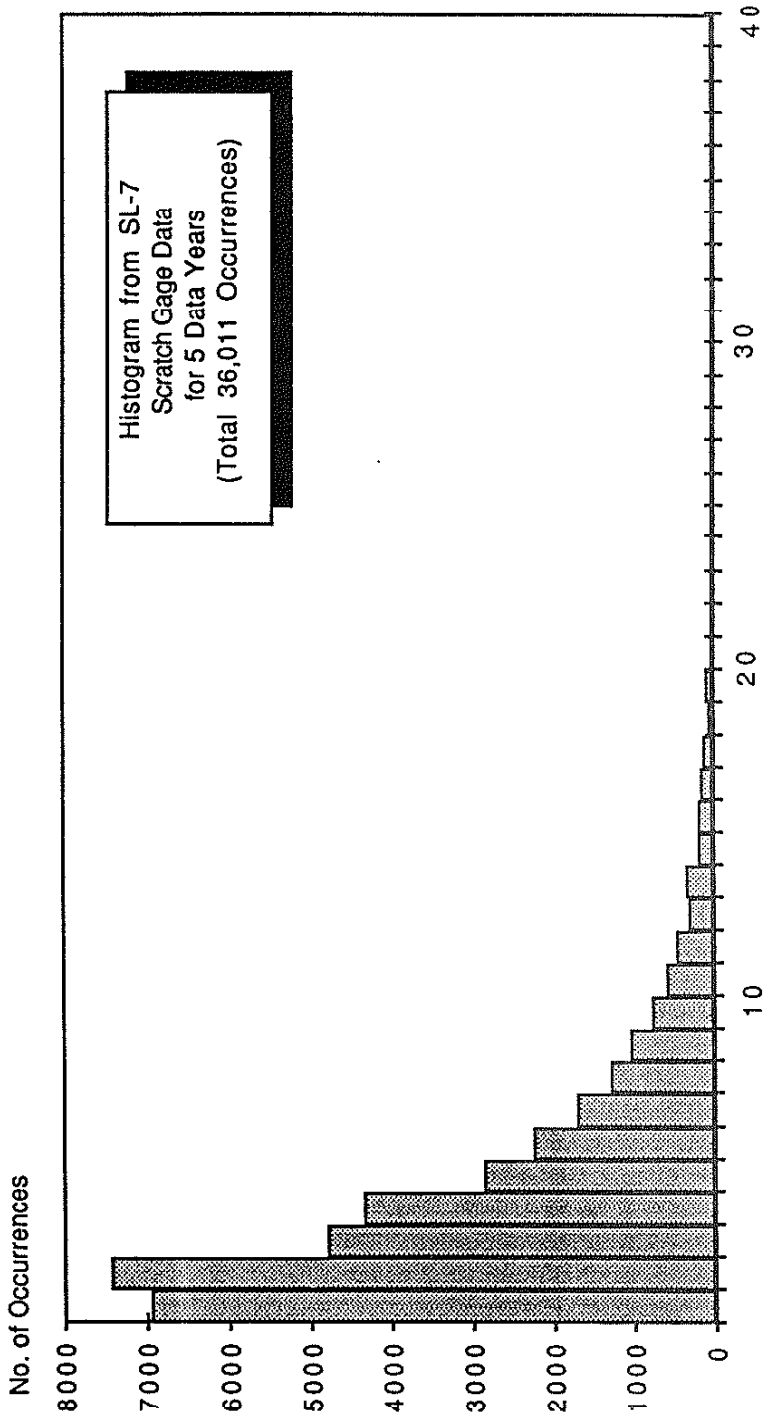

Fig. B5 Histogram from the SL-7 container ship scratch gage data. The number of occurrences during a 5 year history is plotted as a function of maximum peak-to-trough stress range [52].

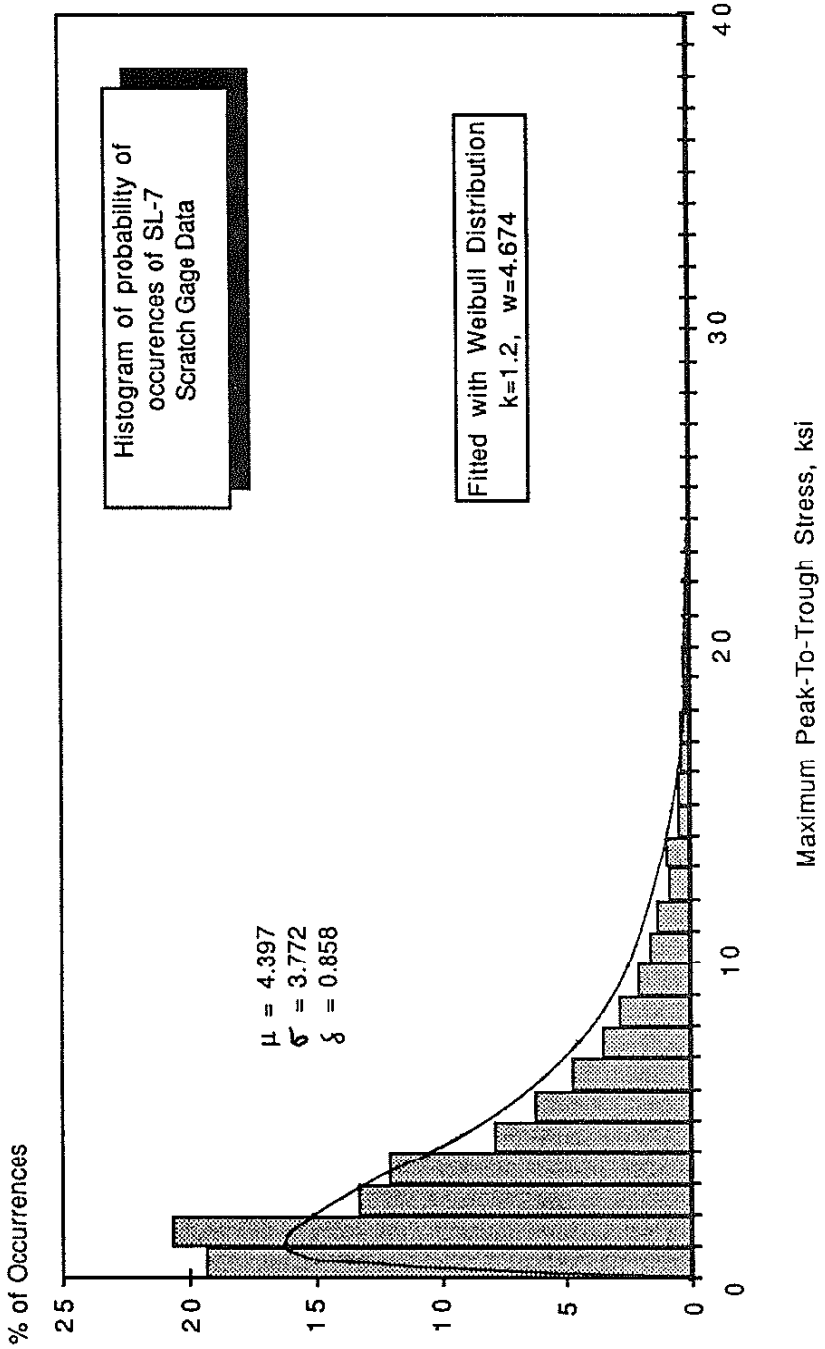

Fig. B6 Histogram from the SL-7 container ship scratch gage data fitted with a Weibull distribution [9].

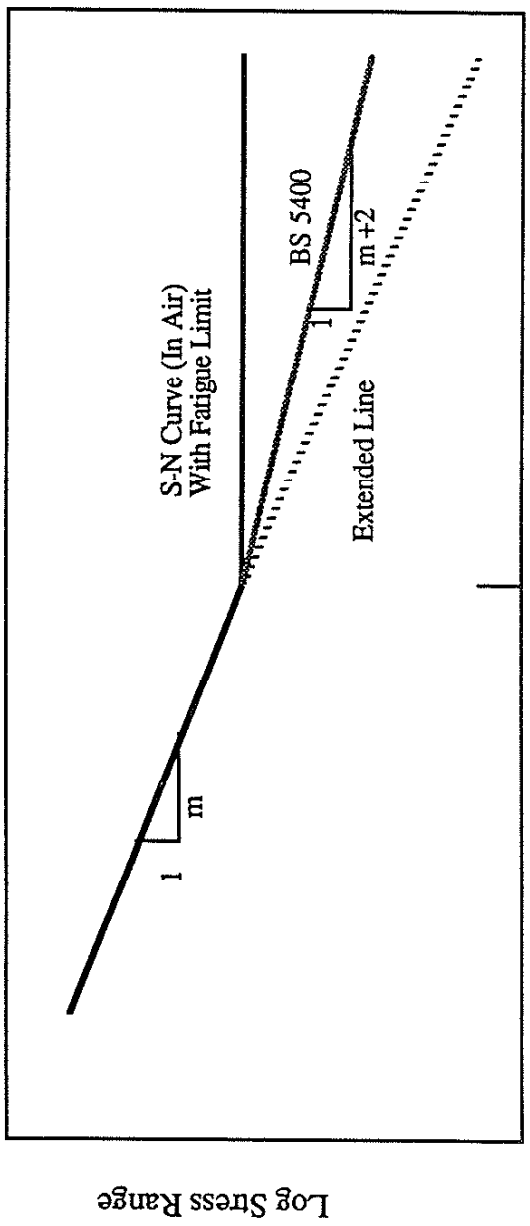

Fig. B7 Three suggested shapes of the S-N diagram in the long-life region.

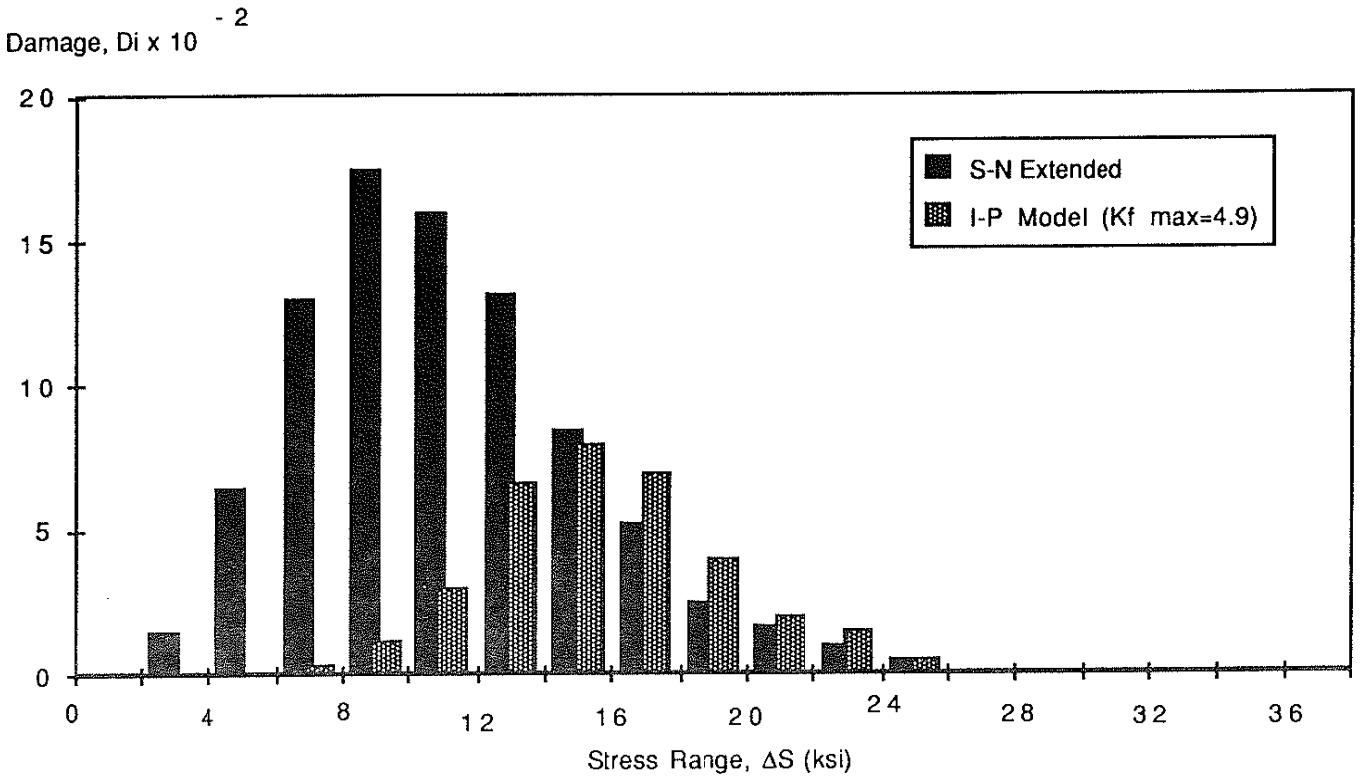

Fig. B8 Calculated damage attributable to each stress range interval for a Weibull distribution based on the 108 cycle container ship history [44]. Damage was calculated using both the extended S-N curve and the I-P model as shown. The damage estimated depend upon the assumed shape of the S-N diagram in the high cycle region as well as the severity of the stress concentration K_{fmax}.

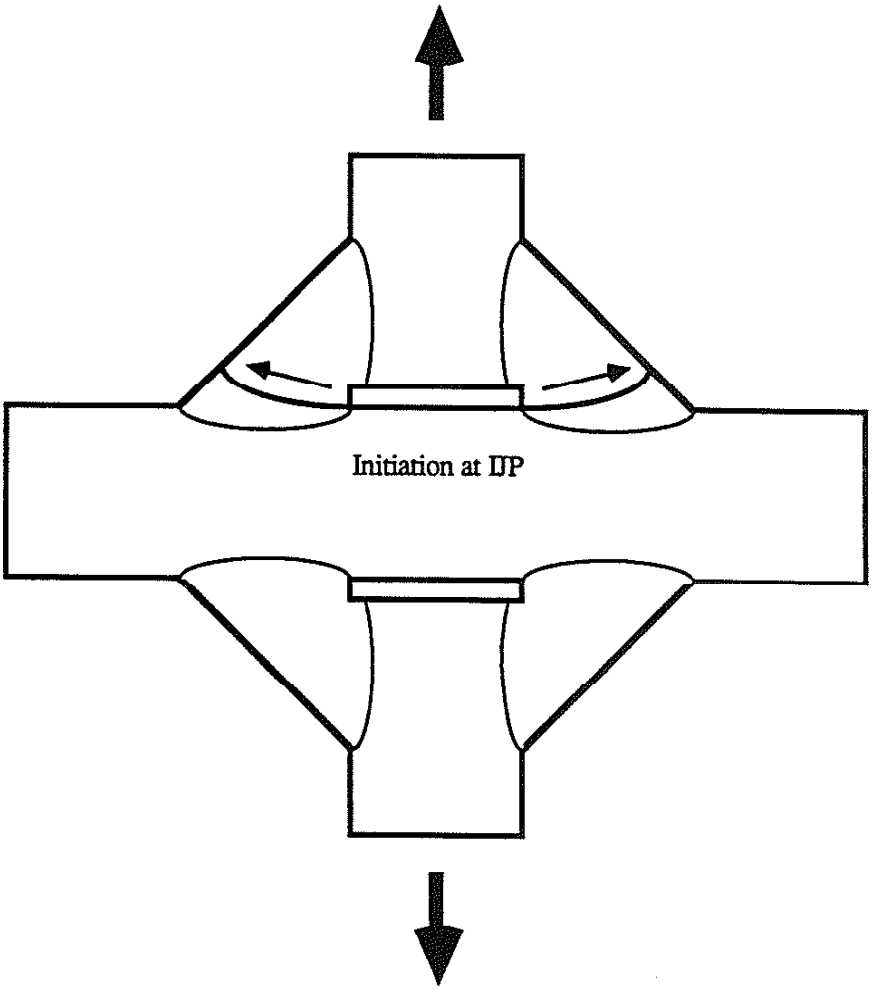

Fig. B9 Schematic description of fatigue failure mode at the IJP failure.

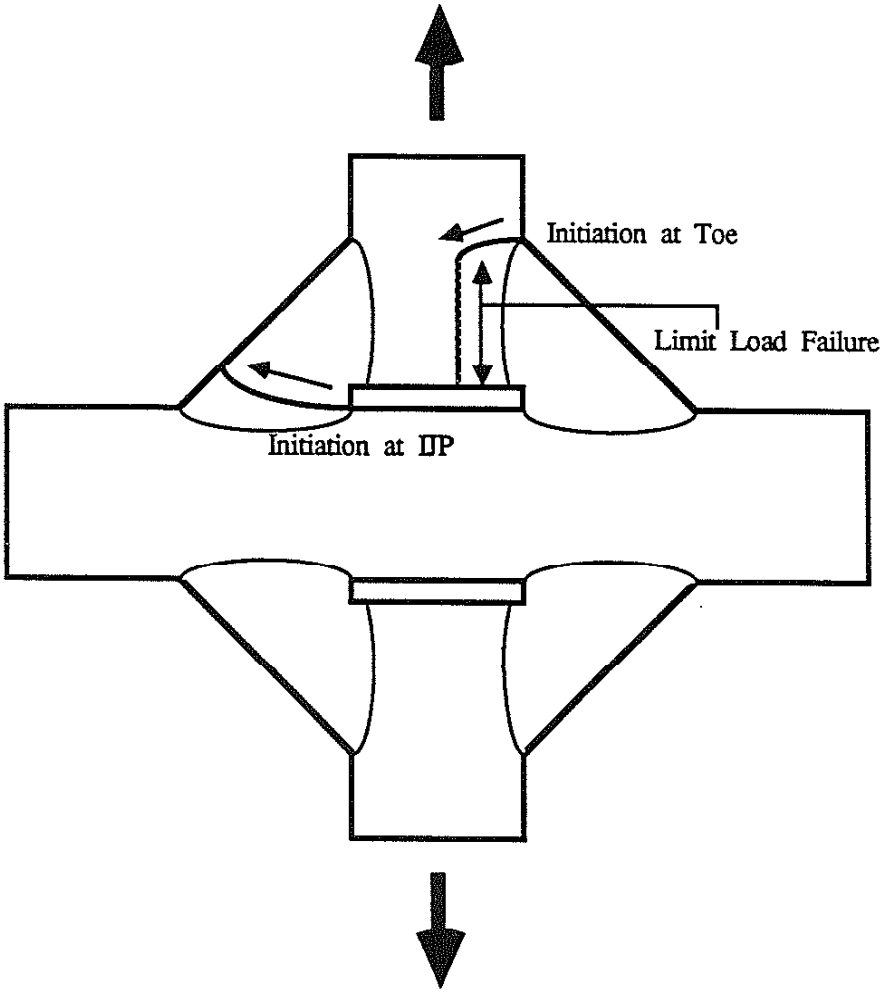

Fig. B10 Schematic description of combined fatigue failure mode at the toe site and the IJP site.

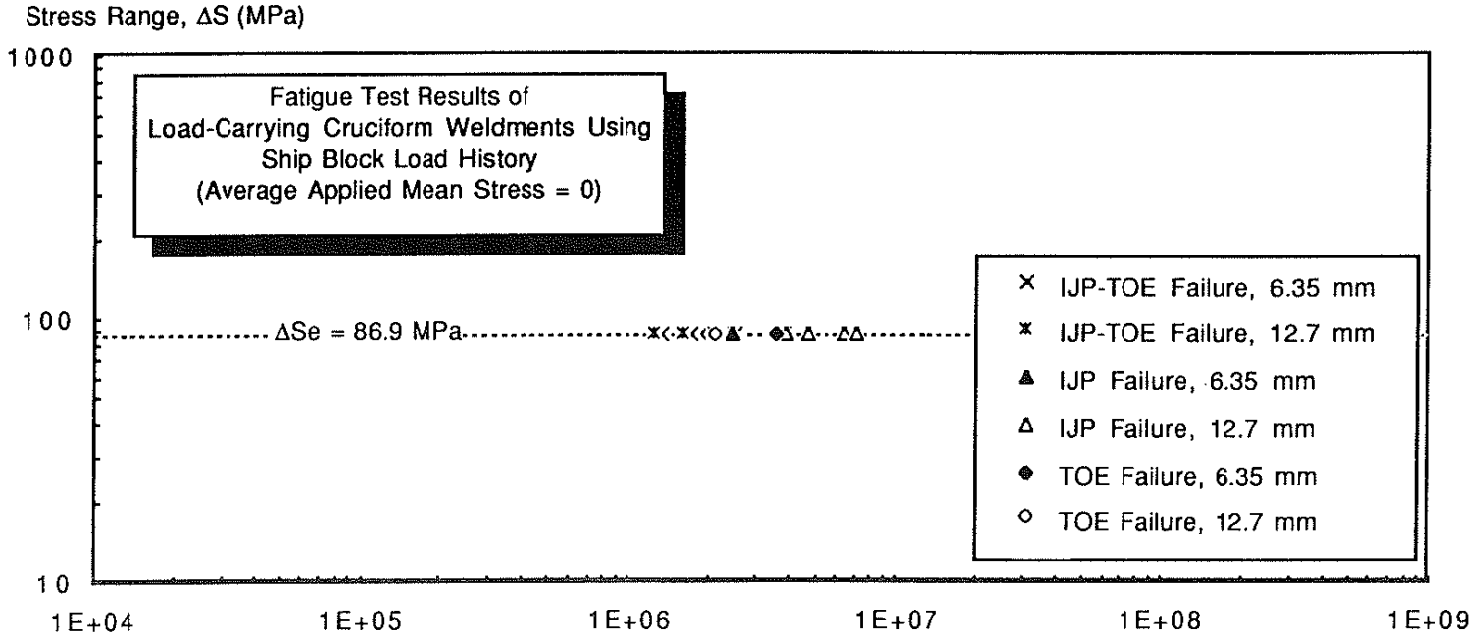

Fig. B11 Fatigue test results for load-carrying cruciform weldments using ship block load history with zero average applied mean stress. One block (5047 cycles) of ship block load history had same damage as 5047 cycles of equivalent stress range (ΔSe) of 86.9 MPa based on the linear damage rule and S-N relationship from UIUC fatigue data bank [10]. The fatigue life was calculated by multiplying the blocks to failure by 5047 cycles.

APPENDIX C. STATISTICAL ANALYSIS OF FATIGUE VARIABLE DATA

C.1 Load-Carrying Cruciform Weldments

Material Properties Effects (P): The measured hardness (DPH) of the HAZ, weld metal and base metal of 12.7 mm and 6.35 mm plate-thickness specimens was given in Tables C.1 and C.2. The average hardness of the grain-coarsened HAZ and the weld metal were applied to Eqs. 17 to estimate the average value of fatigue properties (σ_f', b) at the crack initiation sites, the toe and IJP. The standard deviation of fatigue strength coefficient (s_σ) was estimated using Eq. 19. Since all the specimens were fabricated from the steels with same specification (ASTM A-36), a typical s_{Su} value of 29 MPa (4.2 ksi) was assumed as a standard deviation of ultimate tensile strength (s_{Su}) of crack initiation sites.

Geometry and Fatigue Notch Effects (G): The data for the variation in geometry is listed in Tables B1, B2 and B3. This data was used to obtain the distribution of the nondimensional geometric coefficients (α^A and α^B) through the analytical relationships developed by Lawrence et.al. (Fig. 8) [28]:

For toe;

$$\alpha^A = .35\ (L_2/L_1)^{.25}\ [\ 1 + 1.1\ (c/L_1)^{1.65}\ ]$$

$$\alpha^B = .21\ (L_2/L_1)^{.167} \qquad \text{(C1)}$$

Foe IJP;

$$\alpha^A = 1.15\ (L_2/L_1)^{-.25}\ (c/L_1)^{0.5}$$

$$\alpha^B = 3.2\ (c/t)^{.12} \qquad \text{(C2)}$$

The statistics of α^A and α^B for the toe and IJP for the 12.7 mm weldments are given in Table C3, and those for the 6.35 mm weldments are given in Table C4. A Monte Carlo simulation using the statistics in Tables C3 and C4 together with the statistics of ultimate tensile strength of crack initiation sites was employed to estimate the statistics of corresponding fatigue notch factors at the crack initiation sites. The average ultimate tensile strength of crack initiation sites was estimated using average measured hardness and their empirical relationship [37]:

$$S_u = 3.45 \text{ DPH} \tag{C3}$$

A standard deviation of 29 MPa was used for the variation of ultimate tensile strength as discussed above.

For the simulation, Eq. 24 was used for the cases of axial loading both at the toe and IJP, and for the case of bending loading at the toe. For the fatigue notch factor at the IJP under bending stress, Eqs. 24 should be modified as:

$$K^B_{fmax} = .5(1 + \delta) + .00325\ \alpha^B\ \delta\ (S_u)^{0.9}\ t^{0.5} \tag{C3}$$

where $\delta = \dfrac{2\ c\ t^2}{(t+2L_1)^3 - (2c)^3}$

since $K_t = \delta\ (1 + \alpha(t/r)^{.5})$, where δ is a geometric parameter which designates the nominal stress which is to be multiplied by resulting K_{fmax} value by the remote bending stress: See Fig. C1 [28]. Tables C3 and C4 also shows the statistics of δ. The statistics of simulated fatigue notch factors are listed in Tables C5 and C6, also their distributions on a normal probability paper are shown in Figs. C2 and C3.

Distortion Effects (B): The bending factor (x) of each specimen was calculated from the strain gauge measurements of induced bending stress as in Tables B1, B2, and B3. Only positive values which caused tensile stress components were used for the simulation to model the situation of symmetrical weldments such as the double-V butt weld or cruciform joint in which distortions induce both tensile and compressive bending stresses so that the fatigue life is always reduced.

The statistics of the bending factor (x) data set of 12.7 mm and 6.35 mm thick specimens are given in Table C7, and the distributions of both data set on a normal probability paper are shown in Fig. C4.

Mean Stress and Residual Stress Effects (LS): Since testing was carried out using a variable load history, the R ratio is not defined. Thus, the average applied mean stress (S_m^A) was controlled during testing. Also, strain gauge measurements for the gripping mean stress were available (Tables B1, B2 and B3). Therefore, Eq. 28 was used for the simulation of fatigue strength instead of Eq. 16. Equation 28 considers the applied mean stress and notch-root residual stresses through a combined LS term instead of individual RS and MS terms.

The statistics of tensile gripping mean stress data for 12.7 mm and 6.35 mm specimens are given in Table C7, and the data was fitted to a lognormal distribution as shown in Fig. C5. The negative values were ignored in the simulation for the reason discussed above for the bending factor of symmetric joints. The applied mean stress level (S_m^A) was treated as a deterministic value since it was an experimentally controlled variable. The maximum tensile notch-root residual stress (σ_r) was assumed to be equal to the base metal yield strength ($+S_y$) [43]. The average base metal yield

strength was 310 MPa for 12.7 mm thick plate and 332 MPa for 6.35 mm thick plate [44]. A typical value of standard deviation of 28 MPa (4 ksi) was assumed as a standard deviation of base metal yield strength: see Section 3.4.

C.3 Non-Load-Carrying Cruciform Weldments (Engesvik and Moan)

Material Properties Effects (P): The average ultimate tensile strength (S_u) of the base metal reported in [45] (Table C8) were used to estimate the S_u of the fatigue crack initiation sites (assumed as the grain-Coarsened HAZ at the toe) in Table C9 using Eq.18. The average fatigue properties (σ_f' and b) were estimated by using the estimated average value of S_u of the crack initiation site and Eq. 17

Since all the specimens were fabricated from steels with same specification, the standard deviation of fatigue strength coefficient (s_σ) was estimated based on the standard deviation of ultimate tensile strength (s_{Su}) using Eq. 19 and a typical s_{Su} value of 29 MPa (4.2 ksi): see section 3.1.

Geometry and Notch Effects (G): The statistical distribution of the toe flank angle (θ) in Table C10 was used to reformulate the term representing geometry and notch effects (G) by using its analytical relationships with of α^A and α^B as:

$$\begin{aligned} \alpha^A &= .35(\tan\theta)^{.25} \quad \text{for Axial Load} \\ \alpha^B &= .21(\tan\theta)^{.167} \quad \text{for Bending Load} \end{aligned} \tag{C5}$$

since the IJP size (2c) equal to zero.

Then the geometry and notch factor (G) in Eq. 16 can be rewritten as:

$$G = \frac{1}{1 + 1.1375\text{x}10^{-3}(\tan\theta)^{.25}(S_u)^{0.9}\ t^{0.5}} \qquad (C6)$$

Distortion Effects (B): Engesvik and Moan performed strain gauge measurements of induced bending stress for twenty specimens out of forty two specimens, and measurements results of nineteen of twenty measurements were reported [45]. These results were converted into the data for the bending factor (x) in Table C11. The statistics of the bending factor (x) were directly applied to the simulation.

Mean Stress and Residual Stress Effects (MS, RS): The mean stress effects (MS) was treated as a deterministic variable since the nominal mean stress ratio was reported as a controlled variable to be R = 0 for all the test specimens. Since the specimens were reported to be stress-relieved, the residual stress was considered to be a deterministic variable having the value zero.

C.3 Non-Load-Carrying Cruciform Weldments (Lassen and Eide)

Lassen and Eide reported the statistics of Toe Flank Angle (θ) (Table C10), and they were used in simulation. They also performed the strain gage measurements of induced bending stresses, and those were converted to the data of the bending factor (x) as in Table C11 to be used in simulation.

Other simulation procedures were same as for the data from Engesvik and Moan as in Appendix C.2.

C.4 JIS-SM50B 20 mm Thick Butt Weldments

Material Properties Effects (P): Similar to the non-load-carrying cruciform weldments, the average ultimate tensile strength (S_u) of the base metal reported in [48] (Table C12) were used to estimate the S_u of the fatigue crack initiation sites (assumed as the grain-Coarsened HAZ at the toe) using Eq.18 (Table C13). The average fatigue properties (σ_f' and b) were estimated by using the estimated average value of S_u of the crack initiation site and Eq. 17.

Since all the specimens were fabricated from steels with same specification, the standard deviation of fatigue strength coefficient (s_σ) was estimated based on the standard deviation of ultimate tensile strength (s_{Su}) using a typical s_{Su} value of 29 MPa (4.2 ksi) and Eq. 19: see section 3.1.

Geometry and Notch Effects (G): The term representing geometry and notch effect (G) in Eq. 16 was modified to use directly the statistics of toe flank angle (θ) in the simulation. The analytical relationship of the toe flank angle (θ) with geometric coefficient (α) for the butt weldment at the toe was [28] (Fig. 8):

$$\begin{aligned} \alpha^A &= .27(\tan\theta)^{.25} && \text{for Axial Load} \\ \alpha^B &= .165(\tan\theta)^{.167} && \text{for Bending Load} \end{aligned} \qquad (C7)$$

Then the geometry and notch effect term (G) in Eq. 16 can be rewritten by using Eqs. 24 and C5 as:

$$G = \frac{1}{1 + 8.775\text{x}10^{-4}(\tan\theta)^{.25}(S_u)^{0.9}\ t^{0.5}} \qquad (C8)$$

Distortion Effects (B): The statistical distributions of angular distortion (d/2) and the reported values of other related geometric parameters influencing bending parameter (x) were directly applied to the simulation. The distortion factor (B) was modified as follows:

For the fixed gripping end condition,

$$S^B = d\ \left(\frac{3\ S^A\ E}{4}\right)^{.5}\ \tanh\ (\ y\ ) \qquad (26)$$

where $y = \frac{L_G}{2t}\left(\frac{3\ S^A}{E}\right)^{.5}$

S^B = Induced Bending Stress Level

S^A = Applied Nominal Axial Stress level

E = Young,s Modulus

L_G = Gripping Distance

t = Thickness of Loading Plate

d = Amount of Angular Distortion

The distance between grips (L_G) was adjusted according to the relationship [47]:

$$L_G = 2\ W + W_B \qquad (C9)$$

where W is the specimen width, and W_B is the bead width.

Then the term (y) in Eq. 26 was very smaller than unity in the long life regime whose stress level is low (For example, when S^A = 207 Mpa, W = 25 mm

and W_B = 20 mm, y = .07668). Expanding $\tanh(y) = y - y^3/3 + y^5/15 \ldots$, and ignoring higher order terms, Eq. 26 can be rewritten as:

$$S^B = d \frac{3 S^A L_G}{4 t} \tag{C10}$$

Then the bending parameter (x) can be obtained as:

$$x = \frac{S^B}{S^A + S^B} = \frac{.75 \, d \, L_G/t}{1 + .75 \, d \, L_G/t} \tag{C11}$$

The distortion factor (B) becomes:

$$B = \frac{1}{1 + .75 \frac{K^B_{fmax}}{K^A_{fmax}} d \, L_G/t} \tag{C12}$$

where: the statistical distributions of bending and axial fatigue notch factors can be obtained by using Eqs. 24 and C7.

Mean Stress Effects (MS): The mean stress effects (MS) was treated as a deterministic attribute to the fatigue strength since the mean stress ratio was a controlled variable for all the test specimens (R=0).

Residual Stress Effects (RS): The maximum tensile notch-root residual stress (σ_r) was assumed to be equal to the base metal yield strength ($+S_y$) [43]. The average base metal yield strength was given in Table C12. A typical value of standard deviation of 28 MPa (4 ksi) was assumed as a standard deviation of base metal yield strength: see section 3.4.

C.5 JIS-SM50A 6 mm Thick Butt Weldments

Since the statistical distributions for this particular group of specimens were not available, the statistic of Angular distortion (d) and Toe Flank Angle (θ) for 9 mm butt weldments tested by the same investigators [47] were used. The 9mm butt weldments were fabricated with similar welding procedure to the 6 mm butt weldments, especially the heat input and the welding sequence which are the most significant parameters to the angular distortion amount and weld toe geometry. The parameters used in the fabrication in both group of weldments are compared in Table C14.

Other simulation procedures were same as those for the 20 mm butt weldments in Appendix C.4.

C.6 Single-V Butt Weldments from UIUC Fatigue Data Bank

Material Properties Effects (P): The statistics and histogram of ultimate tensile strength (S_u) for base material of all the specimens considered in this simulation were given in Table C15 and Fig. C6. The average of S_u was 422 MPa (61.2 ksi), and the standard deviation was 54 MPa (7.8 ksi). The average value of S_u for the fatigue crack initiation sites (assumed as the grain-Coarsened HAZ at the toe) were estimated using Eq. 18, and that was used to estimate the average fatigue properties (σ_f' and b) at the crack initiation sites using Eq. 17.

The variation in ultimate tensile strength (s_{Su}) of crack initiation site was assumed same as the variation of the base metal. The standard deviation of ultimate tensile strength (s_{Su}) of base material (54 MPa, 7.8

ksi) was used to estimate the standard deviation of fatigue strength coefficient (s_σ) using Eq. 17.

Geometry and Notch Effects (G): The statistics of toe flank angle (θ) was estimated based on the measured data of those for the butt weldments by Nihei et. al. [47]. They measured seven different groups of butt weldments, and their statistical estimators for each group are as listed in Table C16. Those statistical estimators (mean, standard deviation and distribution function) were used to regenerate the random data of flank angle through a Monte Carlo simulation. One-hundred data for each group, total seven-hundreds data were generated, and those were statistically tested to estimate the statistics of toe flank angle to use in the simulation of fatigue strength.

Since the plate-thickness of most of specimens was not known, a best guess was used to estimate the uncertainty of the thickness of specimens. Since in practice, the single-V butt weldments are designed for the relatively thinner specimens, a uniform distribution between 6 mm to 20 mm was guessed.

The statistics of toe flank angle and plate-thickness, together with the statistical estimators of ultimate tensile strength, were used in a Monte Carlo simulation of the term representing geometry and notch factor (G) using Eq. C7.

Distortion Effects (B): Since neither direct data for the bending factor (x) nor the angular distortion were given, the statistics of distortion amount was estimated in the similar manner for the toe flank angle. The measured data of angular distortion (d/2) for seven groups of butt weldments

from Nihei et. al. [47] were used to estimate the statistics of angular distortion through a Monte Carlo Simulation: see Table C16.

Since the gripping distance for specimens were not specified, a conservative assumption that the gripping distance was over 100 times of plate-thickness was used. When the gripping distance reaches about 100 times of plate-thickness, Eq. 26 showed a maximum plateau independent to the geometrical parameters (gripping distance and plate-thickness) [42] as:

$$S^B = .866\ d\ (E\ S^A)^{.5} \tag{C13}$$

Using Eq. 15 and C13, the Basquin-Morrow equation can be rewritten as:

$$\begin{aligned} S_a^A + X\ S_a^B &= S_a^A + .866\ d\ X\ E^{.5}\ (S_a^A)^{.5} \\ &= \sigma_f' \frac{1}{K_{fmax}^B} \left(1 - \frac{\sigma_r}{\sigma_f'}\right) \frac{1}{\left[1 + \frac{1+R}{1-R} (2N_I)^b\right]} (2N_I)^b \\ &= (P)(G)(RS)(MS)\ (2N_I)^b \\ &= C \end{aligned} \tag{C14}$$

Then, Eq. C14 can be rewritten as:

$$S_a^A + .866\ d\ X\ E^{.5}\ (S_a^A)^{.5} - C = 0 \tag{C15}$$

Taking only positive root of Eq. C15,

$$\begin{aligned} (S_a^A)^{.5} &= -.433\ d\ X\ E^{.5} + .5\ (.75\ d^2\ X^2\ E + 4C)^{.5} \\ S_a^A &= C + .375\ d^2\ X^2\ E - .433\ d\ X\ E^{.5}(.75d^2X^2E + 4C)^{.5} \end{aligned} \tag{C16}$$

Then the equivalent distortion factor (B) can be:

$$B = S_a^A/C = 1+.375d^2X^2E/C - .433d \text{ X } E^{\cdot 5}(.75d^2X^2E + 4C)^{\cdot 5}/C \qquad (C17)$$

The estimated statistics of angular distortion (d/2) and Eqs. C16 and C17 to simulate the fatigue strength and the distortion effects.

Mean Stress Effects (MS): The mean stress effects (MS) was treated as a deterministic attribute to the fatigue strength since for all the specimens considered, the mean stress ratio was a controlled variable either R=-1 or R=0.

Residual Stress Effects (RS): The maximum tensile notch-root residual stress (σ_r) was assumed to be equal to the base metal yield strength ($+S_y$) [43]. The histogram of base metal yield strength was given in Fig. C7. The average yield strength of base metal was 250 MPa (36.2 ksi), and the standard deviation was 28 MPa (4.1 ksi). These values were used in the simulation of fatigue strength.

Table C1

Statistics of Measured Hardness (DPH) Data for the 12.7 mm Thick Load-Carrying Cruciform Weldments

	Base Metal	Weld Metal	Heat Affected Zone		
			G.C.Z.*1	G.R.Z.*2	G.C.Z.*3 & G.R.Z.
No. of Measurements	50	50	78	78	156
Min.	162	172	169	136	136
Max.	113	235	237	211	237
Estimated Mean	142.4	206.6	200.7	173.9	187.3
Estimated Standard Deviation	11.06	15.41	15.19	17.30	21.09
Coefficient of Variation	.078	.075	.076	.100	.113
Distribution	Normal	Normal	Normal	Normal	Normal

*1 : Grain-Coarsened Heat Affected Zone
*2 : Grain-Refined Heat Affected Zone
*3 : Summed Results of Grain Coarsened and Refined HAZ

Table C2

Statistics of Measured Hardness (DPH) Data for the 6.35 mm Thick Load-Carrying Cruciform Weldments

	Base Metal	Weld Metal	Heat Affected Zone		
			G.C.Z.*1	G.R.Z.*2	G.C.Z.*3 & G.R.Z.
No. of Measurements	50	50	50	50	100
Min.	158	201	168	123	123
Max.	125	281	244	203	244
Estimated Mean	142.8	241.1	201.4	159.7	180.6
Estimated Standard Deviation	6.78	14.67	17.13	20.46	28.11
Coefficient of Variation	.047	.061	.085	.128	.156
Distribution	Normal	Normal	Normal	Normal	Normal

*1 : Grain-Coarsened Heat Affected Zone
*2 : Grain-Refined Heat Affected Zone
*3 : Summed Results for Grain Coarsened and Refined HAZ

Table C3

Statistics of Geometric Coefficients (α^A and α^B) of 12.7 mm Thick Load-Carrying Cruciform Weldments

	Geometric Coefficient under Axial Loading		Geometric Coefficient under Bending Loading		
	α^A at Toe	α^A at IJP	α^B at Toe	α^B at IJP	δ
Data Size	60	60	60	60	60
Min.	.4439	.8076	.2048	2.908	.0369
Max.	.7911	.9879	.2279	2.963	.1292
m*1	.5684	.8952	.2156	2.952	.0690
s*2	.0599	.0370	.0052	.0141	.0156
COV*3	.1055	.0414	.0241	.0048	.2258
p(x)*4	Normal	Normal	Normal	Normal	Normal

*1: Estimated Mean
*2: Estimated Standard Deviation
*3: Coefficient of Variation
*4: Probability Distribution Used in Simulation

Table C4

Statistics of Geometric Coefficients (α^A and α^B) of 6.35 mm Thick Load-Carrying Cruciform Weldments

	Geometric Coefficient under Axial Loading		Geometric Coefficient under Bending Loading		
	α^A at Toe	α^A at IJP	α^B at Toe	α^B at IJP	δ
Data Size	40	40	40	40	40
Min.	.4995	.8364	.2047	2.963	.0513
Max.	.9123	1.118	.2291	3.089	.1594
m*1	.6205	.9489	.2162	2.975	.0847
s*2	.0931	.0516	.0066	.0348	.0243
COV*3	.1501	.0544	.0307	.0117	.2866
p(x)*4	Normal	Normal	Normal	Normal	Normal

*1: Estimated Mean
*2: Estimated Standard Deviation
*3: Coefficient of Variation
*4: Probability Distribution Used in Simulation

Table C5

Statistics of Simulated Fatigue Notch Factors (K^{A}_{fmax} and K^{B}_{fmax}) for the 12.7 mm Thick Load-Carrying Cruciform Weldments

	Axial Fatigue Notch Factor, K^{A}_{fmax}		Bending Fatigue Notch Factor, K^{B}_{fmax}	
	IJP	TOE	IJP	TOE
Size of Simulation	100	100	100	100
Min.	4.335	2.831	1.026	1.803
Max.	5.458	4.193	1.915	2.002
m*1	4.829	3.363	1.407	1.898
s*2	.219	.277	.197	.041
COV*3	.045	.082	.140	.022
p(x)*4	Normal	Normal	Normal	Normal

*1: Estimated Mean
*2: Estimated Standard Deviation
*3: Coefficient of Variation
*4: Probability Distribution Used in Simulation

Table C6

Statistics of Simulated Fatigue Notch Factors (K^{A}_{fmax} and K^{B}_{fmax}) for the 6.35 mm Thick Load-Carrying Cruciform Weldments

	Axial Fatigue Notch Factor, K^{A}_{fmax}		Bending Fatigue Notch Factor, K^{B}_{fmax}	
	IJP	TOE	IJP	TOE
Size of Simulation	100	100	100	100
Min.	3.864	2.230	.929	1.565
Max.	4.943	3.712	2.058	1.726
m*1	4.296	2.829	1.420	1.639
s*2	.218	.296	.254	.032
COV*3	.051	.105	.179	.020
p(x)*4	Normal	Normal	Normal	Normal

*1: Estimated Mean
*2: Estimated Standard Deviation
*3: Coefficient of Variation
*4: Probability Distribution Used in Simulation

Table C7

Statistics of Bending Factor (x) and Gripping Mean Stress (S_m^B) from Strain Gauge Measurements for the Load-Carrying Cruciform Weldments

	Bending Factor, x		Gripping Mean Stress, S_m^B (MPa)	
	12.7 mm	6.35 mm	12.7 mm	6.35 mm
Data Size	60	40	60	40
Min.	0.0	0.0	1.38	29.0
Max.	.39	.32	205	214
m*1	.114	.133	75.7	84.4
s*2	.0899	.0895	65.4	48.2
COV*3	.790	.676	.863	.571
p(x)*4	Normal	Normal	Lognormal	Lognormal

*1: Estimated Mean
*2: Estimated Standard Deviation
*3: Coefficient of Variation
*4: Probability Distribution Function Used in Simulation

Table C8

Mechanical Properties of Marine Structural Steel Plates
Used for the Base Metal of 32 mm and 25 mm Thick
Non-Load-Carrying Cruciform Weldments

	32 mm Thick	25 mm Thick
Data Source	[45]	[46]
Yield Strength (S_y, MPa)	251	370
Ultimate Tensile Strength (S_u, MPa)	420	510
Elongation (%)	30.3	28.5

Table C9

Estimated Statistics of Mechanical Properties of Grain-Coarsened HAZ for the 32 mm and 25 mm Thick Non-Load-Carrying Cruciform Weldments

	32 mm Thick			25 mm Thick		
	m*1	s*2	p(x)*3	m	s	p(x)
Ultimate Tensile Strength (S_u, MPa)	630	29	normal	765	29	normal
Fatigue Strength Coefficient (σ_f', Mpa)	999	34	normal	1127	34	normal
Fatigue Strength Exponent (b)	-.09182	-	D*4	-.08639	-	D

*1 Estimated Mean
*2 Estimated Standard Deviation
*3 Probability Distribution Function Used in Simulation
*4 Deterministic Variable

Table C10

Statistics of Toe Flank Angle (θ) for the Specimens of 32 mm and 25 mm Thick Non-Load-Carrying Cruciform Weldments

	32 mm Thick	25 mm Thick
Data Source	[45]	[46]
No. of Measurements	384	400
Min.	15 Degrees	30 Degrees
Max.	69	95
m*1	30	58
s*2	9	9
COV*3	.31	.157
p(x)*4	Lognormal	Lognormal

*1: Estimated Mean
*2: Estimated Standard Deviation
*3: Coefficient of Variation
*4: Probability Distribution Function Used in Simulation

Table C11

Statistics of Bending Factor (x) for the Specimens of 32 mm and 25 mm Thick Non-Load-Carrying Cruciform Weldments

	32 mm Thick	25 mm Thick
Data Source	[45]	[46]
No. of Measurements	19	39
Min.	.0060	.0
Max.	.4859	.1697
m^{*1}	.0894	.0421
s^{*2}	.1060	.0328
COV^{*3}	1.185	.7784
$p(x)^{*4}$	Lognormal	Lognormal

*1: Estimated Mean
*2: Estimated Standard Deviation
*3: Coefficient of Variation
*4: Probability Distribution Function Used in Simulation

Table C12

Mechanical Properties of JIS-SM50A and SM50B Steel Plates Used for the Base Metal of 6 mm and 20 mm Thick Butt Weldments

	JIS-SM50A (6 mm Thick)	JIS-SM50B (20 mm Thick)
Data Source	[49]	[48]
Yield Strength (S_y, MPa)	357	397
Ultimate Tensile Strength (S_u, MPa)	558	534
Elongation (%)	32.5	31.0

Table C13

Estimated Statistics of Mechanical Properties of Grain-Coarsened HAZ For the 6 mm and 20 mm Thick Butt Weldments

	6 mm Thick			20 mm Thick		
	m*1	s*2	p(x)*3	m	s	p(x)
Ultimate Tensile Strength (S_u, MPa)	837	29	Normal	801	29	Normal
Fatigue Strength Coefficient (σ_f', MPa)	1195	34	Normal	1161	34	Normal
Fatigue Strength Strength Exponent (b)	-.08409	-	D*4	-.08520	-	D
Maximum Tensile Residual Stress (σ_r, MPa)	357	28	Normal	397	28	Normal

*1: Estimated Mean
*2: Estimated Standard Deviation
*3: Probability Distribution Function Used in Simulation
*4: Deterministic Variable

Table C14

Comparison of welding parameters between 6 mm JIS-SM50A butt weldments and 9 mm JIS-SM50B Butt weldments [47]

Parameters	6 mm JIS-SM50A Butt Weldments	9 mm JIS-SM50B Butt Weldments
Filler Material	JIS D5016, 4 mm dia.	JIS D5016, 4 mm dia.
Welding Current	150-160 A	170 A
Welding Speed	9-10 cm/min.	10-20 cm/min.
Arc Voltage	19-23 V	19-23 V
Heat Input	17-22 kJ/cm	15-20 kJ/cm
Preheating	none	none
Welding Position	flat	flat

Table C15

Data of Toe Flank Angle (θ) and Angular Distortion (d/2)
for Butt Weldments from Nihei et. al. [47]

	Toe Flank angle (θ) degree			Angular Distortion (d/2) radian x 10^{-3}		
	m	s	p(x)	m	s	p(x)
JIS-SM50B 9 mm	34.0	5.2	Lognormal	3.68	1.84	Normal
JIS-SM50B 20 mm	41.1	5.7	Lognormal	9.21	5.83	Normal
JIS-SM50B 40 mm	34.4	8.4	Lognormal	6.07	4.91	Normal
JIS-SM58Q 9 mm	32.5	10.4	Normal	5.17	2.31	Normal
JIS-SM58Q 20 mm	32.2	10.2	Normal	3.2	2.13	Normal
JIS-HT80QT 9 mm	23.8	10.8	Normal	1.79	1.37	Normal
JIS-HT80QT 20 mm	31.0	17.5	Normal	3.36	1.86	Normal
Simulation Results	32.2	10.5	Lognormal	4.61	3.94	Normal

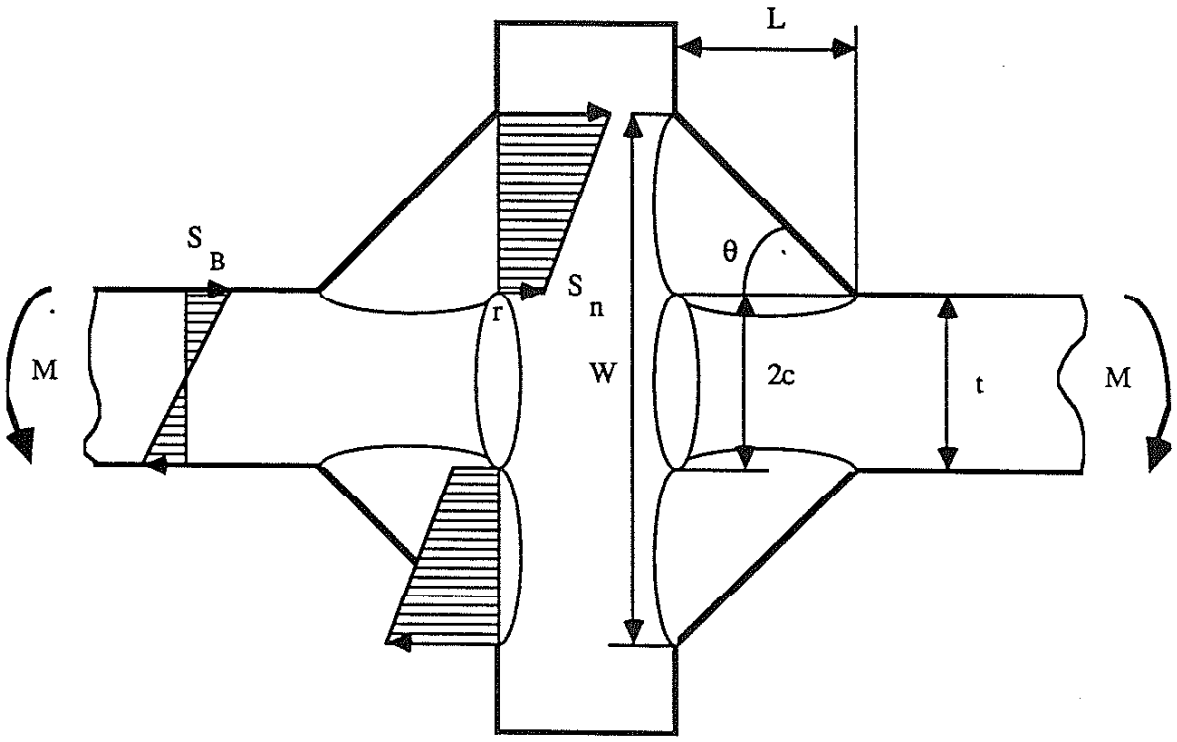

$$K_{t,B}^{IJP} = \frac{\sigma_{max}}{S_n} = 1 + \alpha_B \left(\frac{t}{r}\right)^{.5}$$

$$\alpha_B = 3.22 \left(\frac{c}{t}\right)^{.15}$$

$$S_n = \frac{S_B}{\left(W^3 \left(\frac{1}{2ct^2}\right) - \left(\frac{2c}{t}\right)^2\right)}$$

Fig. C1 Stress concentration factor for the IJP of the cruciform weldment under pure bending conditions.

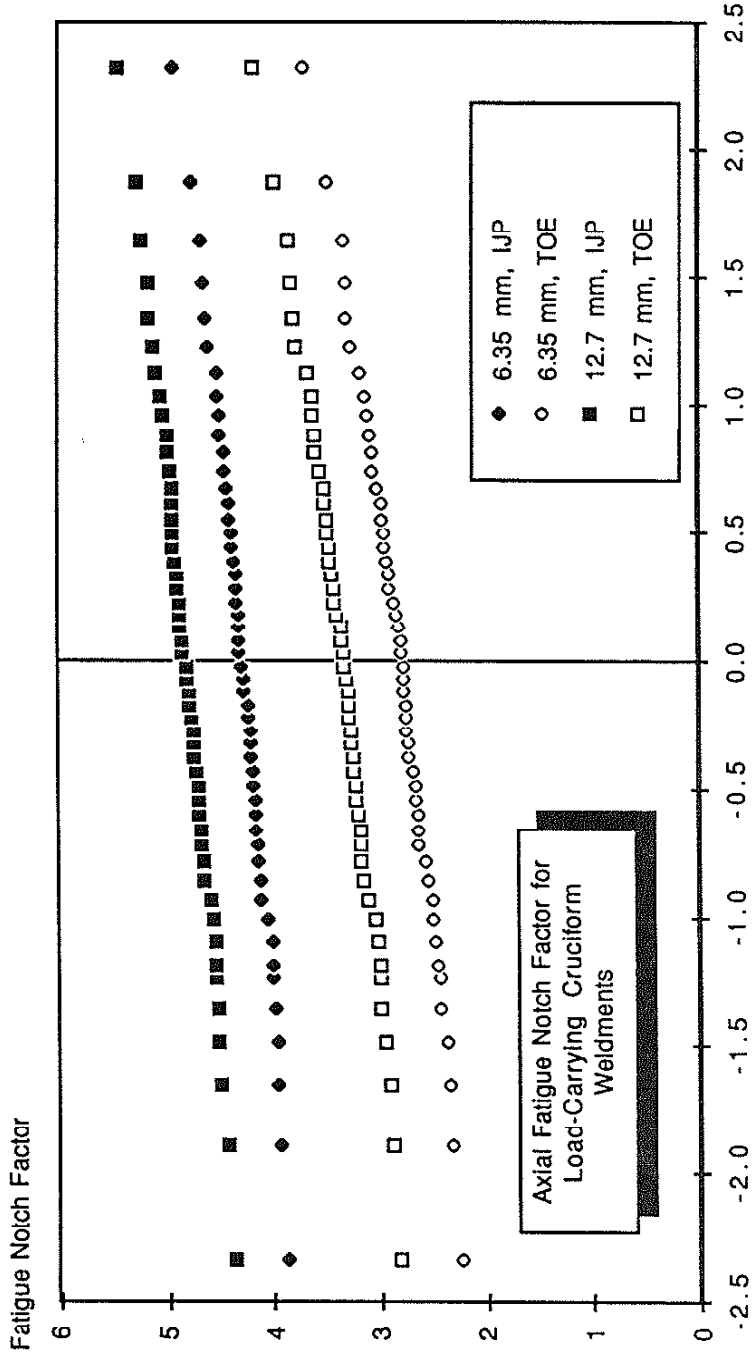

Fig. C2 Distribution of the axial fatigue notch factor (K_{fmax}) for the load-carrying cruciform weldments on the normal probability paper.

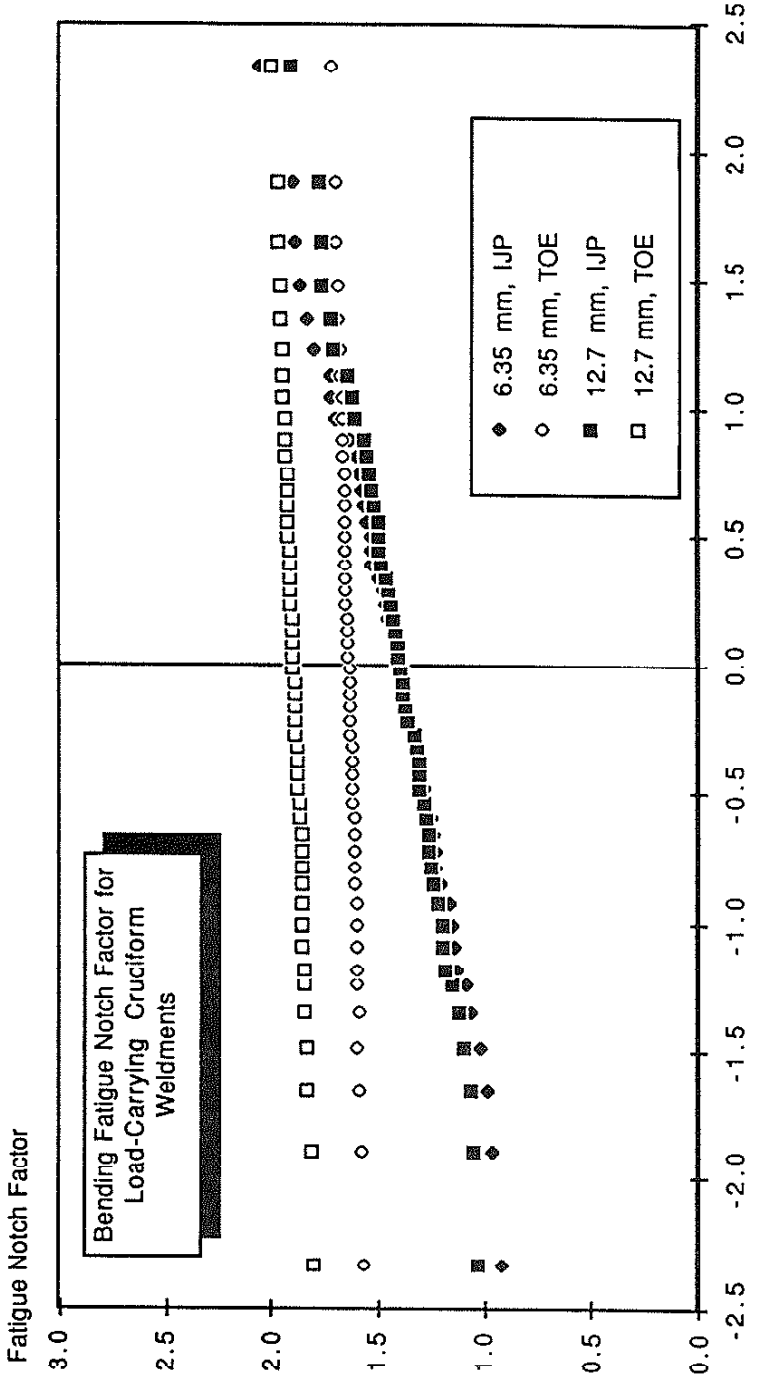

Fig. C3 Distribution of the bending fatigue notch factor ($K_{f_{max}}^{R}$) for the load-carrying cruciform weldments on the normal probability paper.

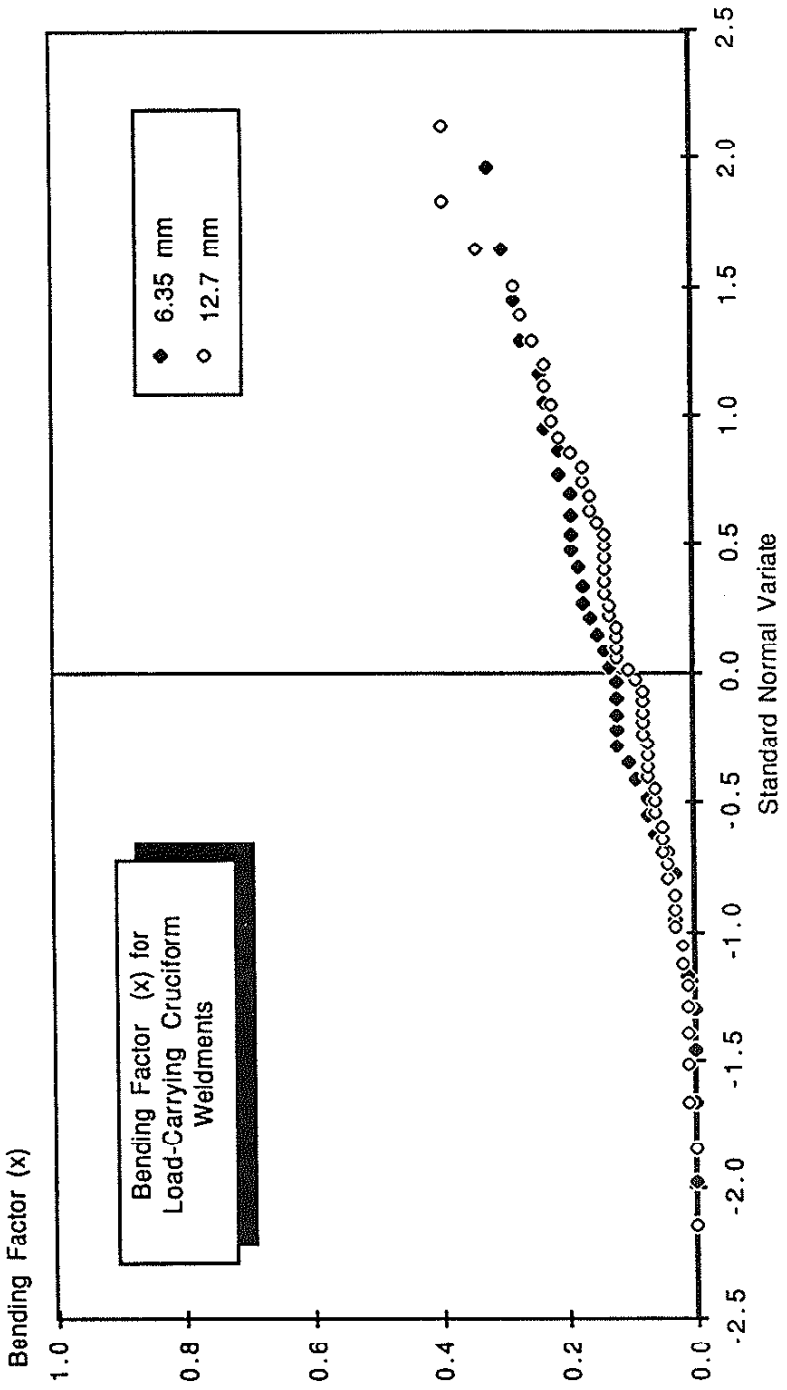

Fig. C4 Distribution of the bending factor (x) for the load-carrying cruciform weldments on the normal probability paper.

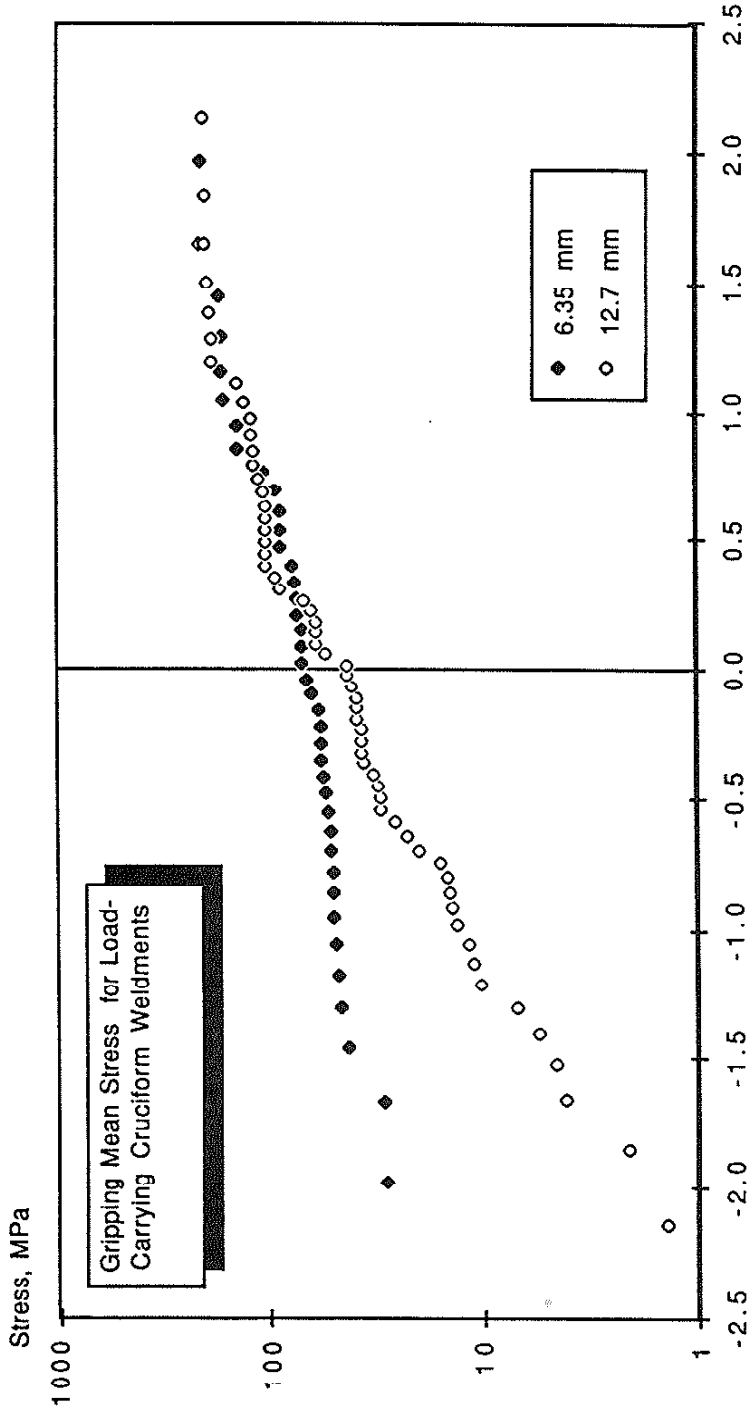

Fig. C5 Distribution of the gripping mean stress (S_m^B) for the load-carrying cruciform weldments on the lognormal probability paper.

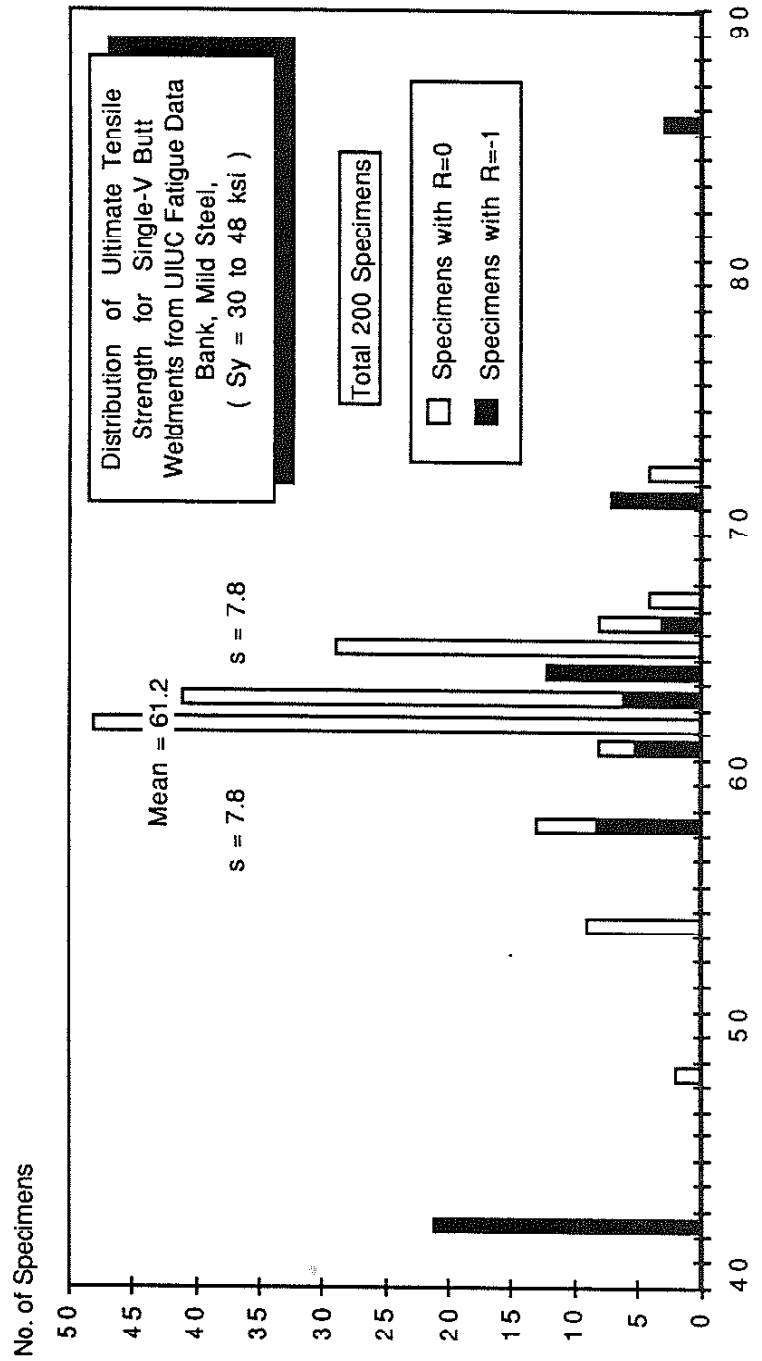

Fig. C6 Distribution of ultimate tensile strength (S_u) for as-welded mild steel (Sy = 30 to 48 ksi) Single-V butt weldments from UIUC fatigue Data bank.

REFERENCES

1. Munse, W.H., "Fatigue of Welded Steel Structures," Welding Research Council, New York, 1964. (L.Grover, editor)

2. The Welding Institute, Proceedings of the Conference on Fatigue of Welded Structures," July 6-9, 1970, The Welding Institute, Cambridge, England, 1971.

3. Gurney, T.R., "Revised Fatigue Design Rules," Metal Construction, Vol. 15, No. 1, 1983, pp. 37-44.

4. Yung, J.-Y., "Further Development of the Total Life Model for Weldments and Its Application to Fatigue Design," Ph. D. Thesis, Department of Metallurgical Engineering, University of Illinois at Urbana-Champaign, 1985.

5. Ang, A. H-S. and Tang, W.H., Probability Concepts in Engineering Planning and Design, Vol. II, John Wiley and Sons, 1975.

6. Wirsching, P.H., "Probability-Based Fatigue Design Criteria for Offshore Structure," Final Project Report API-PRAC Project #81-15, College of Engineering, The University of Arizona, Jan.,1983.

7. ASCE Committee on Fatigue and Fracture Reliability of the Committee on Structural Safety and Reliability of the Structural Division, " Fatigue Reliability," Journal of the Structural Division, ASCE, Jan.,1982, pp. 3-45.

8. Ang, A. H-S. and Munse, W.H., "Practical Reliability Basis for Structural Fatigue," Preprint No. 2494 for ASCE National Structural Engineering Convention at New Orleans, Louisiana during Apr. 14-18, 1975

9. Munse, W. H., Wilbur, T. W., Tellalian, M. L., Nicoll, K. and Wilson K., "Fatigue Characterization of Fabricated Ship Details for Design," Ship Structure Committee, SSC-318, 1983.

10. Radziminski, J. B., Srinivasan, R., Moore, D., Thrasher, C. and Munse, W. H., " Fatigue Data Bank and Data Analysis Investigation," Structural Research Series No. 405, Civil Engineering Studies, University of Illinois at Urbana-Champaign, June, 1973.

11. Paris, P.C., and Erdogan, F. , "The Critical Analysis of Crack Propagation Law," J. of Basic Engineering, ASME Trans., Vol. 85, Ser. D, No.4, 1963, p.528.

12. Engesvik, K. M. and Moan, T., "Probabilistic Analysis of the Uncertainty in the Fatigue Capacity of Welded Joints," Engineering Fracture Mechanics, Vol. 18, No. 4, pp 743-762, 1983.

13. Maddox, S.J., "A Fracture Mechanics Approach to Service Load Fatigue in Welded Structures," Welding Research International, Vol. 4, No. 2, 1974.

14. Barsom, J.M., "Fatigue-Crack Propagation in Steel of Various Yield strength," Journal of Engineering Ind., Vol.93,No. 4, 1971.

15. Schilling, C.G., Klippstein, K.H., Barsom, J.M. and Blake, G.T., "Fatigue of Welded Steel Bridge Members under Variable Amplitude Loading," NCHRP Project Final Report 12-12, Aug. 1975.

16. Simth, I.F. and Smith R.A., "Defects and Crack Development in Fillet Welded Joints," Fatigue of Engineering Materials and Structures, Vol. 5, No.2, pp.151-165,Pergamon Press, 1982.

17. Signes, E.G., Baker, R.G., Harrison, H.D., and Burdekin, F.M., "Factors Affecting the Fatigue Strength of Welded High Strength Steels," British Welding Journal, 14, pp. 108-116, 1967.

18. Watkinson, F., Bodger, P.H. and Harrison, J.D., "The Fatigue Strength of the Welded Joints in High Strength Steels and Methods for its Improvement," Proceedings of the Conference on the Fatigue of Welded Structures, The Welding Institute, England, 1971.

19. Kottgen, V.B., Oliver, R. and Seeger, T., " The Influence of Plate Thickness on Fatigue Strength of Welded Joints, A Comparison of Experiments with Prediction by Fatigue Notch Factors," Steel in Marine Structures, ed. by C. Noordhoek and J. de Back, Elsevier Science Publishers, Amsterdam, 1987

20. McMahon J. C. and Lawrence F. V., "Fatigue Crack Initiation and Early Growth in Tensile Shear Spot Weldments," FCP Report No. 131, College of Engineering, University of Illinois at Urbana-Champaign, 1986.

21. Socie, D. F., " Fatigue Damage Map," Fatigue 87, The Third International Conference on Fatigue and Fatigue Thresholds, Charlottsville, VA, June 1987.

22. Nowak H. and Marissen R., "Fatigue Crack Propagation of Short and Long Cracks:Physical Basis, Prediction Methods and Engineering Significance," Fatigue 87, The Third International Conference on Fatigue and Fatigue Thresholds, Charlottsville, VA. June 1987.

23. Lankford, J., " On the Small Crack Fracture Mechanics Problems," Int. J. of Fracture, Vol. 16, P.R7, 1980.

24. Smith, R.A., "On the Short Crack Initiation of Fracture Mechanics," Int. J. of Fracture, Vol. 13, P. 717, 1977.

25. Kitagawa, H. and Takahashi, C., " Applicability of Fracture Mechanics to Very Small Cracks or Cracks in the Early Stage," Proceedings of The Second Int. Conf. on Mechanical Behavior of Materials, ASM, P. 627, 1976.

26. Schjive J., "Difference between the Growth of Small and Large Fatigue Cracks in Relation to Threshold K Values," Fatigue 84, Proceedings of The Second Int. Conf. on Fatigue and Fatigue Threshold, Vol. II, PP. 881-908, EMAS,1984.

27. Verreman, Y., Ballion, J.-P. and Masounave, J., " Closure and Propagation Behavior of Short Fatigue Cracks at Different R-Ratios," Fatigue 87, Proceedings of The Third International Conference on Fatigue and Fatigue Thresholds, Charlottsville, VA. June 1987.

28. Ho, N.-J. and Lawrence, F. V., Jr., "The Fatigue of Weldments Subjected to Complex Loadings," FCP Report No. 45, College of Engineering, University of Illinois at Urbana-Champaign, Jan. 1983.

29. Mattos, R. J.,and Lawrence, F. V., Jr., "Estimation of the Fatigue Crack Initiation Life In Welds Using Low Cycle Fatigue Concepts," FCP Report No. 45, College of Engineering, University of Illinois at Urbana-Champaign, Jan. 1983.

30. Morrow, J. D., and Socie, D.F., "Review of Contemporary Approaches to Fatigue Damage Analysis," Risk and Failure Analysis for Improved Performance and Reliability, Edited by Burke,J.J.,and Weiss, V., Plenum Publishing Corporation, 1980.

31. Chang S.-T. and Lawrence, "Improvement of Weld Fatigue Resistance," FCP Report No. 46, College of Engineering, University of Illinois at Urbana-Champaign, Jan. 1985.

32. Yung, J.-Y. and Lawrence, " Analytical and Graphical Aids for the Fatigue Design of Weldments," FCP Report No. 115, College of Engineering, University of Illinois at Urbana- Champaign, Nov. 1984.

33. User's Manual for IMSL STAT/PC-LIBRARY, IMSL, Texas, 1984.

34. Landgraf, R.W., "The Resistance of Metals to Cyclic Deformation, " Achievement of High Fatigue Resistance in Metals and Alloys, ASTM STP 467, 1970.

35. Socie, D.F., Mitchell, M.R. and Caulfield, E.M., "Fundamentals of Modern Fatigue Analysis," FCP Report No.26, University of Illinois at Urbana-Champaign, 1978.

36. Mitchell, M.R., "Fundamentals of Modern Fatigue Analysis for Design," Fatigue and Microstructure, ASM, 1979.

37. McMahon, J. C., and Lawrence, F.V., Jr., "Predicting Fatigue Properties Through Hardness Measurements," FCP Report No. 105, College of Engineering, University of Illinois at Urbana-Champaign, Feb.1984.

38. Baht, S., Private Communication, Inland Steel Company, 1987.

39. Lawrence, F.V., Private Communication, University of Illinois at Urbana-Champaign, 1987.

40. Peterson, R.E., "Notch Sensitivity," Chap. 13, Metal Fatigue, Sines and Waisman (ed.), Mcgraw-Hill, New York, 1959.

41. Matsubuchi, K., Analysis of Welded Structure," Pergamon, 1980

42. Burk, J.D. and Lawrence, " Influence of Bending Stresses on the Fatigue Crack Propagation Life in Butt Welds," FCP Report No. 21, College of Engineering, University of Illinois at Urbana-Champaign, Nov. 1984.

43. Lawrence, F.V., Burk, J.D. and Yung, J.Y.," Influence of Residual Stress on the Predicted Fatigue Life of Weldments," ASTM STP 776, ASTM, 1982.

44. Park, S.K. and Lawrence, F.V., "Fatigue Characterization of Fabricated Ship Structure Design, Phase II," Report to Coast Guard, Project DTCG-12-84-C-20018, Feb., 1987.

45. Engesvik, K. M., "Analysis of Uncertainties in the fatigue Capacity of Welded Joints," Report No. UR-82-17, Department of Marine Technology, The University of Trondheim, Trondheim, Norway,1982.

46. Lassen T. and Eide O.I., "Data for Fracture Mechanics Derivation of S-N Curves," Report 5.1, The Ship Research Institute of Norway, Apr., 1984.

47. Nihei, M., Sasaki, E., Kanao, M., Inagaki, M., "Statistical Analysis of Fatigue Strength of Arc Welded Joints Using Covered Electrodes under Various Welding Conditions with Particular Attention to Toe Shape," Transaction of National Research Institute for Metals, Vol. 23, No. 1, 1981.

48. Ohta, A., Kamakura, M., Nihei, M., Maeda, Y., Inagaki, M., Sasaki, E., "An Automatic Detection of Fatigue Initiation Life of a Welded Joints," Transaction of National Research Institute for Metals, Vol. 22, No. 3, 1980.

49. Nihei, M., Yohda, M., Sasaki, E., "Fatigue Properties for Butt Welded Joints of SM50A High Tensile Strength Steel Plate," Transaction of National Research Institute for Metals, Vol. 20, No. 4, 1978.

50. Munse, W.H., Private Communication, Department of Civil Engineering, University of Illinois at Urbana-Champaign, 1988.

51. Gurney, T.R., "Fatigue Design Rules for Welded Steel Joints,"The Welding Institute Research Bulletin, Vol. 17, May, 1976.

52. Fain, R.A. and Booth, E.T., "Results of the First Five Data Years of Extreme Scratch Gauge Data Collected Aboard Sea Land's SL-7/s," SSC-286, Ship Structure Committee, March, 1979.

53. Yung, J.-Y. and Lawrence, " A Comparison of Method for Predicting Weldment Fatigue Life under Variable Load Histories,"Design of Weldments," FCP Report No. 117, College of Engineering, University of Illinois at Urbana-Champaign, Feb. 1985.

VITA

Sahng Kyoo Park received his B.S.E. in Welding Engineering from Seoul National University, Seoul, Korea in 1978. He then worked as a sales engineer of steel mill products at the Daewoo Industrial Co. Ltd., in Seoul for three years. He received his M.S. degree in Welding Engineering from The Ohio State University at Columbus, Ohio in 1983. He joined the University of Illinois at Urbana-Champaign in August, 1984 to pursue his graduate study leading to the Ph.D. degree in Metallurgical Engineering.